

Characterisation of Gallium Nitride
Grown by
Pulsed Laser Deposition



**A thesis submitted for the degree of
Doctor of Philosophy**

by

Kia Woon Mah B.Eng. M.Eng.

**School of Physical Sciences
Dublin City University**

**Research Supervisor
Dr. Jean-Paul Mosnier**

January 2002

Declaration

I hereby certify that the material, which I now submit for assessment on the programme of study leading to the award of Doctor of Philosophy is entirely my own work and has not been taken from the works of others save and to the extent that such work has been cited and acknowledged within the text of my work

Signed 

ID number 99144980

Kia Woon Mah

Date 24/01/02

Acknowledgements

I would like to express my sincere gratitude to Dr Jean-Paul Mosnier, my supervisor, for his great supports, encouragement, suggestions, valuable discussion and unfailing advice throughout this research project. My hand-on skills have been greatly enhanced under his continuous guidance. I am also very grateful for his proof reading of this thesis. I would also like to thank Prof James Lunney, Trinity College, for giving me the opportunity to carry out PLD experiments in his laboratory and for placing other research equipment at my disposal. Special thanks also to Dr Enda McGlynn and Prof Martin Henry, for their insight and discussions of the PL measurements.

I would also like to thank other lecturers within the departments, Prof Eugene Kennedy, Dr Paul van Kampen, Dr John Costello and Dr Tony Cafolla for their valuable helps in the DLP and AFM measurements. I would also like to thank Dr Juan Castro from Trinity College for his advice and valuable suggestions during my time in TCD. Special thanks to Donagh O'Mahony from TCD for his helps and support in setting up the PLD system, as well as the tedious but enjoyable time we spend in the sample preparation and the dump XRD measurements. Thanks also to all the lab fellows in DCU, Pat Yeates, Mark Stapleton, Alan McKiernan, Mohamed Abbas, Oonagh Meighan and John Hirsch, for their dirty jokes and encouragement, either in the lab, canteen or in the pub.

I would like to thank Des Lavelle in the workshop for machining of all those parts in my chamber, particularly to those tiny little holes in the heater. Also, I greatly appreciate the assistance of Pat Wogan and Alan Hughes for the electrical connection in the heating element.

Most of all, my thanks to my family, for their support and understanding throughout the period I am in Dublin. Last, but not the least, to my girlfriend, Kitty, for her love, full support and understanding during the course.

Abstract

This main aim of this thesis is to study the photoluminescence (PL) properties of Gallium Nitride (GaN) grown by either the solid- or the liquid- target Pulsed Laser Deposition (PLD) technique

Most thin films were deposited on sapphire(0001) substrate in a pure nitrogen (N_2) atmosphere GaAs(001) was also used as a substrate for the first time The properties of the material systems were characterized using PL, X-Ray diffraction (XRD), Raman spectroscopy and atomic force microscopy (AFM) The expansion dynamics of Ga and GaN laser-ablation plumes were also studied using time- resolved extreme ultraviolet dual laser photoabsorption (DLP) spectroscopy

The PL, XRD and Raman results indicated the possibility of a mixed cubic- and hexagonal- structure in GaN grown using the solid target PLD system PL full width at half maximum (FWHM) as narrow as ~ 9 meV for the donor-exciton transitions (D-X) was achieved for GaN/sapphire(0001) grown by liquid target PLD system Significantly enhanced low temperature PL emissions at 3.361 eV (I_3) and 3.310 eV (I_4) were observed for the material deposited on a GaAs(001) substrate at $\sim 800^\circ\text{C}$ A model has been proposed to explain the emission mechanism for I_3 and I_4 in which the electrons and holes are confined in cubic inclusions within the hexagonal material, analogously to a type I quantum well

The DLP results showed the marked difference between Ga and GaN laser-ablation plumes, and suggested that metallic Ga is a more suitable target material for the PLD growth of GaN compared to a GaN target

Table Of Contents

Acknowledgments	2
Abstract	3
Table of Contents	4
1 Introduction	
1 1 Motivation	7
1 2 Objectives	9
1 3 Contents and Organization of the Thesis	11
1 4 References	14
2 Gallium Nitride Material System - Epitaxial Growth and Physical Properties	
2 1 GaN Properties	
2 1 1 Hexagonal GaN	17
2 1 2 Cubic GaN	21
2 2 Brief History of the growth of GaN	23
2 3 Pulsed laser deposition of GaN	27
2 4 References	32
3 Description of the Experimental Setups	
3 1 Pulsed Laser Deposition System	
3 1 1 Solid Target Pulsed Laser Deposition System	37
3 1 2 Liquid Target Pulsed Laser Deposition System	39
3 2 X-Ray Diffraction (XRD) System	44
3 3 Photoluminescence	
3 3 1 Photoluminescence in Semiconductor	45
3 3 2 Experimental Setup	49

3 4	Dual Laser Plasma (DLP) Photoabsorption Technique	
3 4 1	Experimental Setup	51
3 4 2	Experimental Description	53
3 5	References	54
4	Properties of GaN grown by Solid Target Pulsed Laser Deposition Technique in Nitrogen Atmosphere	
4 1	Surface Morphology	56
4 2	Crystalline Structure	58
4 3	Optical Properties	
4 3 1	Photoluminescence Study	60
4 3 2	Raman Spectroscopy Study	68
4 4	Conclusion	70
4 5	References	71
5	Properties of GaN grown by Liquid Target Pulsed Laser Deposition Technique in Nitrogen Atmosphere	
5 1	Growth Rate	74
5 2	Crystalline Structure	76
5 3	Photoluminescence Study	79
5 4	Conclusion	93
5 5	References	94
6	Study of the expansion dynamics of Ga and GaN plasma plume using time-resolved extreme UV photoabsorption spectroscopy	
6 1	Gallium Metal Target	97
6 2	Polycrystalline Gallium Nitride Target	102
6 3	Conclusion	107
6 4	References	108

7 Conclusion and Recommendations for Future Works	
7.1 Conclusion	110
7.2 Recommendations for Future Works	112
7.3 References	114
Author's Publications	115
List of Figures	117
List of Tables	120
Appendices	
A Quantum Well Theory	121
B Band Theory	126
C Physical Properties of Gallium Nitride	131
D Optical Setup of the DLP System	133

CHAPTER 1

INTRODUCTION

1.1 Motivation

Silicon (Si) is presently the most important semiconductor for the microelectronics industry which makes up over 90% of all semiconductor devices sold world-wide. However, Si is not widely used in optoelectronic applications, mainly due to the fact that it is not a direct bandgap semiconductor and hence not an efficient photonic material. Since the first report by Welker *et al* [1] in 1952, which suggested that compound materials made up of group-III and group-V elements of the periodic table exhibit semiconductor properties, III-V semiconductor compounds and their applications have been extensively investigated. Nowadays, III-V compound semiconductors are attracting more and more interest especially in the field of optical devices such as lasers, waveguides or optical modulators, as well as in high frequency electronic devices. III-V compounds such as Gallium Arsenide (GaAs) and Indium Phosphide (InP) have superior transport properties (i.e. higher electron mobility and drift velocity) over Si, which make them more suitable for application in high frequency microwave devices. Furthermore, III-V compounds can form heterojunctions with each other, which are the basic structure for modern electronic and optical devices [2].

Chapter 1 Introduction

The family of III-V compound nitrides such as *Indium Nitride* (InN), *Gallium Nitride* (GaN) and *Aluminium Nitride* (AlN) is one of the promising classes of optoelectronic materials. The bandgap and the corresponding wavelength for InN, GaN and AlN are given in table 1.1 respectively [3-4].

	InN	GaN	AlN
Bandgap (eV) @300K	1.95	3.40	6.25
Wavelength (nm) @300K	636	365	198

Table 1.1 Summary of the bandgap and wavelength values for *Indium Nitride* (InN), *Gallium Nitride* (GaN) and *Aluminium Nitride* (AlN)

All three binaries and their alloys are direct bandgap semiconductors and their energy gaps cover the spectral region from red to deep ultraviolet. This makes them ideal candidates for carefully tailored optoelectronic devices, such as light emitting diodes (LED), which up to now, are difficult to fabricate in the blue and green regions [5].

Up to date, high brightness visible GaN based LED's are commercially available, a development which has transformed the market for full colour displays [6-8], and which has opened the way to many other applications, such as in traffic lights and highly efficient low voltage white light sources. Recently, GaN based CW UV laser diodes [9] have also been demonstrated, which paved the way for applications in high density optical storage systems and UV lithography.

Chapter 1 Introduction

Until now, most of the high quality GaN materials have been grown by advanced epitaxial techniques such as molecular beam epitaxy (MBE) [10] or organometallic vapor phase epitaxy (MOCVD) [11]. Most studies have been devoted to understand the growth kinematics and properties of the GaN materials grown by these techniques. Apart from MBE and MOCVD, the pulsed laser deposition (PLD) technique has, more recently, also been used successfully to grow GaN by a number of workers [13, 17-19]. In PLD, a pulsed laser is used to vaporize the surface of a target material (i.e. GaN or Ga metal) to create a laser plasma which condenses on a suitable substrate.

1.2 Objectives

The present work was initiated by the need to further understand and characterise the GaN material grown by either solid GaN- or liquid Ga- target PLD systems [13]. More than 40 samples were prepared in this work, and characterised by a number of methods such as x-ray diffraction (XRD), temperature dependent photoluminescence (PL), Raman scattering spectroscopy and atomic force microscopy (AFM).

The PL technique is widely used for analyzing the optical properties of GaN material grown by MBE, MOCVD, gas source molecular beam epitaxy (GSMBE) and halide vapour phase epitaxy (HVPE) [10, 14-16]. However, detailed reports on the PL on GaN grown by PLD technique are not widely available, i.e. little is known about the activation energies of different PL transitions in PLD grown GaN samples. Hence, it

Chapter 1 Introduction

is important to study the PL properties of GaN grown by the PLD technique in greater detail

Active nitrogen plasma source and ammonia are the most commonly used N sources for the growth of GaN in a liquid target PLD system [13,17-19] However, a very high residual n-type carrier concentration ($\sim 10^{19} \text{ cm}^{-3}$) has been measured on GaN thin films grown by active plasma source [17] In addition, it has been reported that the use of ammonia can create certain problems such as the incorporation of unintentional hydrogen into the films during the epitaxial growth [18] An alternative method for the growth of high purity GaN in liquid target PLD system is the use of pure nitrogen gas (N_2) However, detailed studies on the growth and properties of GaN prepared by this method are not widely reported, for example, the study on the change of the material properties as a function of growth parameters are still not available Thus, it is important to study the influence of the growth parameters (i.e. substrate temperature, N_2 pressure, laser repetition rate and etc) on GaN grown in a liquid target PLD system in N_2 atmosphere

GaN can crystallise either in hexagonal or cubic structure Cubic GaN, which will grow mainly on a cubic substrate such as GaAs (001), has recently attracted some interest [20] This is because epitaxially grown layers of cubic GaN provide some advantages over the hexagonal ones, such as easier cleaving for laser applications [21] Most of the previous researches on PLD grown GaN have mainly focussed on the epitaxial growth of hexagonal GaN on sapphire (0001) [13,18-19,22], fused silica

Chapter 1 Introduction

or Si substrates [22-23] PLD was never used to grow GaN on a GaAs (001) substrate, although much research has been carried out using other techniques such as MBE or MOCVD [20, 24-25] Hence, it is worth looking into the growth and material properties of GaN thin films grown on a GaAs (001) substrate in a PLD system

It is well known in the PLD process that the initial formation of the ablation plume and its expansion are key to the growth of high quality films However, to date, most of the studies on GaN grown by PLD have mainly focussed on the effect of the growth parameters [18-19, 22] rather than the investigation of the ablation plume Consequently, it is necessary to study the laser ablation plume in order to understand aspects of the growth mechanism in a PLD system [14]

1.3 Contents And Organization Of The Thesis

This thesis comprises seven Chapters

Some theoretical background and historical survey related to the growth of GaN material system is presented in Chapter 2 A summary of the current developments in PLD grown GaN thin films is also included

In Chapter 3, the characterisation methods used in this study, such as “ θ -2 θ ” x-ray measurement (XRD), photoluminescence (PL), dual laser plasma (DLP) photoabsorption technique will be described In addition, the fundamental mode of

Chapter 1 Introduction

operation of the two different types of Pulsed Laser Deposition (PLD) growth techniques used in this study, namely solid target PLD and liquid target PLD are also included

Chapter 4 contains a detailed description of the properties of GaN/Sapphire(0001) material system grown by the solid target PLD technique. The GaN epilayers were characterised using “ θ - 2θ ” XRD scans, PL, Raman scattering and atomic scanning microscopy (AFM) measurement. Low temperature PL yield a line-width (FWHM) of 15 meV for the donor-bound exciton (D-X) transitions, comparable with GaN grown by MOCVD [16] and MBE [26] techniques. Subsequently, origins and activation energies for various PL transitions are deduced and discussed in details. The results suggest that GaN grown by solid target PLD in N_2 atmosphere consisted of mixed hexagonal and cubic phases.

Chapter 5 discusses the properties of GaN grown in a liquid target PLD system. GaN material systems grown on sapphire (0001) substrate are studied as a function of substrate temperature and pulse laser repetition rate. PL FWHM as narrow as 9 meV for (D-X) transitions was achieved in the samples grown at a substrate temperature (T_s) of 800°C. Following this, GaN thin film was grown on a GaAs (001) substrate for the first time using the PLD technique. Optical properties for GaN grown on sapphire (0001) and GaAs (001) substrates are compared and studied using temperature dependent PL. Two strong luminescence lines I_3 (3.368 eV) and I_4 (3.310 eV) were observed to dominate the low temperature spectrum, and a significant enhancement

Chapter 1 Introduction

for both luminescence lines were observed in the material deposited on GaAs (001) substrates. We interpret both peaks as transitions involving carriers confined in cubic inclusions in the hexagonal phase, analogously to a type I quantum well.

Chapter 6 contains a study of the dynamics of Ga species in the laser ablation plumes of Ga metal and polycrystalline GaN. Time and space resolved photoabsorption spectra of the ablation plumes were obtained using the time-resolved DLP technique. Marked differences between the Ga and GaN plumes were observed. Based on these observations, we deduce a relationship between the quality of the GaN epilayers and the relevant ablation plume parameters. The results confirmed the remarks by Wang *et al* [27] according to which metallic gallium is a better candidate for the growth of high quality GaN by PLD.

A summary of all the work, as well as recommendations for future research are presented in Chapter 7.

Chapter 1 Introduction

1 4 References

- 1 H Welker, *Z Naturforsch Nature Science* **79**, 744 (1952)
- 2 N Holonyak *Solid State Electronic Devices* Prentice-Hall Ed 1990
- 3 R F Davis *Physicca* **B185**, 1 (1993)
- 4 D A Neumayer and J G Ekerdt *Chem Mater* **8**, 9 (1996)
- 5 F A Ponce and D P Bour *Nature* **386** 351
- 6 S Nakamura *Nikkei Electronics Asia* **6**, 65
- 7 S Nakamura *J Vac Sci Tech* **A13**, 705
- 8 K Itoh, T Kawamoto, H Amono, K Hiramatsu and I Akasaki *Jpn J Appl Phys* **30**, 1924 (1991)
- 9 J I Pankove *RCA Review* **34**, 336
- 10 M Suzuki and T Uenoyama *J Appl Phys* **80**, 6868 (1996)
- 11 R J Molnar, R Singh and T D Moustakas *Appl Phys Lett* **66**, 268 (1995)
- 12 S Nakamura, Y Harada and M Seno *Appl Phys Lett* **58**, 2021 (1991)
- 13 R D Vispute, V Talyansky, R P Sharma, S Choopun, M Downes and T Venkatesan *Appl Phys Lett* **71**, 102 (1997)
- 14 H Z Xu, A Bell, Z G Wang, Y Okada, M Kawabe, I Harrison and C T Foxon *J Crystal Growth* **222**, 96 (2001)
- 15 M Leroux, B Beaumont, N Grandjean, P Gibart, J Massies, J P Faurie *MRS Internet Journal* Vol 1, Article 25
- 16 M Leroux, N Grandjean, B Beaumont, G Nataf, F Semond, J Massies and P Gibart *J Appl Phys* **86**, 3721 (1999)

Chapter 1 Introduction

- 17 P Merel, M Chaker, M Tabbal and H Pepin *Appl Surf Sci* **177**, 165 (2001)
- 18 T F Huang, A Marshall, S Spruytte, J S Harris, *J Crys Growth* **200**, 362 (1999)
- 19 L D Wang and H S Kwok *Appl Surf Sci* **154**, 439 (2000)
- 20 D J As, F Schmilgus, C Wang, B Schottker, D Schikora and K Lischka, *App Phys Lett* **70**, 1311 (1997)
- 21 S Nakamura, M Senoh, S Nagahama, N Lisa, T Yamada, Y Sugimoto *Jpn J Appl Phys* **L74**, 35 (1996)
- 22 D Cole and J G Lunney *Mat Sci Eng* **B50**, 20 (1997)
- 23 R F Xiao, X W Sun, Z F Li, N Cue and H S Kwok, Q Z Liu and S S Lau *J Vac Sci Tech* **A15**, 2207 (1997)
- 24 C H Hong, D Pavlidis, S W Brown, S C Rand *J Appl Phys* **77**, 1705 (1995)
- 25 H Chen, H Fei, Z Li, S Liu, Q Huang, J Zhou and Y Wang *J Crys Growth* **201/202**, 336 (1999)
- 26 T Kurobe, Y Sekiguchi, J Suda, M Yoshimoto, H Matsunami, *Appl Phys Lett* **73**, 2305 (1998)
- 27 L D Wang and H S Kwok *Appl Surf Sci* **154**, 439 (2000)

CHAPTER 2

GALLIUM NITRIDE MATERIAL SYSTEM -- EPITAXIAL GROWTH AND PHYSICAL PROPERTIES

GaN crystallizes either in (1) the hexagonal (wurtzite, h-GaN) structure, (2) the cubic (zinc blende, c-GaN) structure, or (3) a mixture of both these structures. Both cubic and hexagonal structures are very closely related, differing only by their stacking sequences. The hexagonal and cubic structure will be discussed in section 2.1.1 and 2.1.2 respectively. A brief description of the history of the growth of GaN, as well as the pulsed laser deposition of this material will be presented in section 2.2 and 2.3. The major problems associated with its growth will also be discussed.

2.1 GaN Properties

The structure and optical properties of hexagonal GaN have been studied extensively in the past [1-2]. To date, most devices have been fabricated using hexagonal GaN grown on sapphire (0001) [1]. Cubic GaN, which is normally grown on cubic substrates such as GaAs (001) [3], presents some advantages over the hexagonal one, namely, higher carrier mobilities, easy cleaving/etching and better ohmic contact.

2.1.1 Hexagonal GaN

Hexagonal GaN is mainly grown on hexagonal substrates such as sapphire (0001), 6H silicon carbide (SiC) or silicon(001) substrates [3-4]. The hexagonal structure dominates in growth conditions where there is an excess of group V species (i.e. Nitrogen), or at high substrate temperatures. In the hexagonal structure, each atom is tetrahedrally surrounded by four nearest neighbours with the same bond distances. The atomic structure for hexagonal GaN is shown in Figure 2.1 below:

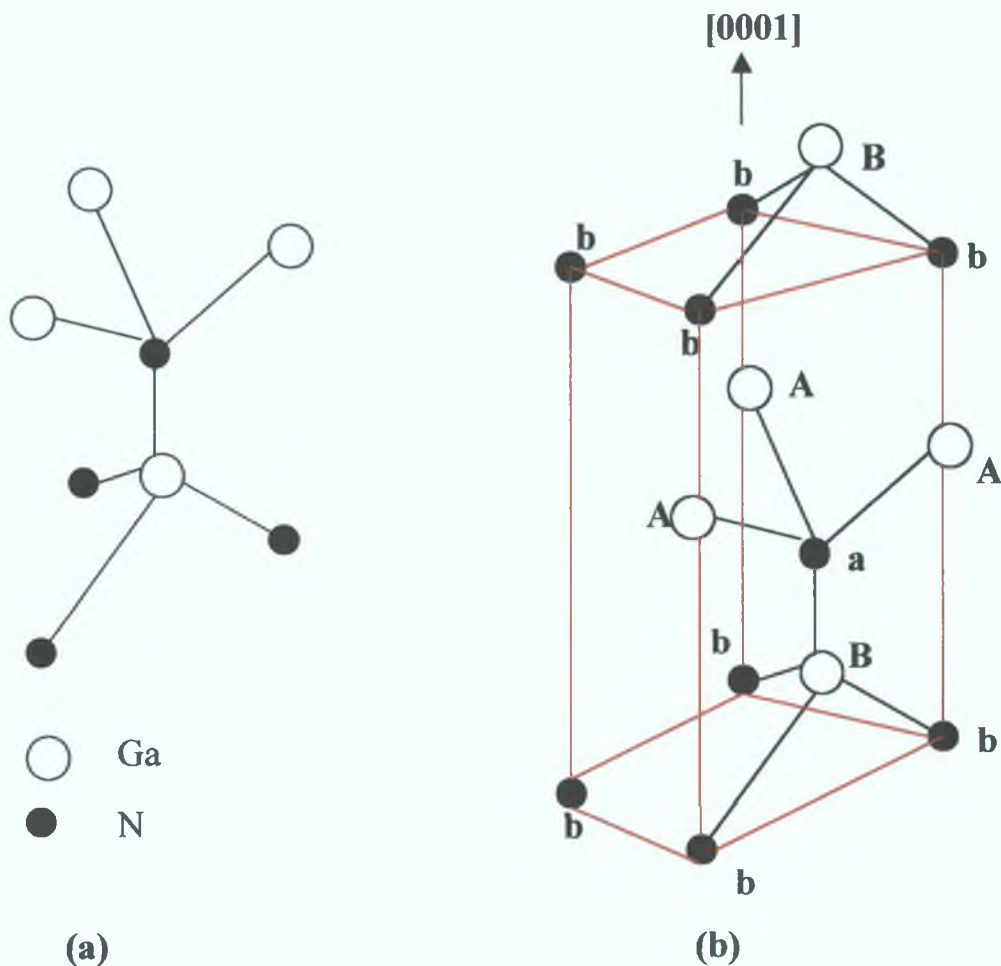


Figure 2.1. (a) The basic interatomic bond (b) Three dimension structure of layers stacking along the [0001] direction in hexagonal GaN structure

Chapter 2 Gallium Nitride Material System - Epitaxial Growth and Physical Properties

The Bravais lattice of the wurtzite structural is hexagonal and the axis perpendicular to the hexagons is labelled as [0001] direction (or "C-axis") Along the [0001] direction, the structure can be imagined as a sequence of layer of atoms of the same elements (all Ga or all N), build up from regular hexagons As shown in Fig 2 1(b), the stacking sequence for the hexagonal structure is



To date, the most accurate lattice parameters for an ideal hexagonal GaN crystal are $a_0 = 3.1879 \pm 0.0002 \text{ \AA}$, $c_0 = 5.1851 \pm 0.0002 \text{ \AA}$ as reported by Leszczynski *et al* [7] Those parameters result in a significant mismatch effect with the commonly used substrates such as sapphire (0001) where $a_0 = 4.785 \text{ \AA}$ and $c_0 = 12.991 \text{ \AA}$ However, the "effective" in-plane mismatch depends on the epitaxial orientations actually adopted Several authors [3,8] have shown that hexagonal GaN films grown on basal plane sapphire grow with their c-axis parallel to the sapphire c-axis but rotated in plane so that $[2\bar{1}\bar{1}0]_{\text{GaN}}$ is parallel to $[1\bar{1}00]_{\text{sapphire}}$, and $[1\bar{1}00]_{\text{GaN}}$ is parallel to $[1\bar{2}10]_{\text{sapphire}}$ In this configuration, the mismatch turns out to be 16%, much less than 49% discrepancy in a_0 , although this is still very large in epitaxy terms

Two types of X-ray diffraction scans are commonly used to characterize GaN films, the ω rocking curve and the θ - 2θ scan In the former, the detector remains fixed and the sample is rotated near the Bragg angle, giving a hnewidth ($\Delta\omega$) dependent on the angular spread of the columnar grains Typical values for $\Delta\omega$ are between 30 and 50

Chapter 2 Gallium Nitride Material System - Epitaxial Growth and Physical Properties

arc min [7,9]. In the latter, the detector is rotated through twice the angle of the sample rotation and the angular width of the resulting x-ray peak provides a measure of the spread in the lattice parameter along the growth axis. The details of the corresponding experimental setup will be covered in Chapter 3 and the results of the θ - 2θ scans for our GaN samples will be discussed in Chapters 4 and 5.

The fundamental energy bandgap for GaN has been extensively measured. The data from Monemar et al.[10] appears to be the most accurate. Monemar [10] obtained his results from thick GaN films grown on sapphire substrates using optical reflectance and PL excitation spectroscopy. As mentioned, both hexagonal and cubic GaN have a direct bandgap and most of the optical transitions occur in Γ point ($k = 0$) in the Brillouin zone. The fundamental transitions in hexagonal GaN are shown in Fig. 2.2.

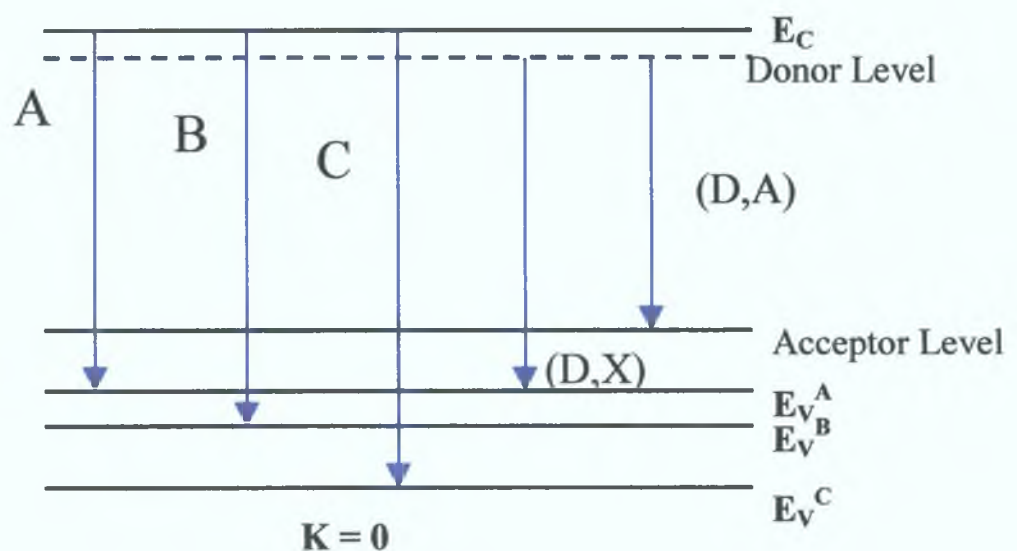


Figure 2.2 The fundamental bandgap of hexagonal GaN

Chapter 2 Gallium Nitride Material System - Epitaxial Growth and Physical Properties

The near band edge transitions at 4.2 K are tabulated in Table 2.1 [12]. The valence band near $k \sim 0$ in hexagonal GaN is split into three separate bands, better known as E_V^A , E_V^B and E_V^C due to spin orbit splitting and the axial crystal field [10-12]. Each band gives rise to an exciton state and each exciton state gives rise to a hydrogenic series of energy levels. This may cause a certain confusion in the interpretation of the experimental data as the energy separation between E_V^A , E_V^B and E_V^C is rather small (see Table 2.1). This situation is further complicated by the fact that excitons may be trapped at impurity sites (donor or acceptor), resulting in transition energies lower by a few to hundreds of meV. The donor exciton (D-X) transition is the most commonly observed transition in hexagonal GaN at temperature less than 30 K [13-14].

A	B	C	(D-X)	(D-A)
3.504 eV	3.510 eV	3.547 eV	3.473 eV	3.275 eV

Table 2.1 Emissions energies for various transitions in hexagonal GaN at 4.2 K

In addition to the near band edge transitions, GaN may also exhibit a broad transition around 2.2 eV, generally known as "yellow band". The yellow bands appear to be a universal feature as it has been observed both in the bulk material and in epitaxially grown GaN. The intensity of yellow band can vary considerably from sample to sample. Good optical quality samples exhibit very weak yellow luminescence. Some authors [3,6] have attributed the yellow band to the transition originating from Ga or N vacancy.

2.1.2 Cubic GaN

Up to now, when compared with hexagonal GaN, little research has been carried out on the properties of cubic GaN. The atomic structure of cubic GaN is shown in Fig. 2.3 below:

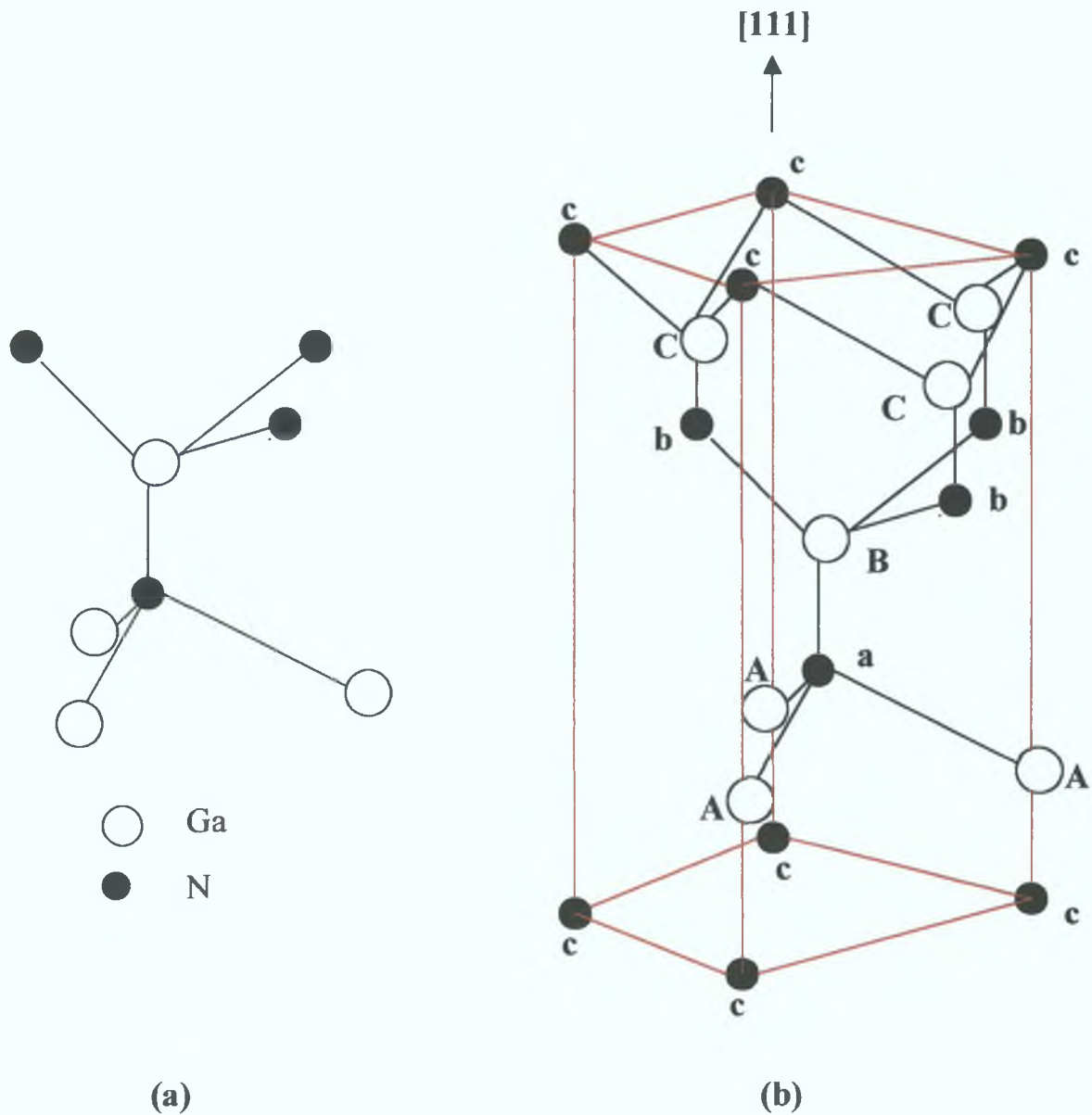


Figure 2.3 (a) The basic interatomic bond (b) Three dimension structure of layers stacking along the [111] direction in cubic GaN structure.

Chapter 2 Gallium Nitride Material System - Epitaxial Growth and Physical Properties

Unlike the hexagonal structure, the second layer of the cubic GaN is rotated through an angle of 60° with respect to the first layer in the [111] direction. As shown in Fig 2.3(b), the stacking sequence for cubic GaN is



A common approach for the growth of cubic material is the use of a cubic substrate such as GaAs (001), Si (111) or 3C SiC [15-17]. However, there is experimental evidence showing that the cubic structures may also occur near the substrate interface in films grown on sapphire (0001) substrates. The films gradually become a single hexagonal structure as the film thickness increases [18]. The lattice parameters for the cubic GaN is obtained experimentally as $a_0 = 4.50 \text{ \AA}$, which is in good agreement with the theoretical value of 4.53 \AA [8,19]. This result also indicates that the lattice mismatch between cubic GaN and GaAs (001), the most commonly used substrate to grow the cubic structure, is nearly 20 %.

The bandgap of cubic GaN is by now reasonably well studied and measured. It is generally accepted in the literature that the bandgap of cubic GaN is approximately 200 meV smaller than the hexagonal one. Recently, by employing photoluminescence (PL) measurements, several authors have assigned an energy of 3.274 eV to the donor exciton transition (D-X) in cubic GaN [20-21]. The 3.274 eV transition line showed the characteristics of an excitonic transition upon change of temperature or excitation energy, analogously to the (D-X) transition at 3.473 eV in hexagonal GaN [22]. The donor-acceptor (D-A) transition energy for cubic GaN is found to be 3.178 eV, which

was further confirmed by the results obtained from temperature dependent PL [20]. The binding energies for the donor and acceptor impurities in cubic GaN were measured to be approximately 25 meV and 90 meV, respectively [19-20]. Recently, Xu *et al* [23] reported that there should exist three different types of acceptor levels (compared to one as reported previously [21]) in cubic GaN, which are about 130 meV, 342 meV and 447 meV above the valence band. At present, there is no evidence concerning the nature of the acceptor or the donor. However, the conclusions of these studies [19-20] seem clear regarding the actual bandgap energy, i.e. the low temperature band gap of cubic GaN is close to 3.30 eV, while the exciton binding energy is about 26 meV below the conduction band [22].

2.2 Brief History of the growth of GaN

Gallium Nitride (GaN) was first synthesized in powder form early in the 20th century by Johnson [24]. This early work was based on the available technique of halide vapour phase epitaxy (HVPE) [25], using gallium chloride to transport Ga and ammonia as the source for the N, respectively. The bulk-like material with the thickness of $\sim 100 \mu\text{m}$ could be easily produced by this technique, and was suitable for the preliminary studies of many physical properties [26].

During the last two decades, the enormous success of advanced epitaxial growth techniques such as organometallic vapor phase epitaxy (MOCVD) [27-28] or

Chapter 2 Gallium Nitride Material System - Epitaxial Growth and Physical Properties

molecular beam epitaxy (MBE) [29-30], have made it possible to grow high quality GaN and related compound semiconductor such as AlGaN or InGaN Layers with thickness down to monolayer dimension with atomic precision have also been grown However, MOCVD appears to be more successful than MBE for GaN mainly due to the higher throughput and demonstrated superior material quality [28]

In the MOCVD process, a thin film is deposited through a chemical reaction occurring between metal organic precursors and hydrides on a hot substrate surface [27-28] GaN, for example, can be grown by introducing trimethylgallium (TMGa) and ammonia (NH₃) simultaneously into the reaction chamber equipped with a substrate heated to high temperatures Although the MOCVD epitaxial growth process is relatively simple, researchers faced several challenges in the 1980s to achieve device quality nitride films One of the main difficulties is due to the stability of NH₃ against dissociation In order to maintain film stoichiometry during growth, a high pressure of NH₃ (~ 0.5-1 atm) and high growth temperature (>1000 °C) are generally required to enhance the thermal dissociation of ammonia However, these extreme MOCVD conditions create a region of turbulence at the substrate This situation becomes worst at higher growth temperatures where thermal convection will cause an even more turbulent flow As a result, GaN islands rather than 2 dimensional epitaxial growth will be formed on the substrate [27]

In early 1990, Nakamura *et al* [31] reported a novel "two flow" reactor design that overcame this problem (see Fig 2.4) The source gases (main flow) were introduced

Chapter 2 Gallium Nitride Material System - Epitaxial Growth and Physical Properties

parallel to the substrate surface similar to the conventional horizontal reactor. A second flow (subflow) consisting of equal amount of N_2 and H_2 was introduced from above the substrate surface (see Fig. 2.4), to suppress thermal convection and thus keep the reactants on the substrate surface. Without the subflow, the growth is not two-dimensional and only GaN islands are formed.

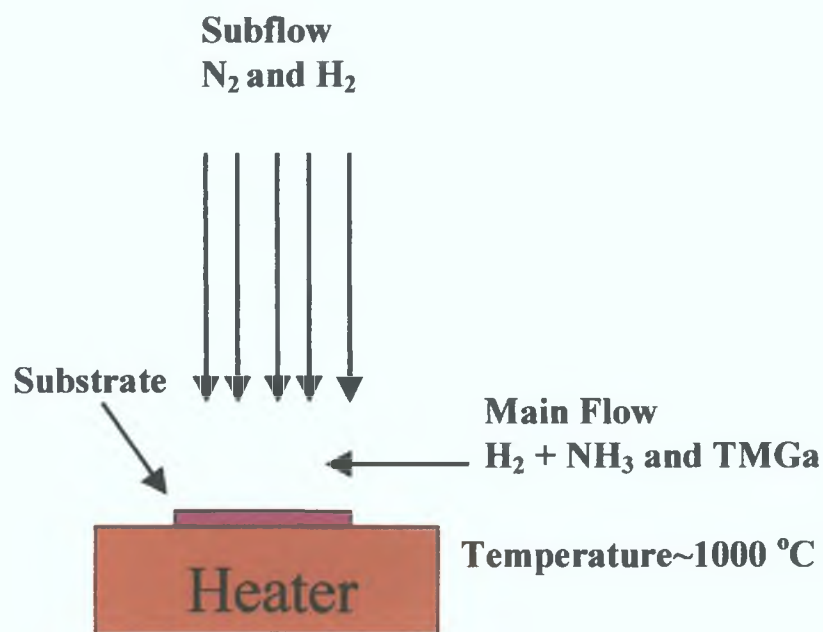


Figure 2.4 A schematic diagram of a typical MOCVD GaN reactor.

Another obstacle to the growth of single crystalline GaN thin films is the lack of substrates with matching lattice constants and thermal expansion coefficients. Sapphire (Al_2O_3) is the most widely used substrate (due to its relatively low cost, availability in large area wafers, and its large band gap energy) in spite of a lattice mismatch of ~16% and a large difference in the thermal expansion coefficient with

Chapter 2 Gallium Nitride Material System - Epitaxial Growth and Physical Properties

GaN In the mid-1980's, the Japanese research group led by Amano [32] developed a two-step process using c-plane sapphire. They first grew a buffer layer of AlN (~200 Å) at low temperature followed by the GaN main layer. The use of a thin buffer layer was believed to enhance two-dimensional nucleation so that a layer by layer growth mechanism was achieved. The crystal quality was good and the layers showed that carrier concentrations of unintentionally n-doped material was reduced from 10^{19} to 10^{17} cm^{-3} while the Hall mobility was increased from 50 to 400 $\text{cm}^2/\text{V s}$ at room temperature. In early 1990, Nakamura and coworkers from the Nichia Chemical Company [33] used a similar approach in which a GaN buffer layer was grown at low temperature. High quality GaN films were achieved with background n-type carrier concentration of 4×10^{16} cm^{-3} and Hall mobility around 600 $\text{cm}^2/\text{V s}$.

GaN thin films grown directly on a sapphire substrate contain high densities of structural line and plane defects. The most dominant defects are threading dislocations that are nearly parallel to the c-axis [34]. Their density ranges between 10^8 to 10^{10} cm^{-3} even with several μm thick films. Besides threading dislocations, stacking faults, inversion domain boundaries and edge dislocations are also present near the interface [35-37]. These structural defects are generated due to the large lattice mismatch (~16%) and thermal expansion coefficient difference (~80%) between the GaN film and the sapphire substrate. However, contrary to other materials used for optoelectronic applications such as III-V arsenides or phosphides, where the dislocation densities above 10^4 cm^{-3} clearly affect the device performance, the fabrication of bright LEDs with long life-time is possible with GaN or other nitride compound semiconductors.

[38] with dislocation densities greater than 10^8 cm^{-3} . It appears that dislocations in III-V nitrides are not associated with electrically active defects, which would act as nonradiative recombination centers and limit the lifetime of the device.

With all the vital contributions from this research, highly efficient blue GaN based LEDs and LDs are now commercially available [38-40]. The high brightness LEDs operate from either a single or multiple quantum well p-n junctions grown on electrically insulating sapphire [40]. Blue (AlN)GaN solid state lasers have also been demonstrated by several groups. Lifetime of these lasers exceeds 10,000 hours [41]. One potential application of the blue laser diode could be their incorporation into optical reading and writing of data on compact disks which would greatly increase the disk storage density, due to the reduction in the diffraction-limited size of the focussed spot.

2.3 Pulsed Laser Deposition of GaN

In this project, the pulsed laser deposition (PLD) [42] technique was employed to grow GaN. In this technique, a pulsed laser is focused on a target to create a plasma, which then expands and recondenses on a suitable substrate (see Fig. 2.5). The growth process is performed either in a vacuum, in the presence of a buffer (i.e. Argon) or a reactive gas (i.e. oxygen or N_2) environment.

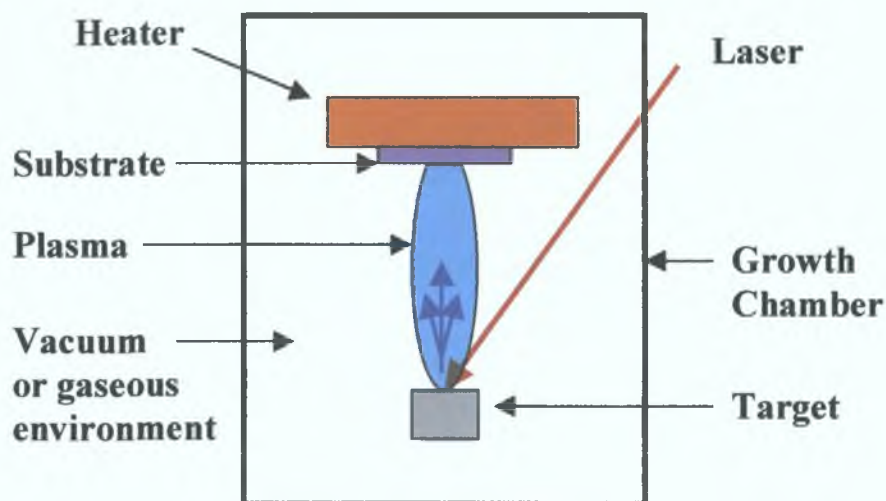


Figure 2.5 A schematic diagram of a typical PLD system.

In brief, the PLD process for the epitaxial growth of GaN can be divided into three stages [42-43]:

- 1) The creation of nitrogen and gallium species in the laser ablation plasma.
- 2) The arrival of those energetic species onto the heated substrate.
- 3) The epitaxial growth of GaN.

Compared to the MOCVD and MBE techniques, PLD is a relatively new growth technique that has been widely used for the growth of oxide thin films- such as ferroelectric or superconducting [42], but rarely used for III-V compound semiconductors. Several features of the PLD technique make it worthy of study as a technique for growing GaN thin films. The congruent nature of laser ablation allows the deposition of multi-component materials using only a single target. Furthermore,

Chapter 2 Gallium Nitride Material System - Epitaxial Growth and Physical Properties

multiple targets can be loaded inside the chamber on a rotating holder, and sequentially exposed to the laser beam, thereby enabling *in situ* growth of heterostructures [43] The growth rate achieved by PLD can be varied by the experimental conditions such as the laser repetition rate

Recently, several authors [43-50] have reported the growth of GaN epilayers using the PLD technique These authors have also studied some of the thin film properties in order to assess and optimize thin film quality The main conclusions from their work are as follows

- a) High quality GaN could be successfully grown by the ablation of polycrystalline GaN targets in vacuum, nitrogen or ammonia backgrounds The optical and structural properties were greatly improved for GaN grown at high substrate temperatures (i.e. >650 °C) However, the growth rate was reduced for material grown at higher temperatures (i.e. > 950 °C), an effect which was attributed to gallium desorption [44-45]
- b) The stacking fault parallel to the interface and screw dislocations along the c-axis were observed in GaN grown by PLD [46]
- c) The thermal cleaning of the substrate surface and the "two-step" (i.e. GaN buffer layer) growth procedure were found to improve the crystalline quality and surface morphology of GaN grown on Sapphire (0001) [47]

Chapter 2 Gallium Nitride Material System - Epitaxial Growth and Physical Properties

- d) GaN thin films were successfully grown on different substrates (sapphire and fused silica) by ablating a liquid target gallium metal, at a substrate temperature of 600°C in the presence of ammonia gas [43]
- e) Wurtzite structure GaN was grown on a Si(111) substrate using liquid target gallium with a pulsed nitrogen gas source. Great improvements in structural and optical properties were observed in GaN grown at the relatively high temperature of 700°C using this experimental configuration [48]
- f) Ternary nitride compounds (i.e. $\text{Al}_x\text{Ga}_{1-x}\text{N}$ [49] and $\text{GaN}_x\text{As}_{1-x}$ [50]) were successfully grown by PLD in an ammonia atmosphere
- g) GaN thin films with very narrow XRD hnewidth (80 arc sec) were successfully grown using a liquid gallium target in conjunction with an atomic nitrogen source. A very low rms surface roughness ($\sim 14 \text{ \AA}$) was observed in these conditions [51]
- h) The effects of the N_2 overpressure on the properties of GaN thin films were studied. The grain sizes were found to decrease for samples grown at higher nitrogen pressure ($> 0.1 \text{ Torr}$)[52]

We note that high quality GaN thin films were successfully grown by those authors although a wide range of different experimental conditions were used [44-52]. For example, target conditions such as liquid or molten Ga, or pressed polycrystalline

Chapter 2 Gallium Nitride Material System - Epitaxial Growth and Physical Properties

GaN, were all used in various growth temperature or pressure of nitrogen or ammonia. This by some means suggests that there may exist certain 'common features' within the laser plasma formation and expansion among all these PLD experimental conditions, which eventually result in the growth of high quality GaN.

Chapter 2 Gallium Nitride Material System - Epitaxial Growth and Physical Properties

2.4 References

- 1 R Gaska and M S Shur Appl Phys Lett **78**, 769 (2001)
- 2 J L Deiss, C Hirlmann, J L Loison, M Robino and G Versini Mat Sci Eng **B82**, 68 (2001)
- 3 J Wu, H Yaguchi, K Onabe, R Ito, Y Shirake, Appl Phys Lett **71**, 2067 (1997)
- 4 R F Xiao, X W Sun, Z F Li, N Cue and H S Kwok, Q Z Liu and S S Lau J Vac Sci Tech **A15**, 2207 (1997)
- 5 P R Willmott and F Antoni Appl Phys Lett **73**, 1394 (1998)
- 6 J I Pankove GaN(1) Semiconductor and Semimetal, Vol 1 Academic Press New York (1998)
- 7 M Leszczynski Appl Phys Lett **69**, 73 (1996)
- 8 R C Powell, N E Lee, Y Kim, J E Greene J Appl Phys **73**, 189 (1993)
- 9 W R L Lambrecht and B Segall *Properties of Group III Nitrides (EMIS Data Review Series)* London INSPEC, IEEE chp 4
- 10 B Monemar Phys Rev **B10** 676 (1974)
- 11 J J Hopfield, J Phys Chems **15**, 97 (1960)
- 12 G D Chen, M Smith, J Y Lim, H X Jiang, S Wei and M A Khan Appl Phys Lett **68**, 2784 (1996)
- 13 C Guenaud, E Deleporte, M Voos, C Delalande MRS Internet Journal Vol **2**, Article 10

Chapter 2 Gallium Nitride Material System - Epitaxial Growth and Physical Properties

- 14 M Leroux, N Grandjean, B Beaumont, G Nataf, F Semond, J Massies and P Gibart *J Appl Phys* **86**, 3721 (1999)
- 15 H Okumura, S Yoshida and T Okahisa *Appl Phys Lett* **64**, 2997 (1994)
- 16 Z X Liu, A R Goni and K Syassen *Appl Phys Lett* **86**, 929 (1999)
- 17 U Kohler, D J As, B Schottker, T Frey and K Lischka *Appl Phys Lett* **85**, 404 (1999)
- 18 Y Xin, P D Brown, C B Boothroyd, A R Preston, C J Humphreys, T S Cheng *Mat Res Soc Sym Proc* **423**, 311 (1996)
- 19 O Madelung *Phys Rev* **B53**, 16425 (1964)
- 20 J Wu, H Yaguchi, K Onabe, R Ito, Y Shirake, *Appl Phys Lett* **71**, 2067 (1997)
- 21 D J As, F Schmilgus, C Wang, B Schottker, D Schikora and K Lischka *Appl Phys Lett* **70**, 1311 (1997)
- 22 J S Foresi and T D Moustakas *Appl Phys Lett* **62**, 2859 (1993)
- 23 D Xu, H Yang, J B Li, D G Zhao, S F Li, S M Zhuang and R H Wu *Appl Phys Lett* **76**, 3025 (2000)
- 24 W C Johnson, J B Parsons, M C Crew *J Phys Chem* **36**, 2561 (1932)
- 25 D D Manchon, A S Barker, P J Dean, R B Zetterstrom *Solid State Comm* **8**, 1227 (1970)
- 26 B Monemar and O Lagerstedt, *J Appl Phys* **50**, 6480 (1979)
- 27 H M Manaservit and K L Hess *J ElectronChem Soc* **126**, 2031 (1971)
- 28 J I Pankove *J ElectronChem Soc* **119**, 1118 (1972)

Chapter 2 Gallium Nitride Material System - Epitaxial Growth and Physical Properties

- 29 S Yoshida, S Misawa, Y Fujii, S Takada, H Hayakawa, S Gonda, A Itoh J Vac Sci Tech **16**, 990 (1979)
- 30 S Yoshida, S Misawa and S Gonda J Appl Phys **53**, 6844 (1982)
- 31 S Nakamura, Y Harada and M Senoh Appl Phys Lett **58**, 2021 (1991)
- 32 H Amano, I Akasaki, K Hiramatsu and N Koide Thin Silif Films **163**, 415 (1988)
- 33 S Nakamura, M Senoh and T Mukai Jpn J Appl Phys **30**, L1708 (1991)
- 34 F A Ponce, MRS bulletin, **22**, 51 (1997)
- 35 Z Lihental Mrs Symp Proc **395**, 351 (1996)
- 36 L T Ramando, J E Northrup and M A O'Keefe **69**, 2394 (1996)
- 37 S D Lester Appl Phys Lett **66**, 1249 (1995)
- 38 S Nakamura, M Senoh, N Iwasa and S Nagahama Appl Phys Lett **67**, 1868 (1995)
- 39 S Nakamura, M Senoh, S Nagahama, T Tamada, T Matsushita, H Kiyoka and Y Sugimoto Jpn J Appl Phys **35**, L74 (1996)
- 40 S Nakamura and G Fasol *Group III-V Nitride Based Ultraviolet Light Emitting Diodes and Laser diodes* Springer 1997
- 41 S Nakamura, M Senoh, S Nagahama, N Iwasa, T Yamada, T Matsushita, Y Sugimoto and H Kiyoku Appl Phys Lett **70**, 1417 (1997)
- 42 D Chrisey, G Hubler *Pulsed Laser Deposition of Thin Films* Wiley-Interscience New York, 1994
- 43 R F Xiao, X W Sun, Z F Li, N Cue and H S Kwok, J Vac Sci Technol A **15(4)**, 2207 (1997)

Chapter 2 Gallium Nitride Material System - Epitaxial Growth and Physical Properties

- 44 R D Vispute, V Talyansky, R P Sharma, S Choopun, M Downes and T Venkatesan Appl Phys Lett **71**, 102 (1997)
- 45 D Cole and J G Lunney Mat Sci Eng **B50**, 20 (1997)
- 46 T F Huang, A Marshall, S Spruytte, J S Harris, J Crys Growth **200**, 362 (1999)
- 47 A Yoshida, K Ouyang, B S Chang and A Wakahara Thin Solid Films **343/344**, 127 (1999)
- 48 P R Willmott and F Antoni Appl Phys Lett **73**, 1394 (1998)
- 49 T Huang and J S Harris Appl Phys Lett **72**, 1158 (1998)
- 50 S Cho and H Okumura Appl Phys Lett **76**, 3861 (2000)
- 51 P Merel, M Chaker, M Tabbal and H Pepin Appl Surf Sci **177**, 165 (2001)
- 52 G S Sundir, H Fujii et al Appl Surf Sci **127**, 471 (1998)

CHAPTER 3

DESCRIPTION OF THE EXPERIMENTAL SETUPS

In this chapter, the experimental principles and techniques used in this work are described. Two different types of Pulsed Laser Deposition (PLD) systems, namely solid target PLD and liquid target PLD, used in this work will be presented in section 3.1 for an understanding of the GaN film preparation process. The main characterisation methods employed in this work, X-ray diffraction (XRD) and photoluminescence (PL), are also described. A brief introduction to the Dual Laser Photoabsorption (DLP) technique is also included and methods used to study the GaN plasma plume are outlined. The growth of GaN and XRD measurements were carried out in the Physics Department of Trinity College, while the PL, DLP, Raman and atomic force microscopy (AFM) measurements were all carried out in the School of Physical Sciences at Dublin City University.

3.1 Pulsed Laser Deposition System

The GaN samples used in our research were grown by using either a solid- or a liquid-target in a PLD system. The former will be covered in section 3.1.1 and the latter will be discussed in section 3.1.2. The PLD system using a solid target was available from previous research work while the liquid target system was built as part of our research.

3.1.1 Solid Target Pulsed Laser Deposition System

The system consisted of an ultra high vacuum (UHV) chamber, equipped with a leak valve to introduce external gases (such as N_2) during deposition. A schematic diagram of this system is shown in Fig. 3.1. It is pumped by a 220 ls^{-1} ion pump backed up by a 60 ls^{-1} turbo-molecular pump. The system was baked up at 120°C for 24 hours and the pressure in the chamber was reduced to less than 10^{-7} Torr. A loadlock was used to transfer targets and substrates without breaking of the vacuum in the main chamber.

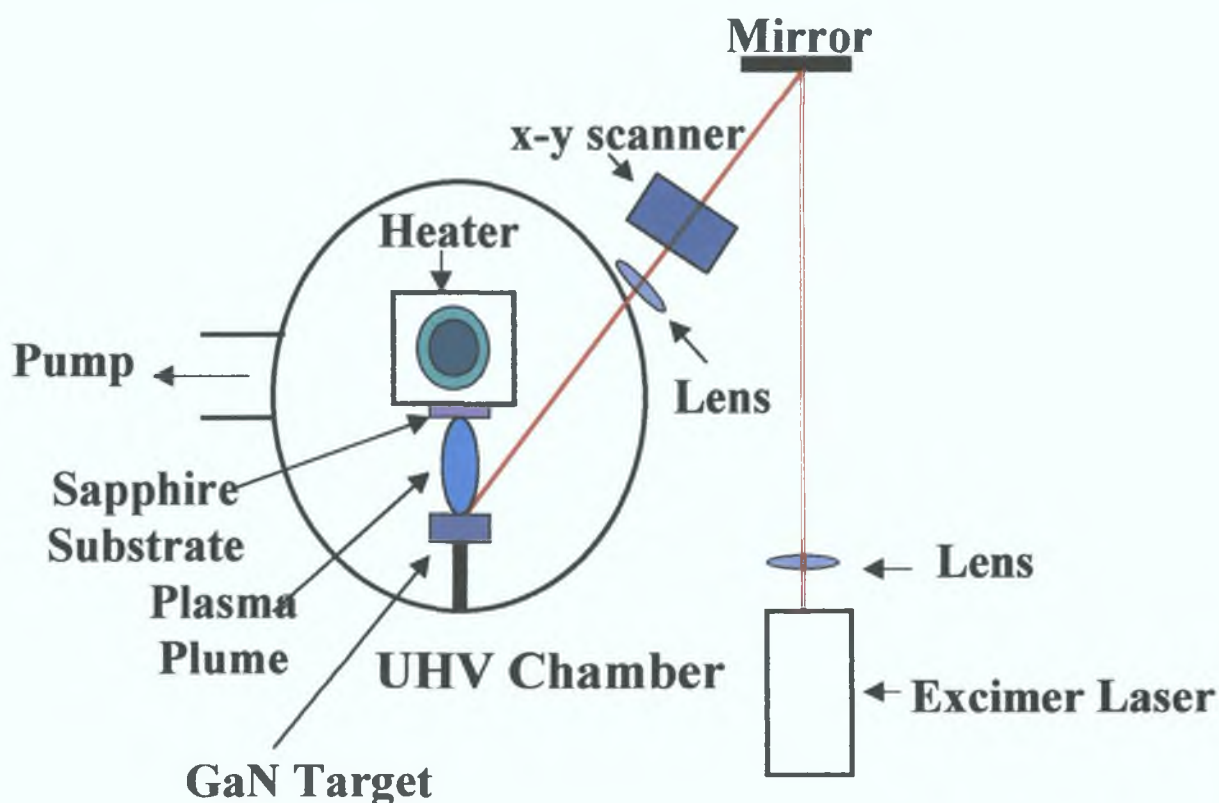


Figure 3.1 Schematic diagram (top view) of PLD system

A multiple target carousel capable of holding up to four different target materials was used in this system. The target pellets were prepared by pressing GaN (99.99%)

Chapter 3 Description of The Experimental Setups

powder at $5 \times 10^4 \text{ N cm}^{-2}$, followed by heating at $700 \text{ }^\circ\text{C}$ in an N_2 atmosphere for 24 hours to improve the mechanical strength of the target. This approach has been used by several authors [1-2] to prepare polycrystalline GaN targets suitable for laser ablation. A Lambda-Physik LPX100 KrF excimer laser, which delivers 23 ns full width at half maximum (FWHM) pulses at a wavelength of 248 nm and energies up to 200 mJ, was used to ablate the target material at a repetition rate of 10 Hz.

Sapphire (0001) was used as the substrate in these experiments. The substrate was heated to 700°C in a radiative-type heater, consisting of a tungsten filament wound on a ceramic tube. The substrate was placed into a stainless steel holder and inserted into the centre of the ceramic tube. The temperature is measured by a K-type thermocouple fixed at the back of the substrate. A schematic diagram of heater is shown in Fig. 3.2. A temperature controller was used to monitor and maintain the temperature. The maximum temperature achievable with this heater is $\sim 700 \text{ }^\circ\text{C}$.

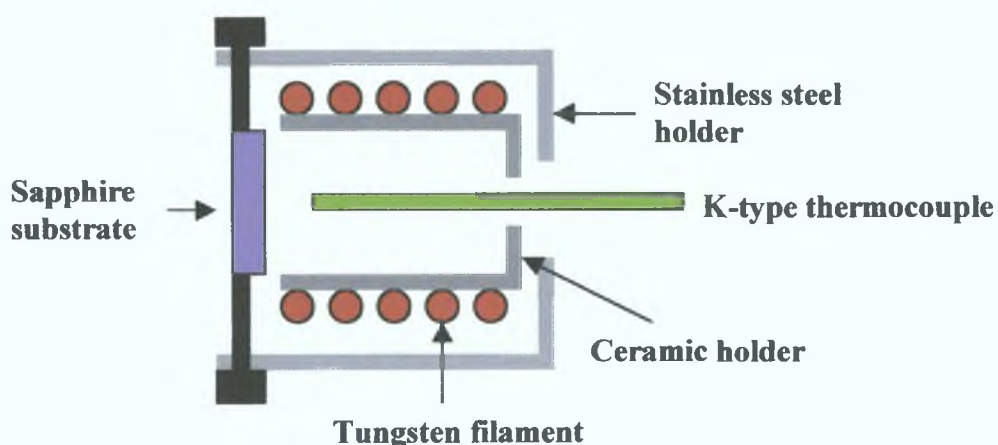


Figure 3.2 Schematic diagram (cross section) of the radiative-type heater used in the system

Chapter 3 Description of The Experimental Setups

In this work, the GaN thin films were grown in a nitrogen (N_2) atmosphere at substrate temperature of $\sim 700^\circ C$. The substrate was kept at a distance of ~ 3 cm from the target surface at a pressure of 2.2×10^{-1} Torr. No intentional buffer layer was used in this study and the thickness of the GaN films grown were $\sim 0.4 \mu m$, which was measured by atomic force microscopy (AFM) measurements (see Chapter 4).

3.1.2 Liquid Target Pulsed Laser Deposition System

This system consisted of an upright (i.e. vertical) UHV chamber with a liquid gallium (Ga) target positioned horizontally at the bottom of the chamber. A schematic diagram of this system is shown in Fig. 3.3.

The KrF excimer laser was focussed by a quartz lens using two mirrors (Fig. 3.3: Mirror 1 – normal “45°” mirror, mirror 2 – custom made “22.5°” mirror), and guided through a quartz window onto the Ga target. The Ga target was kept liquid in a stainless steel cup. A two lens system was used to achieve a uniform beam on the target. An aperture was used to select the uniform portion of the beam. This aperture is then imaged, and then de-magnified, onto the target surface. By moving Lens 1 with respect to the aperture, the fluence on the target could be varied while keeping the spot size on target constant. The maximum energy density arriving on the liquid gallium target was $\sim 8 J/cm^2$.

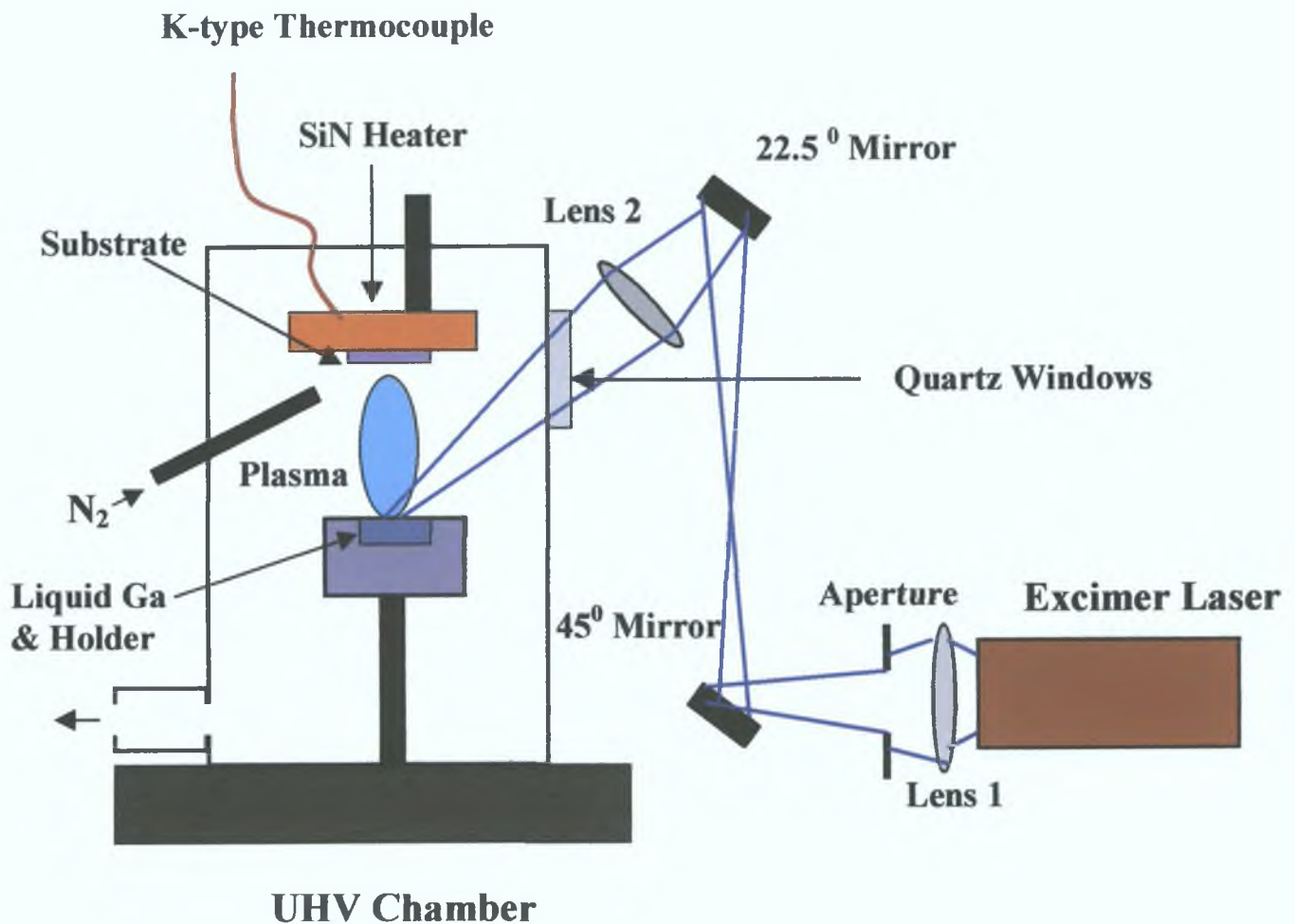


Figure 3.3 Schematic diagram (side view) of the liquid target PLD system

Prior to the growth, the chamber was evacuated to $\sim 10^{-6}$ Torr by a 60 l s^{-1} turbo pump backed by a rotary pump. The turbo pump was turned off during the growth and a mechanical pump was used to maintain the necessary vacuum conditions during the growth process. High purity N₂ (99.995%) gas was used as the nitrogen source during the growth. N₂ gas was introduced into the growth chamber through a needle valve, with a flow rate of ~ 3 sccm (i.e. standard centimetre cube per minute) as measured by

Chapter 3 Description of The Experimental Setups

a flowmeter and sprayed over the surface of the growing GaN film (see Fig 3 3) We found that better films were grown when the end of the nozzle supplying the N₂ was placed at a distance of ~5 mm close to the substrate The chamber pressure was kept constant at 5 Torr for all the experiments We found that no epitaxial growth could be achieved for pressures less than 3 Torr The target-substrate distance was kept at 5 cm such that the glow of the ablation plume was seen to just touch the surface of the substrate

Silver paint was used to attach the substrate to the silicon nitride (SiN) heater The temperature is measured by a K-type thermocouple which was attached directly on the substrate The substrate temperature could be adjusted by regulating the alternating voltage applied across the heater via a temperature controller The calibration curve for temperature vs voltage is shown in Fig 3 4 below

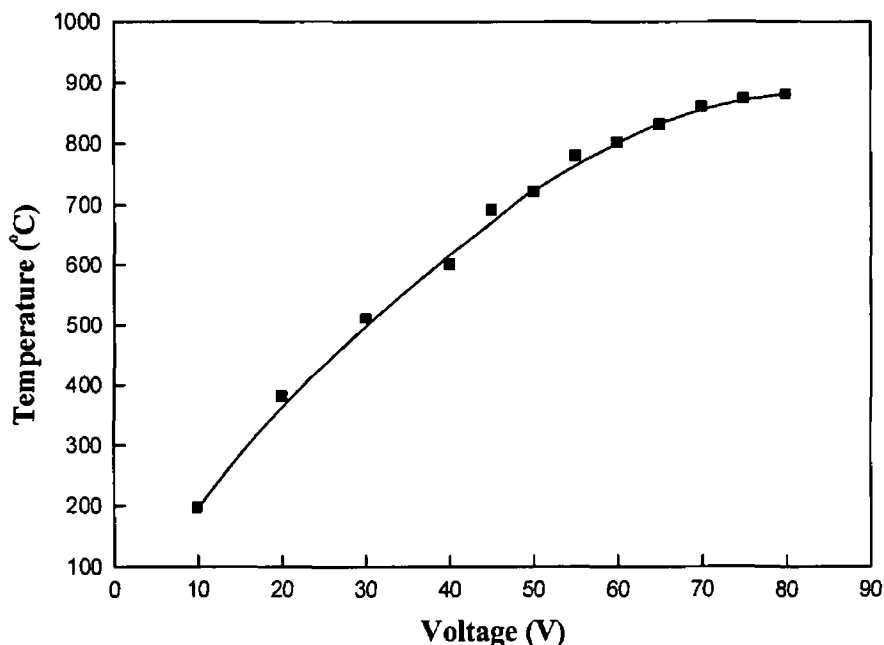


Figure 3 4 Calibration curve for substrate heater

Chapter 3 Description of The Experimental Setups

The thin film growth was monitored by measuring the *in situ* thin film reflectivity during the deposition process. A schematic diagram for the system is shown in Fig. 3.5 below.

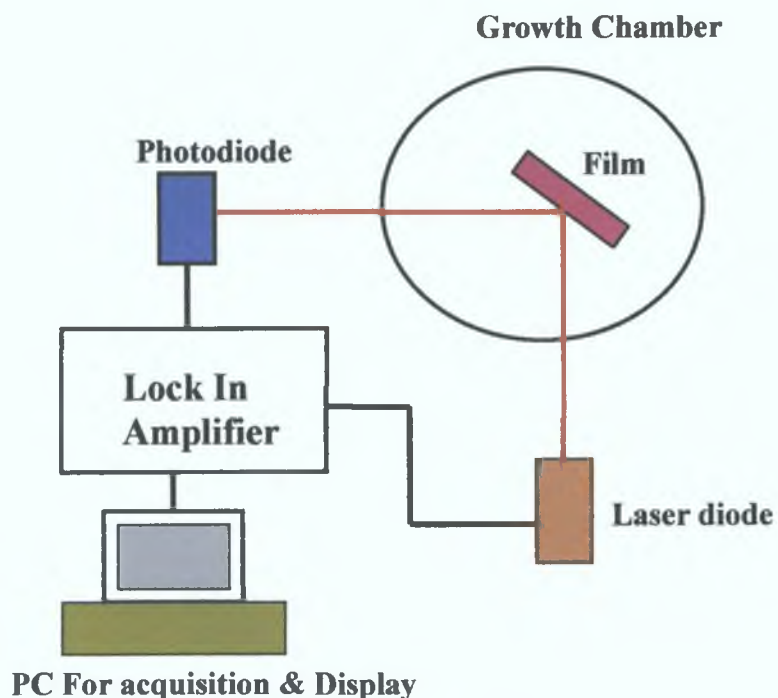


Figure 3.5 Schematic diagram of the Reflectivity System

A laser beam light from a laser diode was incident on the growing film at an angle of 45° . The reflected signal was collected by a fast Si photodiode and sent through a lock in amplifier. This signal was sampled at 0.5 Hz and observed in real time on a computer. This method has the advantages of being non-destructive and applicable to most deposition environments. The theoretical interpretation of the optical reflectivity can be found in [3]. In our work, we only used the reflectivity measurements to check the presence of a thin film during growth through the observation of a fringe pattern. We did not use the reflectivity data to extract any thin film parameters. A typical reflectivity curve is shown in Fig. 3.6.

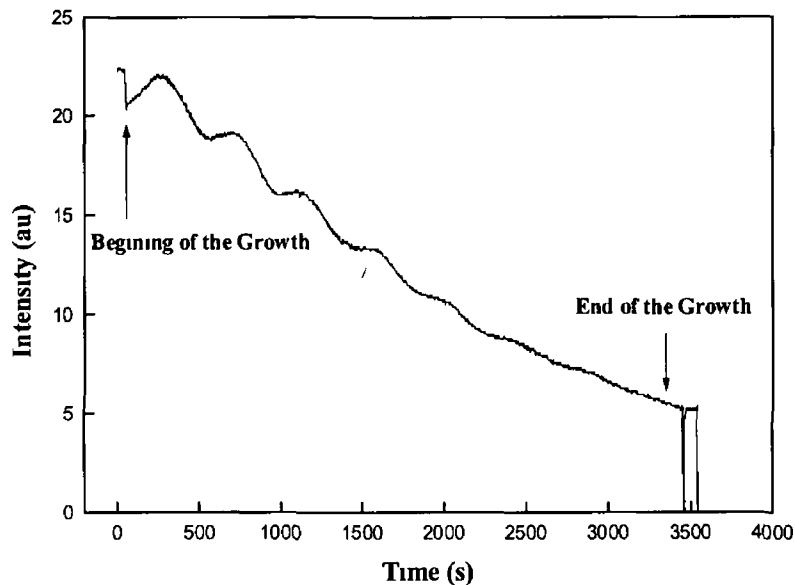


Figure 3.6 Typical reflectivity curve of GaN thin film grown under nitrogen atmosphere

In our first set of experiments on the growth of GaN using a liquid Ga target, the substrate temperature was varied between 500 °C and 860 °C for samples grown directly on the sapphire (0001). We did not employ any buffer layer or substrate pre-treatment for these samples. The optimum growth temperature of ~ 800 °C was found for these samples based on the results obtained from photoluminescence and x-ray diffraction data.

Keeping the optimum growth temperature constant, we replaced the sapphire by a "epi-ready" semi-insulating GaAs (001) substrate. A 40 nm thin GaN buffer layer was grown on the GaAs (001) substrate at 500 °C prior to the growth of the main layer. This was to prevent thermal decomposition of the GaAs substrate at the growth temperature of 800 °C. The thickness of all the samples grown with the liquid target was ~1 μm as measured by a profilometer.

Chapter 3 Description of The Experimental Setups

3.2 X-Ray Diffraction (XRD) System

All the films prepared in this study were characterised immediately after deposition by an X-Ray diffraction system (Model: Siemens Diffrac 500) operated in " θ - 2θ " mode. The geometry of the system is illustrated in Fig. 3.7 below.

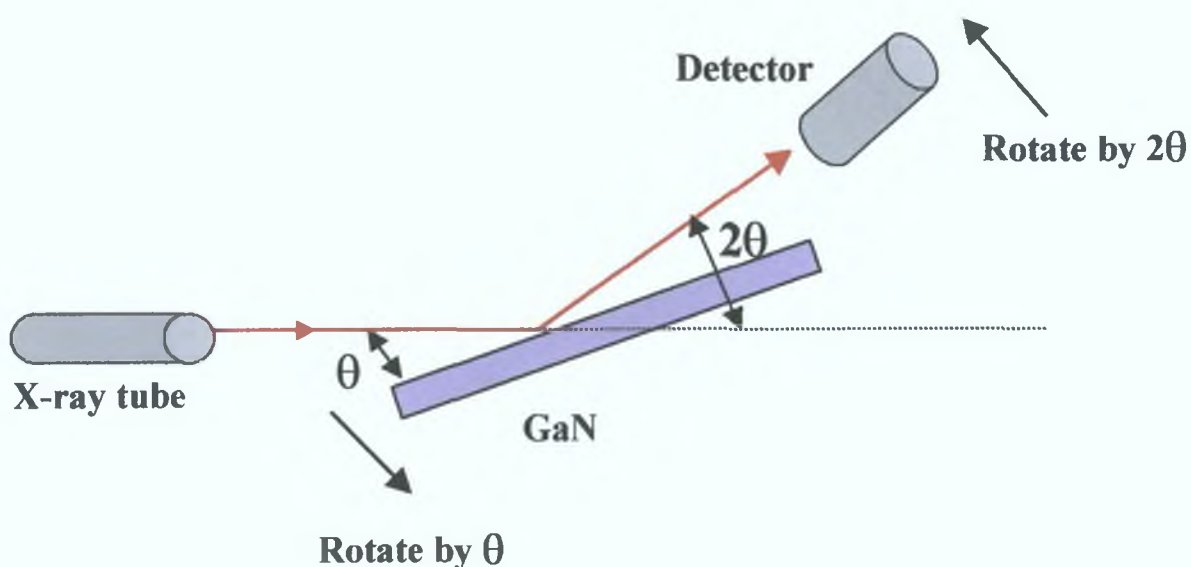


Figure 3.7 Schematic diagram of the XRD system operated in " θ - 2θ " mode

In this configuration, the film is held at the center of the diffractometer and is rotated by an angle of θ through an axis in the sample, while the detector is rotated through the same axis by the corresponding angle of 2θ . The reflection from $\text{CuK}\alpha_1$ radiation was detected from the samples. A voltage of 40 kV and current of 30 mA were used in all the XRD measurements. The theoretical $2 \times$ Bragg angles for both cubic and hexagonal GaN are tabulated in table 3.1[11].

Chapter 3 Description of The Experimental Setups

Cubic GaN			Hexagonal GaN		
Peak	2 x Bragg Angle (2θ)	Relative Intensity (Theory)	Peak	2 x Bragg Angle (2θ)	Relative Intensity (Theory)
(111)	34.4	18.80	(10 $\bar{1}$ 0)	32.2	7.60
(002)	40.0	7.98	(0002)	34.6	18.50
(220)	57.8	4.86	(10 $\bar{1}$ 1)	36.8	8.47
(311)	69.0	2.10	(10 $\bar{1}$ 2)	48.4	1.63
(222)	72.6	1.33	(11 $\bar{2}$ 0)	57.8	4.84

Table 3.1 Theoretical XRD data for cubic and hexagonal GaN

3.3 Photoluminescence (PL)

3.3.1 Photoluminescence in Semiconductors

Photoluminescence (PL) [4] is a widely used optical probing technique for the characterization of III-V semiconductors and their alloys. This is because PL is a simple and direct method for providing adequate information on the material for a reasonable investment in equipment and time. PL is used to understand the fundamental band structure (i.e. bandgap energy), as well as to characterise the optical quality (i.e. PL linewidth) of the material. A general description of the band structure in semiconductors is included in Appendix B.

The optical properties of a semiconductor are connected with both intrinsic and extrinsic effects. Intrinsic optical transitions are the band-to-band transition, including

Chapter 3 Description of The Experimental Setups

exciton effects, and also carrier- related absorption processes Extrinsic properties are related to dopants or defects, which usually create discrete electronics states in the bandgap, and therefore influence both the optical absorption and emission processes It will be shown in Chapter 4 and 5 that the optical properties of our GaN material are indeed strongly influenced by both intrinsic- and extrinsic- effects

In brief, PL in semiconductors is the radiative recombination of non-equilibrium individual or coupled charge carriers generated by absorption of electromagnetic radiation with suitable energy The charged carriers may be (a) free electrons or holes occupying energy levels in the conduction or valence bands respectively, (b) electrons and holes bound to ionized impurities, or (c) excitons (electron-hole pairs coupled by Coulomb interaction at low temperature) Excitons may move through the crystal lattice of the semiconductor (free excitons), or become localised at active point defects such as impurity atoms or at interfaces (known as bound excitons) Normally, the photoluminescence will involve three separate steps

- *Excitation* Charge carriers have to be excited by an external source of energy such as He-Cd laser
- *Thermalisation* The excited charge carriers relax towards a quasi-thermal equilibrium distribution
- *Recombination* The thermalised charge carriers recombine radiatively to produce emission which may be detected by a suitable detector

Chapter 3 Description of The Experimental Setups

Most of the PL measurements are performed at low temperature (typically 5K). This is because in this temperature region, only the ground level of the defect is appreciably populated and the recombination spectra only involve the ground state. Optical band to band transition is the process whereby an electron in the valence band can be excited into the conduction band by absorbing a photon from an incident light beam. For this to happen the photon energy in the beam must clearly be greater than the bandgap energy. In our study, the He-Cd laser, which delivered a photon energy of 3.82 eV (325 nm), is used to excite electron-hole pairs in GaN which has a fundamental bandgap of 3.5 eV. The commonly observed PL emission lines in GaN have been discussed in Chapter 2 (section 2.1).

The manner in which the total photoluminescence intensity of a material system varies with the sample temperature, will provide detailed information on both the defects and the corresponding activation energy of the shallow levels arising from the crystal imperfection within the material. In most semiconductors, the behaviour of the carriers can be well represented by an Arrhenius-type plot. For simplicity, consider a case where all the different types of traps or defects can be represented by a single energy level. This can be visualised in the following manner. In the low temperature region, the electrons are captured by an intermediate energy level (due to defects or impurities). However, as the temperature increases the defect centres can no longer capture the electrons since they are ionized off due to the increase in the thermal energy.

Chapter 3 Description of The Experimental Setups

In general, the PL emission efficiency (η) can be written as [5]

$$\eta = \frac{P_r}{P_r + P_{nr}} \quad (3.1)$$

where P_r and P_{nr} are the radiative and non-radiative transition probabilities respectively

As the electrons are thermally ionised to higher energy level, the non-radiative transitions can be assumed to have a temperature dependence represented by the following expression

$$P_{nr} = {}^0P_{nr} \exp\left(\frac{-\Delta E_a}{kT}\right) \quad (3.2)$$

where ${}^0P_{nr}$ is the temperature-independent constant for the carrier, ΔE_a and k are the activation energy and Boltzman constant, respectively In practise at a given T , the PL intensity should behave according to [5]

$$\frac{I(T)}{I_0} \sim \eta \quad (3.3)$$

where I_0 is the maximum value of the PL intensity for a material system

From (3.1), (3.2) and (3.3) one can obtain the following expression for a single energy level system

Chapter 3 Description of The Experimental Setups

$$\frac{I(T)}{I_0} = \frac{1}{1 + C_1 \exp\left(\frac{-\Delta E_a}{kT}\right)} \quad (3.4)$$

where $C_1 = \frac{{}^0P_m}{P_r}$. However, equation (3.4) should be modified to accommodate the case of a material system with multiple energy levels (due to various types of impurities or defect centres). The PL intensity in this situation is given by the following expression

$$I(T) = \frac{I_0}{1 + \sum_{n=1}^{n=N} C_n \exp\left(\frac{-\Delta E_n}{kT}\right)} \quad (3.5)$$

This equation will be applied later in this work to investigate the material properties of our PLD-grown samples. The corresponding activation energies for the exciton, the donor and the acceptor energy level in the samples will also be deduced, and the origin of these carriers will be discussed as well.

3.3.2 Experimental Setup

The PL apparatus used in this work is schematically shown in Fig. 3.8. The excitation source is a He-Cd laser with a power density of 0.3 W/cm^2 and a laser spot size of about 2 mm. A low pass glass filter placed directly in the front of the laser serves to suppress UV laser lines. Samples are mounted in an Oxford Instruments continuous flow He cryostat (CF1204) and can be cooled down to 4K with liquid Helium. A PID temperature controller was also connected to the 25Ω heater on the sample mount.

Chapter 3 Description of The Experimental Setups

This temperature controller was specifically intended for use in cryogenic applications and by controlling the output of the heater the desired experimental temperature can be achieved. This temperature controller allowed the temperature to be adjusted within 0.1K. The PL radiation from the sample is collected by lens 1 and then focussed by the second lens 2 onto the slit of the monochromator (see Fig. 3.8). The PL signal was dispersed by a grating monochromator with a resolution of 0.1 nm, and was detected using a GaAs photomultiplier (PMT). The output signals were digitized and displayed on a computer which controls the whole PL apparatus.

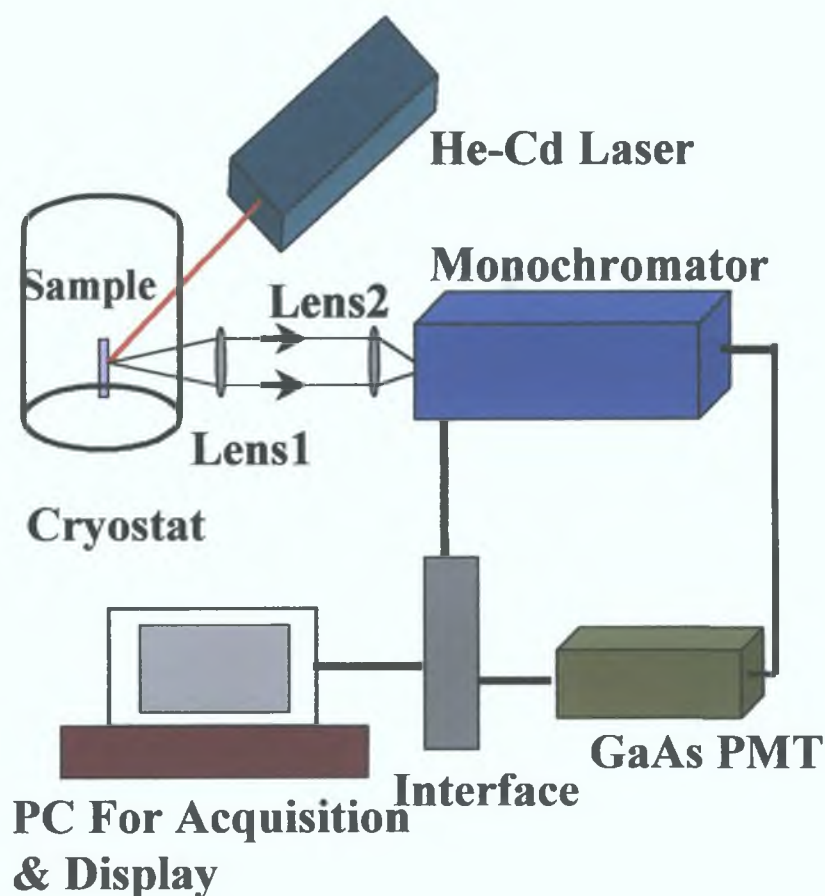


Figure 3.8 Schematic diagram of the PL experimental apparatus

Chapter 3 Description of The Experimental Setups

3 4 Dual Laser Plasma (DLP) Photoabsorption Technique

When the output of a high power Q-switched laser is focussed on a solid target in vacuum, a dense plasma is formed. It constitutes an intense source of extreme ultraviolet and X-ray radiation. The inherent time-resolved nature of the laser plasma light source is suited to the study of the dynamics of transient species, including plasmas themselves [6]. The technique of probing the structure and dynamics of a laser plasma using the light emitted by another laser plasma is known as the Dual Laser Plasma (DLP) photoabsorption technique [6]. DLP is capable of probing the absorbing plasma in different conditions. Spectra of ionised species are obtained when probing the spectra in different spatial-temporal regimes, thus introducing selectivity of absorbing species. DLP is also a powerful analytical tool, finding application in the study of the processes governing the deposition process in PLD growth technique [7]. In this work, we measured the *in situ* expansion dynamics of ablation plumes of Ga and GaN target using DLP.

3 4 1 Experimental Setup

A DLP photoabsorption experiment involves probing a sample plasma plume under different experimental conditions, with temporal (introduced by the control of the delay between the firing of the lasers) as well as spatial (introduced by the use of X-Y manipulators) resolution. The technique basically involves the recording of two spectra. The first spectrum, denoted I_0 , is the background emission generated by a high Z target plasma such as tungsten. The second spectrum, denoted I_1 , is the

Chapter 3 Description of The Experimental Setups

transmitted spectrum after I_0 has passed through the sample ablation plume (Ga or GaN, see Fig. 3.9). The details of the experimental setup in DCU can be obtained in ref [6]. From Beer-Lambert Absorption Law [8];

$$I_1 = I_0 \exp(-\sigma NL) \quad (3.1)$$

where σN = linear absorption coefficient of plasma

L = absorbing column length

I_1 and I_0 are obtained experimentally. By plotting $\ln(I_1/I_0)$ vs photon energy, it is thus possible to deduce the absorption coefficient of various species (such as Ga^+) in the expanding laser ablation plume.

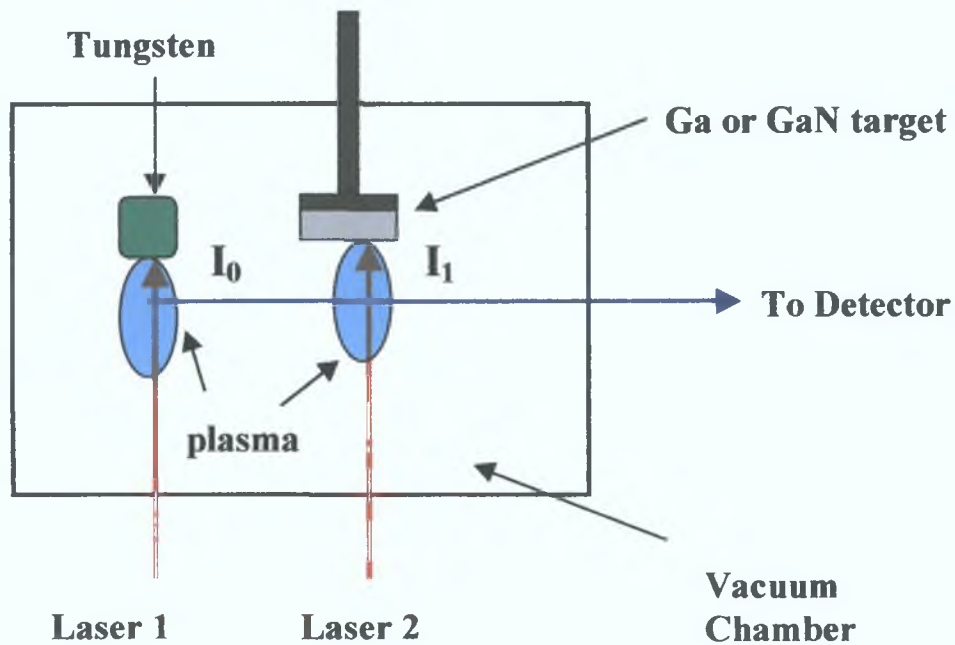


Figure 3.9 Schematic diagram(Top view) of the DLP photoabsorption technique.

Chapter 3 Description of The Experimental Setups

3.4.2 Experimental Description

In our experiments, Ga metal and polycrystalline GaN ablation plasmas were created by the 1064 nm radiation delivered by a 300 mJ, 15 ns Nd YAG laser focussed to a fluence of $(10 \pm 2) \text{ J cm}^{-2}$ on the targets. The background pressure was kept constant at 5×10^{-6} mbar and no gaseous atmosphere was used. The extreme UV probe beam was generated in a second laser produced plasma and had a duration of ~ 10 ns. It could be fired up to 10 μs after the creation of the absorbing plasma, through which it defined a cross-sectional area of $(0.3 \text{ mm} \times 0.5 \text{ mm})$ [9] in the direction perpendicular to the direction of expansion (see Fig 3.10). The target was mounted on a precise X-Y manipulator which allowed different parts of the plasma to be scanned. The photon energy of the probe beam is tuned to the $3d \rightarrow 5p$ transition from the ground state of Ga^+ at ~ 30 eV.

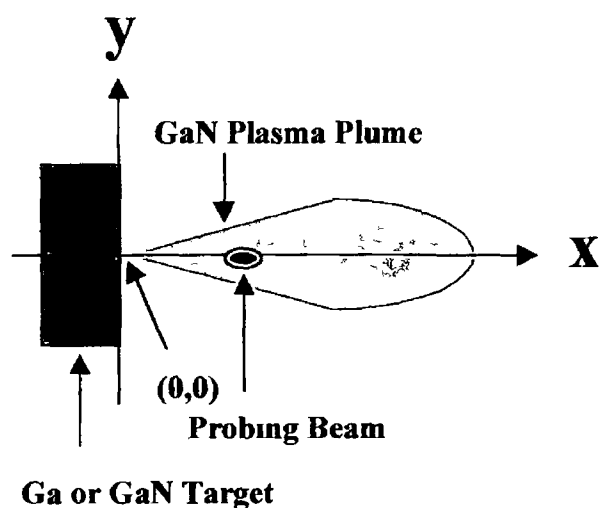


Figure 3.10 Schematic diagram of the GaN plasma plume (side view)

Chapter 3 Description of The Experimental Setups

3 5 References

- 1 R D Vispute, V Talyansky, R P Sharma, S Choopun, M Downes and T Venkatesan *Appl Phys Lett* **71**,102 (1997)
- 2 G S Sudhir, H Fujii, W S Wong, C Kisielowski, N Newman, C Dieker, Z Liliental-Weber, M D Rubin and E R Weber *Appl Surf Sci* **127**, 471 (1998)
- 3 P M Dodd, J G Lunney, J V Armstrong *Optical Engineering* **33**, 3969 (1994)
- 4 S Schmitt-Rink, C Ell and H Haug *Phys Rev* **B33**, 1183 (1992)
- 5 J I Pankove *Optical Processes in Semiconductor* Prentice Hall, NJ 1971
- 6 E T Kennedy et al *Optical engineering* **33**, 3964 (1994)
- 7 W Whitty, J Costello, E T Kennedy, C Moloney and J-P Mosnier, *Appl Surf Sci* **127/129**, 686 (1998)
- 8 J M Bridges, C L Cromer and T J McIlrath *Appl Optics* **25**, 2208 (1986)
- 9 C J Moloney MSc Thesis Dublin City University

Chapter 4 Properties of GaN grown by Solid Target Pulsed Laser Deposition Technique in Nitrogen Atmosphere

CHAPTER 4

Properties of GaN grown by Solid Target Pulsed Laser Deposition Technique in Nitrogen Atmosphere

In this chapter, some properties and characteristics of GaN thin films grown with the solid target pulsed laser deposition (PLD) system are presented, with the emphasis placed on the optical properties obtained using photoluminescence (PL). GaN thin films with $\sim 0.4 \mu\text{m}$ thickness without any intentional buffer layer were successfully grown on a (0001) sapphire in a pure nitrogen atmosphere. In these experiments, a polycrystalline GaN target was used. The target was prepared following the method outlined in Chapter 3. The surface morphology was investigated by atomic force microscopy (AFM) while the crystalline quality was studied using X-ray diffraction (XRD) spectroscopy. The optical properties of the material were studied by photoluminescence down to a temperature of 4.2 K. Activation energies for various transitions lines were derived from the temperature dependent PL measurement. A simple model predicting the origin of the 3.43 eV transition line was suggested. Room temperature Raman scattering measurements were also carried out.

Chapter 4 Properties of GaN grown by Solid Target Pulsed Laser Deposition Technique in Nitrogen Atmosphere

4.1 Surface Morphology

The atomic force microscopy (AFM) results for the edge and centre of our samples are shown in Figs. 4.1 and 4.2 respectively.

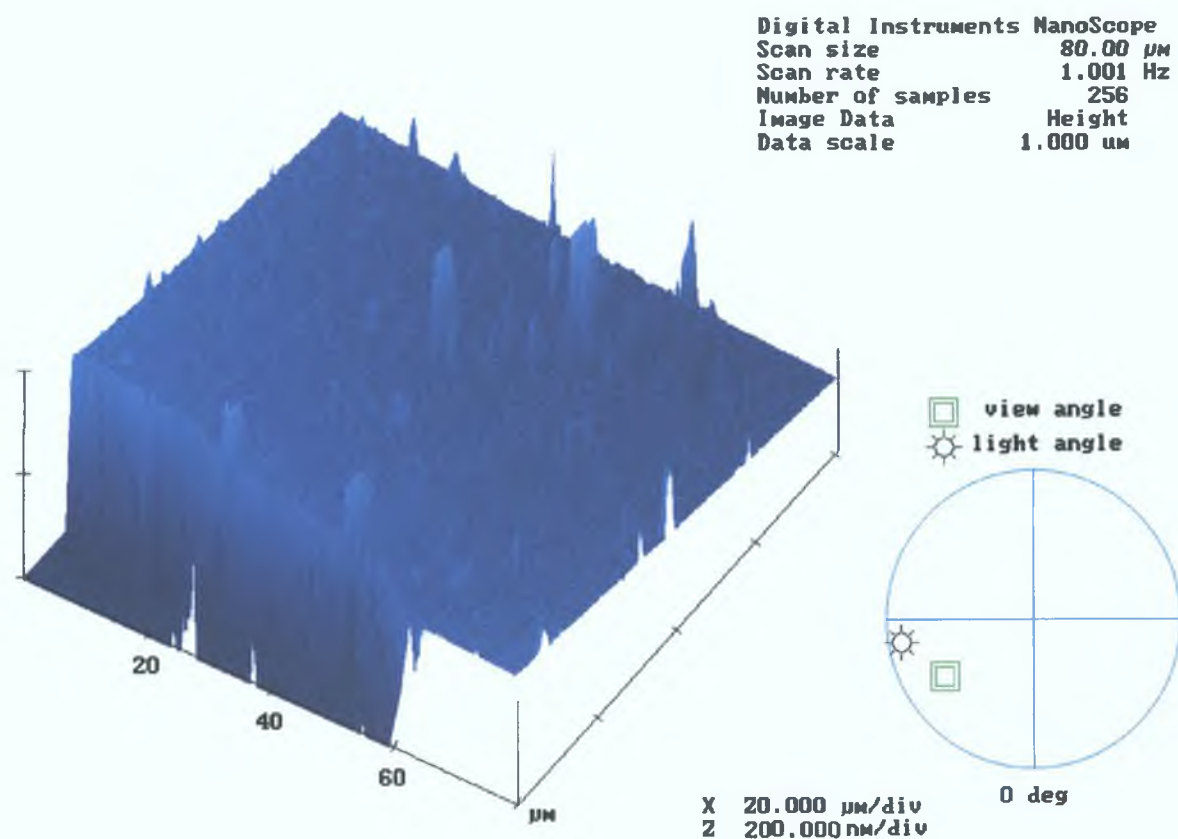


Figure 4.1 3-D AFM image of a GaN thin film taken near the edge of the sample

Fig. 4.1 shows that the thickness of the films is $\sim 0.4 \mu\text{m}$ which indicates a growth rate of $0.1 \mu\text{m}/\text{hr}$ in our experimental conditions (i.e. overall growth time ~ 4 hours). This is an order of magnitude lower than the growth rates achieved by MOCVD [1] and MBE [2-4] techniques (i.e. typical growth rate $\sim 1 \mu\text{m}/\text{hr}$). Since these are carried out in an ammonia environment, one can partly attribute this difference in the growth rate

Chapter 4 Properties of GaN grown by Solid Target Pulsed Laser Deposition Technique in Nitrogen Atmosphere

to the difference in the chemical nature of the nitrogen source. The triple bond of N_2 has dissociation energy of 9.8 eV, which is much higher compared with a value of 3.5 eV for the N-H single bond in ammonia [5-6]. Thus, in PLD a large amount of nitrogen will remain in molecular form at the substrate and will not contribute to the epitaxial growth of GaN. The AFM image taken near the centre of the sample is shown in Fig. 4.2 below.

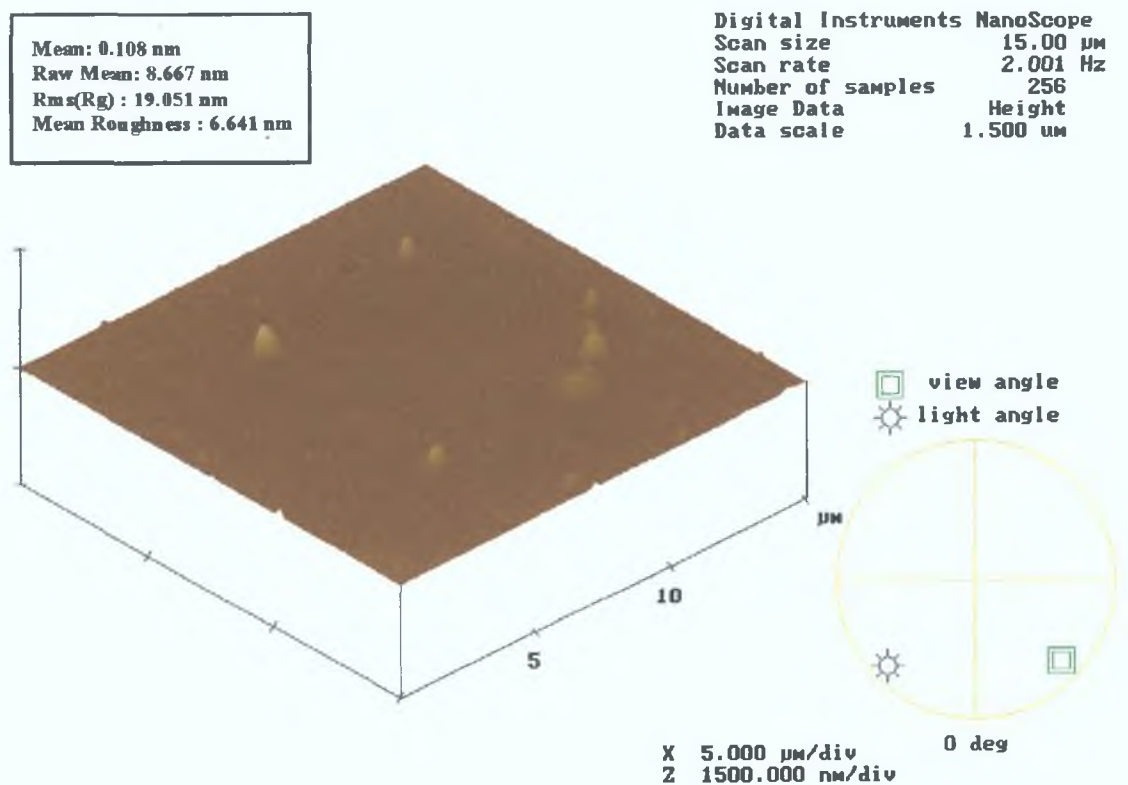


Figure 4.2 3-D AFM image of a GaN thin film taken around the centre of the sample.

Chapter 4 Properties of GaN grown by Solid Target Pulsed Laser Deposition Technique in Nitrogen Atmosphere

The image in Fig 4 2 shows that the sample has a smoother surface morphology near its centre This phenomenon can be attributed to the inhomogeneous nature of a laser ablation plume, which favours droplet formation near the edge of the film [7] The quality of the material in the edge of the PLD grown sample is generally poor due to the relatively non-energetic (smaller kinetic energy) of the species arriving in this region, compared to the species that arrive in the centre of the sample The rms roughness in the centre of our sample is ~ 19.1 nm, which is considerably higher than that of GaN grown by MOCVD [8] or MBE [9] in optimised conditions (i.e. ~ 7 nm) However, the surface morphology of our sample is regarded as comparable to those results as neither a buffer layer or special substrate treatments were used in our growth [10]

4.2 Crystalline Structure

Figure 4 3 shows a typical “ θ - 2θ ” XRD measurement Besides expected sapphire (Al_2O_3) peaks associated with the (0001) orientation at 43.5° and 87.0° , the pattern clearly shows the peaks associated with the (0001) family of planes in hexagonal-GaN which has a strong (0001) texture normal to the substrate [11] (see Table 3 1) The full width at half maximum (FWHM) of the XRD curve for the (0002) peak (labelled as "A") was found to be $\sim 1.4^\circ$ A relatively weak $(10\bar{1}1)$ peak (i.e. $\frac{I(10\bar{1}1)}{I(0002)} \sim 0.2$) was observed at $2\theta \sim 38^\circ$ This peak was not observed in GaN grown by PLD in

Chapter 4 Properties of GaN grown by Solid Target Pulsed Laser Deposition Technique in Nitrogen Atmosphere

ammonia atmosphere [11] The relatively weak shoulder peak (labelled as "B") at lower angle could be due to the presence of a small fraction of cubic GaN($2\theta \sim 34.4^\circ$) embedded in the hexagonal ($2\theta \sim 34.6^\circ$) structure (cubic phase- GaN has a smaller bond length than hexagonal phase- GaN) in our samples [13-14] This will be later confirmed through the temperature dependent PL measurements to be presented in the following sections

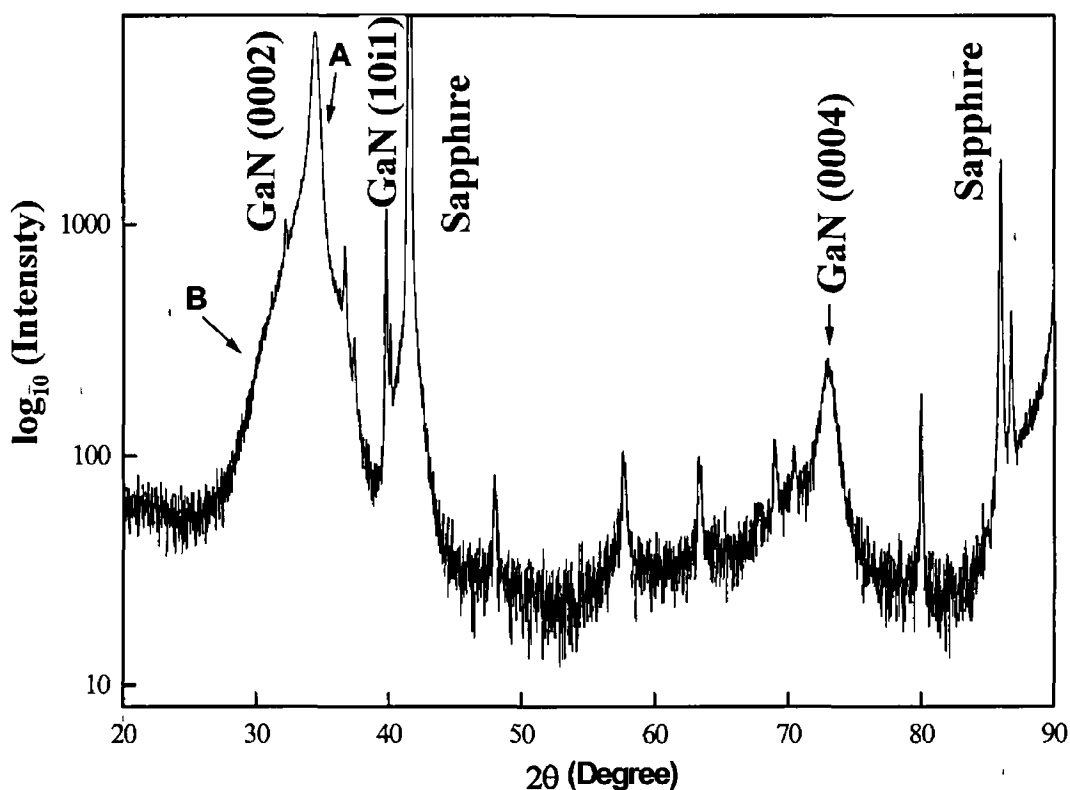


Figure 4 3 2θ X-ray diffraction scans

4.3 Optical Properties

For a detailed evaluation of the film optical properties, temperature dependent photoluminescence (PL) and room temperature Raman scattering measurements were carried out. The results are shown in section 4.3.1 and 4.3.2.

4.3.1 Photoluminescence Study

A typical low temperature (4 K) PL spectrum for GaN as prepared in this study is shown in Figure 4.4. Generally the lineshape of the spectrum appears similar to that of GaN grown by HVPE [15]. The yellow band around 2.2-2.3 eV, which is thought to be related to defects such as Ga vacancy [16-17], is virtually absent in our samples.

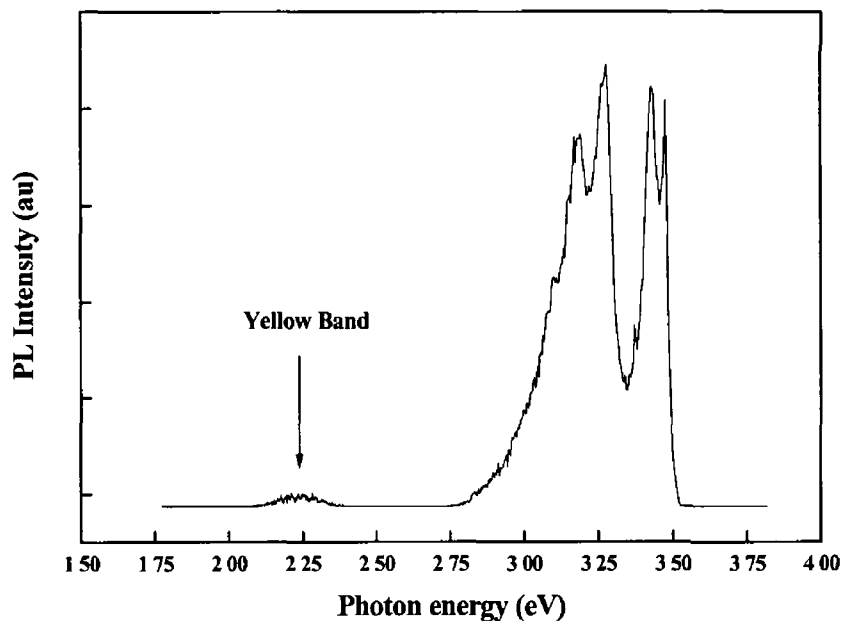


Figure 4.4 4.2 K photoluminescence (PL) spectrum of GaN measured at a laser excitation power of 0.3 W/cm^2 . A very weak yellow band is observed around $\sim 2.2 \text{ eV}$.

Chapter 4 Properties of GaN grown by Solid Target Pulsed Laser Deposition Technique in Nitrogen Atmosphere

Fig. 4.5 shows the expanded view of the PL spectra near the band edge emission. In order to estimate the relative contribution of each transition to the total intensity, all the spectra were fitted by Lorentzian functions with the help of the commercial software package Origin 5.0. The donor-bound exciton (D-X) transition with a FWHM of 16.5 meV (from fitting) is observed at 3.475 eV. This is considered comparable with the values (5-10 meV) obtained for GaN grown by MOCVD or MBE [13, 16]. The neutral donor to acceptor (D-A) transition is observed at 3.278 eV, with a transition corresponding to a phonon replica of 92 meV at 3.186 eV [16]. We also measured a strong band around 3.43 eV (3.4327 eV). It was previously observed only in HVPE grown samples and the corresponding peak energy position varied slightly according to the authors (i.e. peak position: 3.41 eV [5, 21], 3.42 eV [18] and 3.45 eV [15]). The nature of this peak will be discussed by considering the temperature dependent PL measurements in the next paragraph.

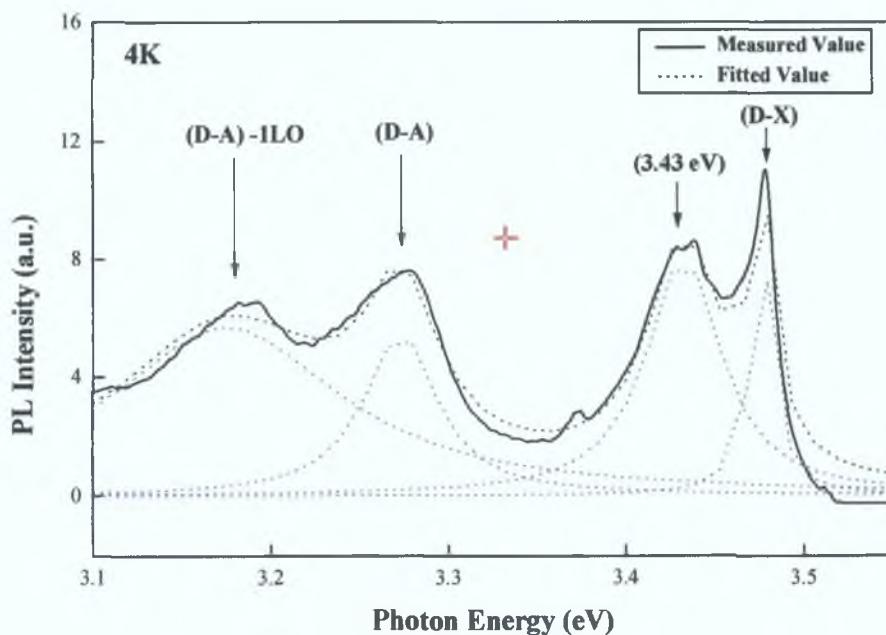


Figure 4.5 Expanded view of the PL spectrum between 3.1 and 3.5 eV

Chapter 4 Properties of GaN grown by Solid Target Pulsed Laser Deposition Technique in Nitrogen Atmosphere

The temperature dependence of our PL spectra is shown in Fig.4.6, The (D-X) line is quenched as the temperature is increased from 4 to 40 K, which is in agreement with the work of other authors [18-19]. This effect is attributed to the thermal dissociation of the bound exciton towards the free exciton. It is of interest to note that the yellow band was almost invisible in our measurement even when the temperature was increased to 150 K. This is considered to be an indication of good film quality [13].

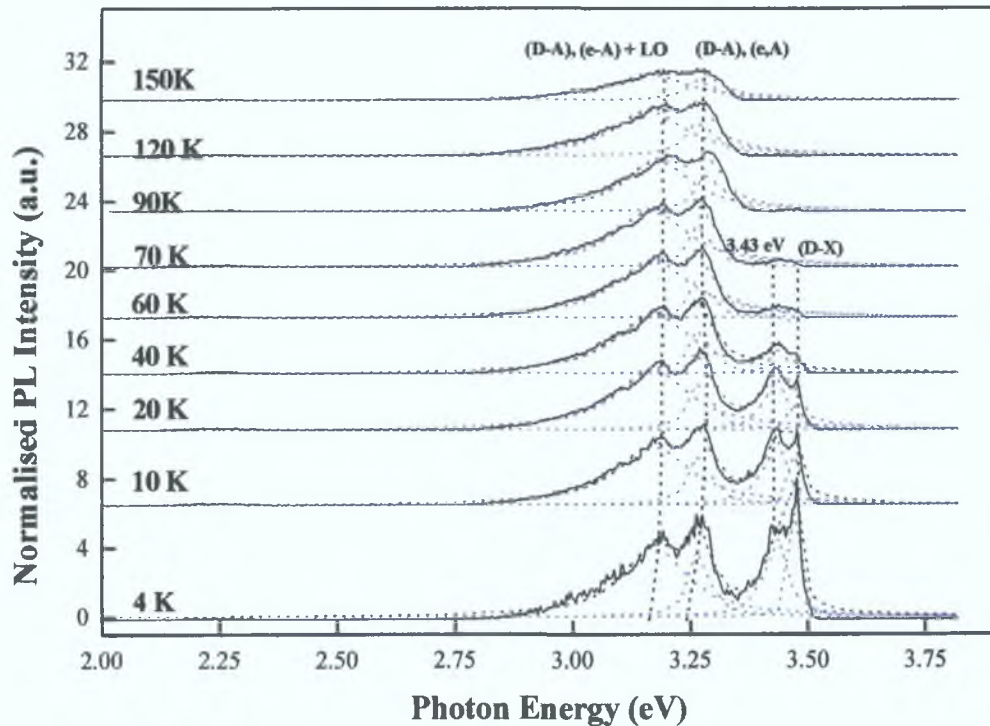


Figure 4. 6 Temperature dependence of PL spectra of GaN

The donor-acceptor (D-A) transitions and the corresponding LO phonon replica located at 3.278 eV and 3.186 eV, shift to higher energy and emerge as the dominant peaks at temperatures above 40 K. This behavior is a common feature for the (D-A) transitions which transform into a band-acceptor (i.e. (e-A)) transition at higher

Chapter 4 Properties of GaN grown by Solid Target Pulsed Laser Deposition Technique in Nitrogen Atmosphere

temperatures due to donor ionisation [16]. The 3.43 eV peak shifts slightly to higher energy by approximately 3 meV as the temperature is increased from 4 K to 20 K. However, a further increase in the temperature (for $T > 20$ K) results in the quenching of this peak. This was also reported by Fischer *et al* [5] for GaN grown by HVPE.

In order to estimate the thermal activation energies of the (D-X), (D-A) and 3.43 eV transitions, their integrated intensities were plotted as a function of $1/T$. The integrated intensities were obtained by numerically integrating the surface area under each of the fitted Lorentzian functions. We observed that the width of the peaks increased with the temperature. For those PL spectra obtained at a temperature less than 40 K, the fitting procedure was performed under the assumption that four different types of peaks (i.e. (D-X), 3.43 eV, (D-A) and 1LA-(D-A)) exist within the spectra. An initial FWHM of 10 meV was used for all four transitions. For the spectra obtained in the temperature range from 70 to 150 K, the fitting was performed under the assumption that only two peaks (i.e. (D-A) and 1LA-(D-A)) substantially contributed to the intensity spectra. This is because the intensities of the (D-X) and 3.43 eV peaks are within the noise level of the spectra (see Fig. 4.6) and the fitted results for these two peaks become unrealistic in this case. The PL spectra taken at 60 K were fitted by assuming that the three transitions (D-A), 1LA-(D-A) and 3.43 eV, respectively, contributed to the overall intensity, the intensity contribution of the (D-X) transition being negligible. The corresponding plots of integrated intensities vs photon energy are presented in Fig. 4.7.

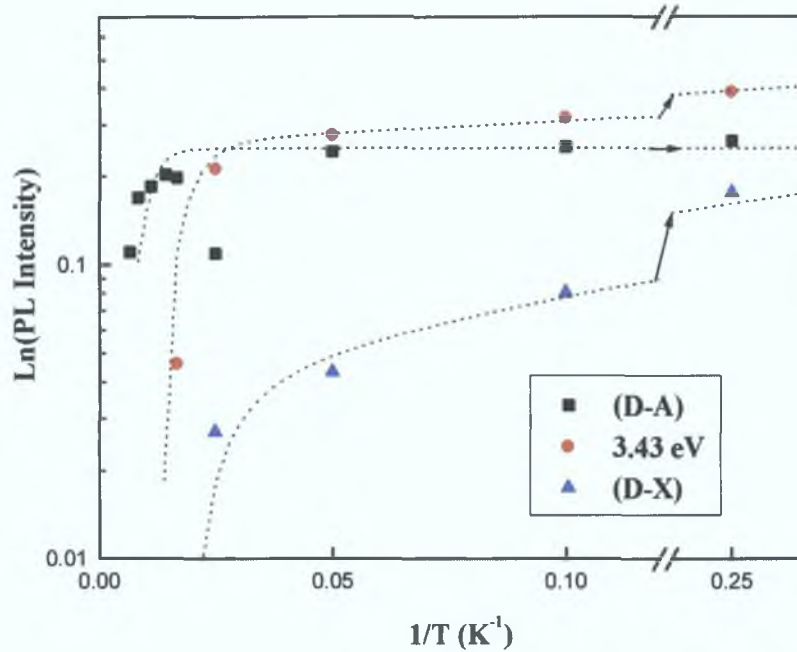


Figure 4.7 Integrated intensities of the (D-X), (D-A) and 3.43 eV transitions as a function of $\frac{1}{T}$. The dotted lines are best fitted curves.

The model presented in Section 3.3 is now used to obtain the required parameters:

$$\frac{I(T)}{I_0} = \frac{1}{1 + C_1 \exp\left(\frac{-\Delta E_a}{kT}\right)} \quad (4.1)$$

$$\frac{I(T)}{I_0} = \frac{1}{1 + C_1 \exp\left(\frac{-\Delta E_a}{kT}\right) + C_2 \exp\left(\frac{-\Delta E_b}{kT}\right)} \quad (4.2)$$

Equation (4.1) should apply when the carriers involved in the recombination are thermally dissociated from the defects with an activation energy E_a . Whereas, Equation (4.2) should hold when the carriers are thermally dissociated from the two defects with activation energies of E_a and E_b , respectively. A non-linear least square

Chapter 4 Properties of GaN grown by Solid Target Pulsed Laser Deposition Technique in Nitrogen Atmosphere

fitting program was used to determine which one of equation (4.1) or (4.2) best fitted the experimental data of Fig. 4.7. The best-fit curves are represented as dotted line on the figure and the activation energies of E_a and E_b derived from the fit are tabulated in Table 4.1 below.

Peaks	E_a (meV)	E_b (meV)
(D-X)	100 ± 3	----
(D-A)	34.5 ± 3	240 ± 20
3.43 eV	180 ± 3	----

Table 4.1 Activation energy of E_a and E_b derived from the best fitted curves

The variations of the intensity of the (D-X) transition as a function of $\frac{1}{T}$ were found to be well presented by Equation (4.1). It quenches with a donor activation energy of (100 ± 3) meV. This value is in good agreement with measurements of the binding energy of the donor bound exciton which range between 5.8 meV and 6.5 meV. Equation (4.2) best represented the behaviour of the (D-A) transition for activation energies in the low and high temperature range of 34.5 meV (E_a) and 240 meV (E_b) respectively. $E_a \sim 34.5$ meV, which dominates at lower temperatures ($T < 80$ K), is reasonably consistent with the shallow Si-like donor (1 e 29 meV) reported by others [19]. The activation energy of $E_b \sim 240$ meV which dominates at higher temperatures

Chapter 4 Properties of GaN grown by Solid Target Pulsed Laser Deposition Technique in Nitrogen Atmosphere

($T > 80\text{K}$) is in good agreement with the residual Mg-like acceptor (i.e. 220-250 meV) reported by several authors [16, 19, 20-21].

For the 3.43 eV peak, a thermal activation energy of ~ 18 meV is obtained in the low temperature range ($T < 40$ K). The origin of the 3.43 eV peak is still debated in the literature and it appears to be a common feature of GaN grown on a GaAs (001) substrate [21] or by the HVPE technique [18, 22]. However, this peak is typically absent from the PL of GaN grown by MBE [23] or MOCVD [17] at the higher end of the growth temperature range. Fischer *et al.* [18] attributed the 3.42 eV peak in their spectra to the exciton bound within structural defects along the c-axis in hexagonal GaN, but the specific nature of the defects was not discussed. A hydrostatic pressure PL experiment reported by Wetzel *et al.* [24] suggested that 3.42 eV band in their spectra may be related to the shallow defects [25] that move with the bandgap. Middleton *et al.* [26] observed a feature at 3.41 eV in the PL measurement of GaN powder. Huang *et al.* [27] observed a PL feature at 3.40 eV which they attributed to oxygen impurities. It is by no means certain, however, that all the peaks around 3.4 eV observed by these authors have the same origin. The substantial spectral line widths in GaN, and the less-readily distinguishable phonon sideband structures make the positive identification of a spectral feature based only on its energy position subject to doubt.

We suggest that the 3.43 eV band may be due to transitions involving carriers bound to extended defects at the interface between cubic and hexagonal phases, with the

Chapter 4 Properties of GaN grown by Solid Target Pulsed Laser Deposition Technique in Nitrogen Atmosphere

electron localized in the cubic phase and the hole in the hexagonal phase. A certain amount of cubic material may be formed in our films since N_2 is less reactive (resulting in a nitrogen deficiency) than ammonia or active nitrogen species, particularly in the low substrate temperature range ($\sim 700^\circ\text{C}$), and such conditions tend to favour the growth of cubic GaN [25]. Indeed, a mixture of cubic and hexagonal phases was directly observed in a TEM study of GaN grown by PLD or MOCVD in N_2 -deficient conditions [28]. Similar results were also reported for GaN grown at low temperature in an MBE system [25, 29]. Our suggestion for the 3.43 eV transition is consistent with the XRD results presented in section 4.2. Hence, we assign 18 meV to the thermal activation energy of carrier bound to the defects at the boundary between the cubic and hexagonal phase. The corresponding band diagram is shown in Fig. 4.8.

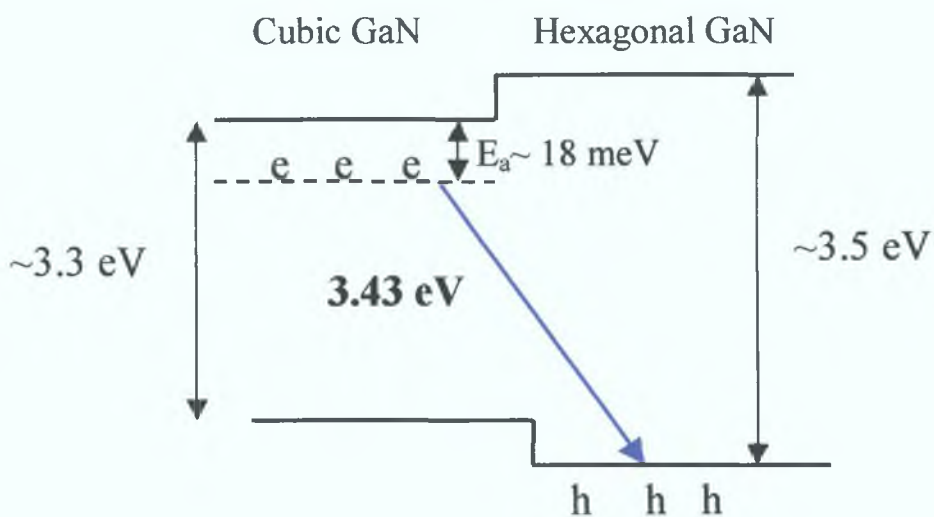


Figure 4.8 Schematic diagram of the band discontinuity at the interface between cubic and hexagonal GaN

Chapter 4 Properties of GaN grown by Solid Target Pulsed Laser Deposition Technique in Nitrogen Atmosphere

This hypothesis may also partially explain the large width of the peaks in the 3.15-3.30 eV energy range in our PL spectra (see Figure 4.5). Several cubic-related GaN peaks (such as FE in the cubic phase [30]) may be superimposed onto the (D-A) bands in this region. In addition, we are able to provide an explanation for the value of several microseconds for the lifetime of the 3.41 eV in ref. [21], as the electron in the cubic phase is spatially separated from the hole in the hexagonal phase before radiative recombination.

4.3.2 Raman Spectroscopy Study

In order to confirm the presence of cubic phase GaN in our samples as indicated by XRD and PL, a further investigation was carried out using room temperature Raman spectroscopy. The measurements were performed on a Micro-Raman spectrometer. A general description of the phonon frequencies in Raman scattering for both cubic and hexagonal GaN are included in Appendix C.

Fig. 4.9 shows the Raman spectra for our GaN thin films. Generally the lineshape of the spectrum appears similar compared to those previously reported [27]. The background scattering due to sapphire substrate is evident due to the transparency of the GaN film. Its contributions therefore was measured separately and shown in the inset in Fig. 4.9. The Raman peaks at 540 cm^{-1} , 560 cm^{-1} and 575 cm^{-1} are identified as the $A_1(\text{TO})$, $E_1(\text{TO})$ and $E_2(\text{high})$ modes of the hexagonal GaN [14, 27-28]. The well resolved peak at $\sim 740\text{ cm}^{-1}$ is due to the $A_1(\text{LO})$ mode in the cubic geometry.

Chapter 4 Properties of GaN grown by Solid Target Pulsed Laser Deposition Technique in Nitrogen Atmosphere

This unambiguously confirms the presence of cubic inclusions within the hexagonal matrix of our samples. The other peaks around 1300-1700 cm^{-1} are due to the scattering from the sapphire substrate as shown from the inset.

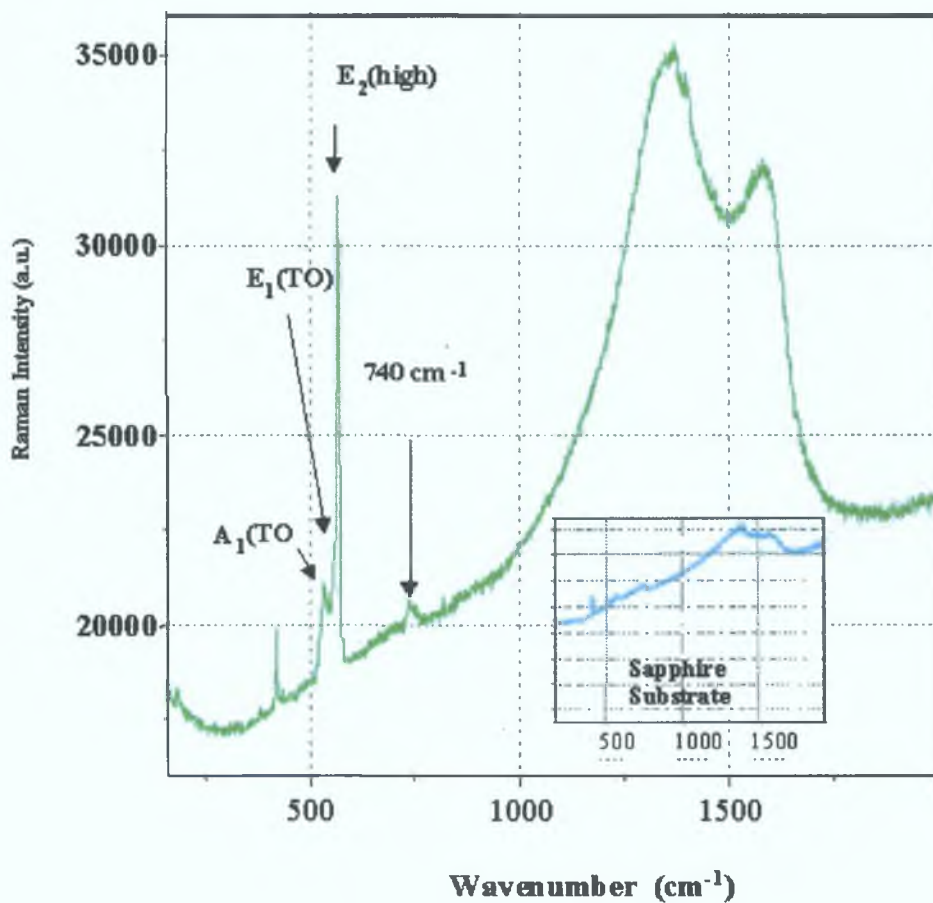


Figure 4.9 Raman spectra for GaN films grown in N_2 atmosphere

Chapter 4 Properties of GaN grown by Solid Target Pulsed Laser Deposition Technique in Nitrogen Atmosphere

4.4 Conclusions

In conclusion, this chapter examined some structural and optical properties of GaN thin films grown by solid target PLD on sapphire substrates at 700 °C in N₂ atmosphere without any intentional buffer layer. GaN films with ~0.4 μm thickness were characterized using "θ-2θ" XRD, temperature dependent PL and Raman spectroscopy. The structural and optical quality of our GaN films were comparable to that of films grown by the MOCVD and MBE techniques. Analysis of the temperature dependence of the PL yielded activation energies of 34.5 meV and 240 meV for the (D-A) transition in low- and high- temperature ranges respectively, in agreement with previous papers. The yellow band which is related to defects, such as Ga vacancy, was almost invisible in our PL spectra even when the temperature was increased to 150 K. An activation energy of 18 meV for the peak at 3.43 eV were obtained in low- and high- temperature ranges respectively, an effect which we attributed to transitions at the interfacial region between hexagonal and cubic phases of the material. We suggested that carriers may be trapped in the interfacial region and are spatially separated from the holes before radiative recombination occurs. The presence of cubic phase material was further confirmed by Raman spectroscopy. Further work would be required to understand the mechanism leading to the formations of cubic GaN in our experimental conditions.

Chapter 4 Properties of GaN grown by Solid Target Pulsed Laser Deposition Technique in Nitrogen Atmosphere

4.5 References

1. S.Nakamura, T.Mukai, M.Senoh, *Appl. Phys. Lett.* **64**, 1687 (1994).
2. V.M.Rao, W.P.Hong, C.Caneau, G.K.Chang, N.Papanicolaou and H.B.Dietrich, *J.Appl. Phys.* **70**, 3943 (1991).
3. R.F.Service, *Science*, **276**, 895 (1997).
4. R.Held, B.E.Ishaug, A.Parkhomovsky, A.M.Dabiran and P.I.Cohen, *J. Appl. Phys.* **87**, 1219 (2000)
5. S.Fischer et al. *J. Crystal Growth.* **189/190**, 556 (1998)
6. D.Cole. Thesis. Trinity College. 1998.
7. M.M.Martynyuk, *Russ. J. Phys. Chem*, **57**, 494 (1983).
8. A.Strittmatter, A.Krost, M.Straburg, V.Turck and D.Bimberg. *Appl. Phys. Lett.* **74**, 1242 (1999).
9. N.Grandjean, J.Massies and M.Leroux, *Appl. Phys. Lett.* **69**, 2071 (1996).
10. D.Wang, Y.Hiroyama, M.Tamura and M.Ichikawa, *Appl. Phys. Lett.* **76**, 1683 (2000).
11. R.D.Vispute, V.Talyansky, R.P.Sharma, S.Choopun, M.Downes and T.Venkatesan, *Appl. Phys. Lett.* **71**, 102 (1997).
12. M.H.Kim, C.Sone, J.H.Yi and E.Yoon. *Appl. Phys. Lett.* **71**, 1228 (1997).
13. T.Kurobe, Y.Sekiguchi, J.Suda, M.Yoshimoto and H.Matsunami. *Appl. Phys. Lett.* **73**, 2305 (1998).
14. L.D.Wang and H.S.Kwok. *Appl. Surf. Sci.* **154**, 439 (2000).
15. B.J.Skromme and J.Jayapalan, *Appl. Phys. Lett.* **74**, 2358 (1999).

Chapter 4 Properties of GaN grown by Solid Target Pulsed Laser Deposition Technique in Nitrogen Atmosphere

- 16 M Leroux, N Grandjean, B Beaumont, G Nataf, F Semond, J Massies and P Gibart *J Appl Phys* **86**, 3721 (1999)
- 17 G Li, S J Chua, S J Xu and W Wang *Appl Phys Lett* **74**, 2821 (1999)
- 18 S Fischer, B K Meyer and E E Haller *Appl Phys Lett* **69** 2716 (1996)
- 19 B Meyer, *Mater Res Soc Symp Proc* **449**, 497 (1997)
- 20 D J As, F Schmilgus, C Wang, B Schmilgus, C Wang, B Schottker, D Schikora and K Lischka *Appl Phys Lett* **70**, 1311 (1997)
- 21 B G Gen, J W Orton, T S Cheng, D J Dewsnip, D E Lackhson, C T Foxon, C H Malloy, X Chen, *MRS Int J Nitride Semicond Res, Art* **22** (1996)
- 22 B Monemar, *J Crys Growth* **189/190**, 1 (1998)
- 23 H Tang and J B Webb *Appl Phys Lett* **74**, 2373 (1999)
- 24 C Wetzel, S Fischer, W Walukiewicz, J Ager, E E Haller, I Grzegory, S Porowski, T Suski, GaN and related material, *Proc 1st Int Symp MRS* **395**, 417 (1996)
- 25 J I Pankove, *GaN(1) Semiconductor and Semimetal, Vol 1* (1998)
- 26 P G Middleton, K P O'Donnell, C T Cowan, D Cole, M Cazzanelli, J Lunney *Mat Sci Eng* **B59**, 133 (1999)
- 27 T F Huang, A Marshall, S Sptuytte, J S Harris Jr, *J Cryst Growth* **200**, 362 (1999)
- 28 S Oktyabrsky *Appl Phys Lett* **74**, 2465 (1997)
- 29 H Okumura, K Balakrishnan, H Hamaguchi, T Koizumi, S Chichibu, H Nakanishi, T Nagatomo, S Yoshida *J Crys Growth* **189/190**, 364 (1998)
- 30 B Daudin, G Feuillet, J Hubner, Y Samson and F Widmann, *J Appl Phys* **84**, 2295 (1998)

CHAPTER 5

Properties of GaN grown by the Liquid Target Pulsed Laser Deposition Technique in Nitrogen Atmosphere

In this chapter, the properties of GaN thin films grown by liquid target pulsed laser deposition (PLD) are presented. Epitaxial GaN films were successfully grown on sapphire (0001) or GaAs (001) substrates in a 5 Torr nitrogen (N_2) atmosphere. The thickness of all these samples was $\sim 1 \mu m$ as verified by a profilometer. The crystalline quality was studied using X-ray diffraction (XRD) operated in the θ - 2θ geometry. The optical properties of the material were studied by low temperature photoluminescence (PL) down to 4 K. Detailed XRD and PL studies as a function of substrate temperature and laser repetition rate were carried out for the samples grown on sapphire (0001) substrates. For both substrates, the optimum temperature for deposition was found to be $\sim 800^\circ C$. In these conditions, the 3.368 eV (I_3) and 3.310 eV (I_4) emission lines dominate the low temperature PL. We propose a model to explain the origin of both emission lines in which the electrons and holes are confined in cubic inclusions in a hexagonal matrix analogous to a type I quantum well.

Chapter 5 Properties of GaN grown by the Liquid Target Pulsed Laser Deposition Technique in Nitrogen Atmosphere

5.1 Growth Rate

Figure 5 1 shows the growth rate of our GaN thin films as a function of substrate temperature(T_s)

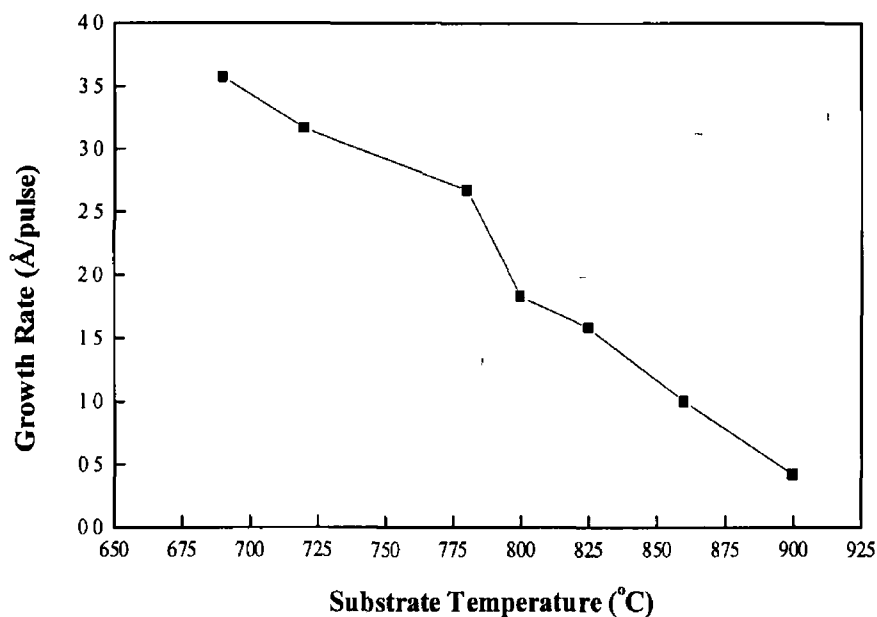


Figure 5 1 Average growth rate per pulse as a function of substrate temperature

During the growth process, if there is an excess of Ga, it could be either desorbed from the growth surface or being trapped in the growing film depending on the pressure of the background gas (i.e. nitrogen) [1]. The desorption of Ga should be reflected in a decrease of the growth rate while the formation of GaN should increase the growth rate at higher T_s . From Fig 5 1, it is clearly seen that the average GaN growth rate per pulse decreased from 3.6 to 0.4 Å/pulse as T_s increased from 690 to

Chapter 5 Properties of GaN grown by the Liquid Target Pulsed Laser Deposition Technique in Nitrogen Atmosphere

900 °C This observation indicates a continuous increase in Ga desorption as T_s increased [1]

The average growth rate per pulse as a function of laser repetition rate at $T_s = 800$ °C is shown in Figure 5.2. It is clearly seen that the growth rate can be controlled by adjusting the laser repetition rate. However, as will be shown in section 5.2 and 5.3, the structural and optical qualities of the samples grown at low repetition rate tended to be poor.

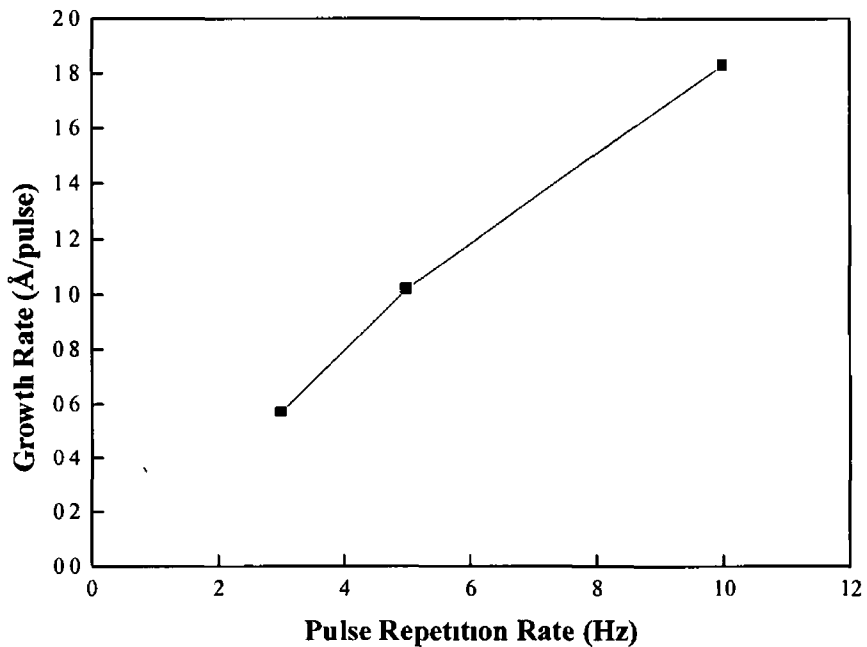


Figure 5.2 Average growth rate per pulse as a function of pulse laser repetition rate (for $T_s = 800$ °C)

5.2 Crystalline Structure

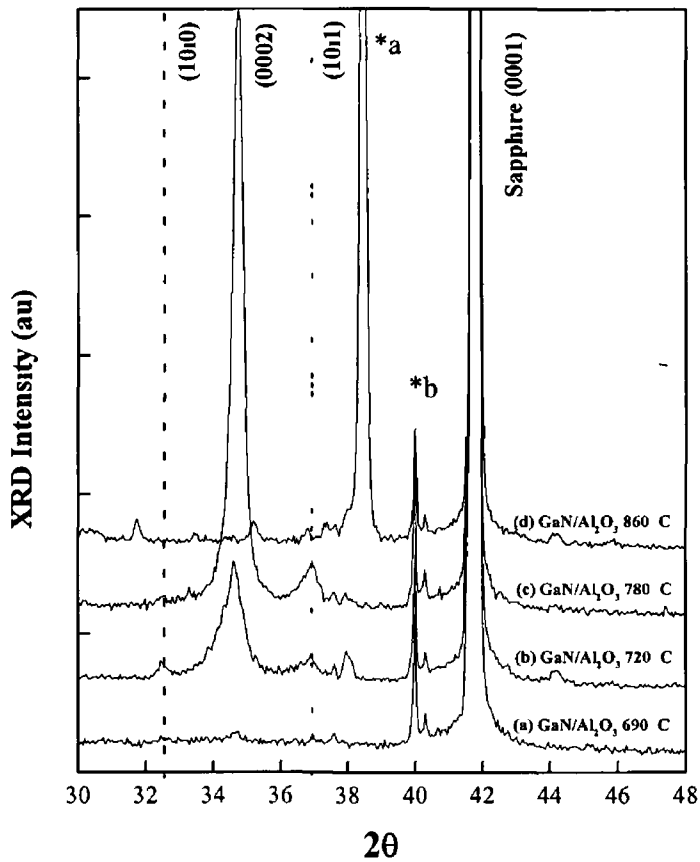


Figure 5 3 XRD scan of GaN samples grown on sapphire (0001) at various temperatures

Figure 5 3 shows the " θ - 2θ " XRD scans for GaN samples grown on sapphire (0001) substrate at various temperatures. The peak labelled *a and *b are due to contamination by x-ray lines from the silver paint on the back of the substrate and the tungsten anode of the XRD system, respectively. No epitaxial growth could be detected for $T_s \sim 690^\circ\text{C}$ (Fig 5 3(a)) or lower, where large amounts of Ga droplets and clusters were visually observed on the films. The absence of the epitaxial XRD

Chapter 5 Properties of GaN grown by the Liquid Target Pulsed Laser Deposition Technique in Nitrogen Atmosphere

peaks at such low temperatures could be related to defects within the films due to an insufficient thermal energy for surface migration of Ga species. A polycrystalline structure including the (0002), (10 $\bar{1}$ 0) and (10 $\bar{1}$ 1) orientations is observed for samples grown at $T_s \sim 720^\circ\text{C}$ (Fig. 5.3(b)) in accord with the work of Xiao *et al* [3]. Fig. 5.3(c) shows the XRD diffraction pattern of a sample grown at $T_s \sim 780^\circ\text{C}$. This sample shows a high degree of crystalline texture along the normal to the substrate. The measured FWHM of 0.33° for the (0002) peak is comparable to those reported elsewhere [2-3]. At $T_s \sim 860^\circ\text{C}$ (Fig. 5.3(d)), no GaN could be detected which may be due to the loss of stoichiometry caused by Ga desorption (i.e. gallium deficiency) as discussed in section 5.1.

Figure 5.4 compares the XRD scans of various samples grown at a substrate temperature of 800°C and a nitrogen pressure of 5 Torr. Fig. 5.4(a) and 5.4(b) compare the XRD diffraction pattern of films grown on sapphire (0001) substrates at laser repetition rates of 10 Hz (a) and 3 Hz (b) respectively. Fig. 5.4(c) shows the XRD diffraction pattern for a film grown on GaAs (001) at a laser repetition rate of 10 Hz. It is interesting to note that no epitaxial growth could be observed for samples grown at 3 Hz (Fig. 5.4(b)) whereas a strong (0002) signal was observed for samples grown at 10 Hz (Fig. 5.4(a)). This could be due to an insufficient level of active nitrogen species created within the ablation plume in sample 5.4(b) due to the low repetition rate, which could affect the stoichiometry during growth. Fig. 5.4(c) shows the diffraction pattern of GaN grown on GaAs (001) at $T_s \sim 800^\circ\text{C}$ [4]. The pattern

Chapter 5 Properties of GaN grown by the Liquid Target Pulsed Laser Deposition Technique in Nitrogen Atmosphere

exhibits both the (0002) and (10 $\bar{1}$ 0) orientations. The slight asymmetry of the (0002) peak on the low 2θ side may be due to the inclusion of cubic phase in the hexagonal structure as suggested in ref [5]

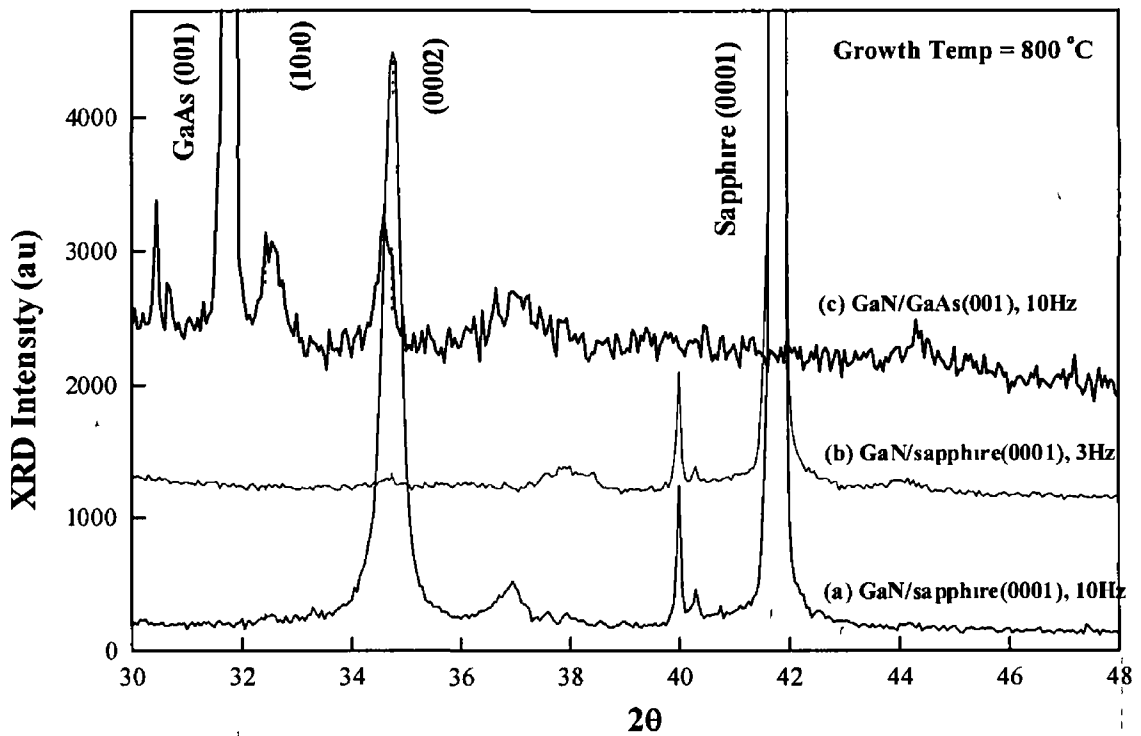


Figure 5 4 XRD scans of GaN thin films in the conditions as indicated on the figure

5.3 Photoluminescence Study

The 10 K PL spectra of GaN thin films samples grown on sapphire (0001) at various substrate temperature (T_s) are presented in Figure 5.5. We observed no photoluminescence for films grown at $T_s \sim 690^\circ\text{C}$ or lower which is consistent with the XRD results of Fig. 5.3. The samples grown at $\sim 800^\circ\text{C}$ exhibit intense near band edge lines between 3.3 eV and 3.5 eV and the yellow band around ~ 2.2 eV. The intensity of the peak of yellow band is about one order of magnitude lower than the band edge emission lines. This suggests that the optical quality of our samples is comparable to those grown by the MOCVD [5] or MBE [6] techniques.

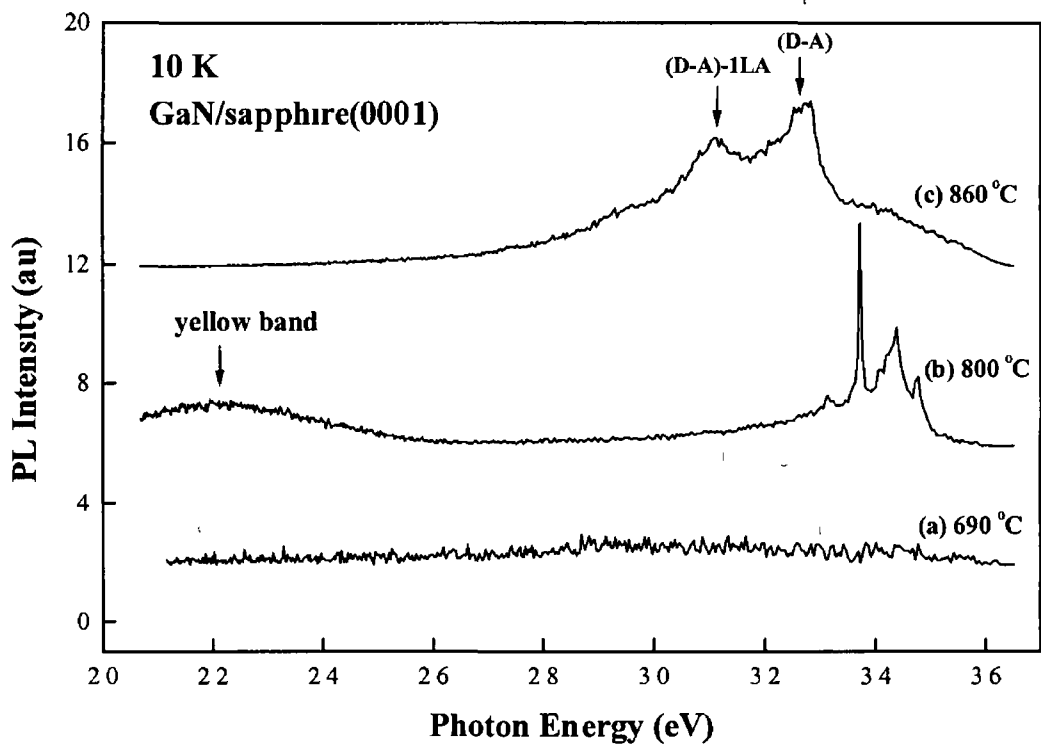


Figure 5.5 10 K photoluminescence spectra of GaN/sapphire(0001) samples grown at various substrate temperatures

Chapter 5 Properties of GaN grown by the Liquid Target Pulsed Laser Deposition Technique in Nitrogen Atmosphere

A further increase in T_s , up to 860 °C resulted in the PL spectra of Fig 5 5(c) Its only features are donor-acceptor (D-A) transitions at 3 273 eV and the corresponding phonon replica (~ 92 meV) at 3 181 eV [7] The absence of band edge emissions indicates an inferior quality of GaN grown in these conditions The shape of this spectrum is in fact almost identical to that of the precursor powder as shown in ref [8], indicating a lack of epitaxial growth, which is again in accord with the XRD measurements in Fig 5 3

Figure 5 6 compares the 5K PL spectrum for three samples grown at $T_s = 800$ °C and nitrogen pressure of 5 Torr Fig 5 6(a) and 5 6(b) show the spectra of films grown on sapphire (0001) at a laser repetition rate of 3 Hz (a) and 10 Hz (b) respectively Fig 5 6(c) shows the PL spectrum of a GaN film grown on a GaAs (001) substrate at 10 Hz It is interesting to observe that the PL of the film grown at 3 Hz is dominated by the yellow band only and the band edge transition is virtually absent, whereas strong band edge emissions are observed for the sample grown at 10 Hz (Fig 5 6(b)) The relatively weak PL intensity in sample (a) coupled with the absence of the band-edge emission, further confirms poor optical quality for GaN grown at the lower repetition rate This result is in agreement with the XRD results shown in Fig 5 4 For the sample grown at 10 Hz (Fig 5 6(b)), the donor-bound exciton (D-X) also known as I_2) with a FWHM of 8 meV was observed ~ 3.45 eV These values are very close to those obtained in GaN grown by MOCVD or MBE [5,7] This result also indicates an improvement in the optical quality when compared to our GaN films grown with a solid target (FWHM ~ 15 meV) as discussed in Chapter 4

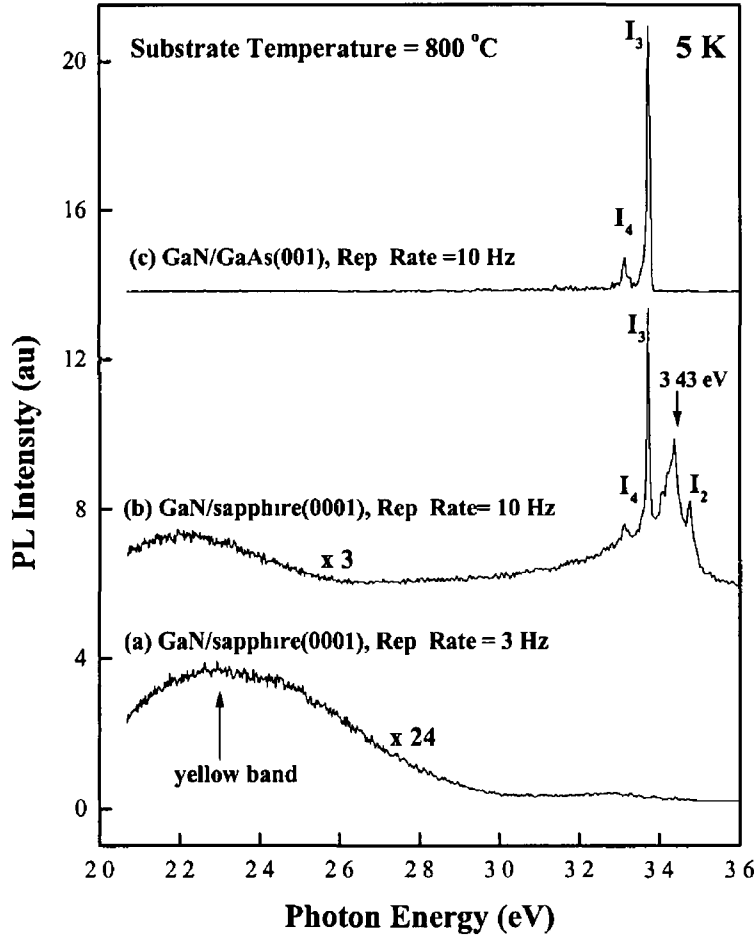


Figure 5.6 5 K PL spectrum for GaN thin films grown at $T_s \sim 800$ °C and 5 Torr in the conditions indicated in figure

The 3.43 eV transition, which we have interpreted as originating in a mixed cubic/hexagonal structure in section 4.3.1, was also observed in sample (b) in Fig. 5.6. Since it does not appear in the spectrum of the other samples grown in the same conditions (Fig. 5.6(a) & Fig. 5.6(c)), this further invalidates its interpretation as a residual impurity such as oxygen as was suggested in ref [9]. Fig. 5.6(c) shows the PL spectra of our GaN grown on a GaAs (001) substrate at a laser repetition rate of 10

Chapter 5 Properties of GaN grown by the Liquid Target Pulsed Laser Deposition Technique in Nitrogen Atmosphere

Hz It is interesting to note that no hint of yellow band ~ 2.2 eV was detected in this sample. We point out that the PL spectrum of Fig. 5.6(c) is very similar to the PL spectrum of the GaN thin films grown on a GaAs (001) substrate by the MOCVD technique [10].

Fig. 5.7 compares the 10 K PL spectrum measured at different positions on our GaN samples grown on GaAs (001). The spectrum in Fig. 5.7 (a) is taken at the centre of the sample while spectrum in Fig. 5.7 (b) is taken at the edge of the sample. It is interesting to note that the intensity of the PL spectrum varies when the measurements are taken at different positions on the sample (i.e. the optical quality is better in the centre). This is similar to the observation of Chapter 4 (section 4.1). It was previously reported that GaN grown on GaAs (001) should consist of a mixture of cubic and hexagonal phases [11-13]. However, we observe that the band edge transitions expected around 3.26 eV (cubic) and 3.47 eV (hexagonal) are absent in our spectra (Fig. 5.6 (c) & Fig. 5.7). We shall provide an explanation for this point later in this chapter.

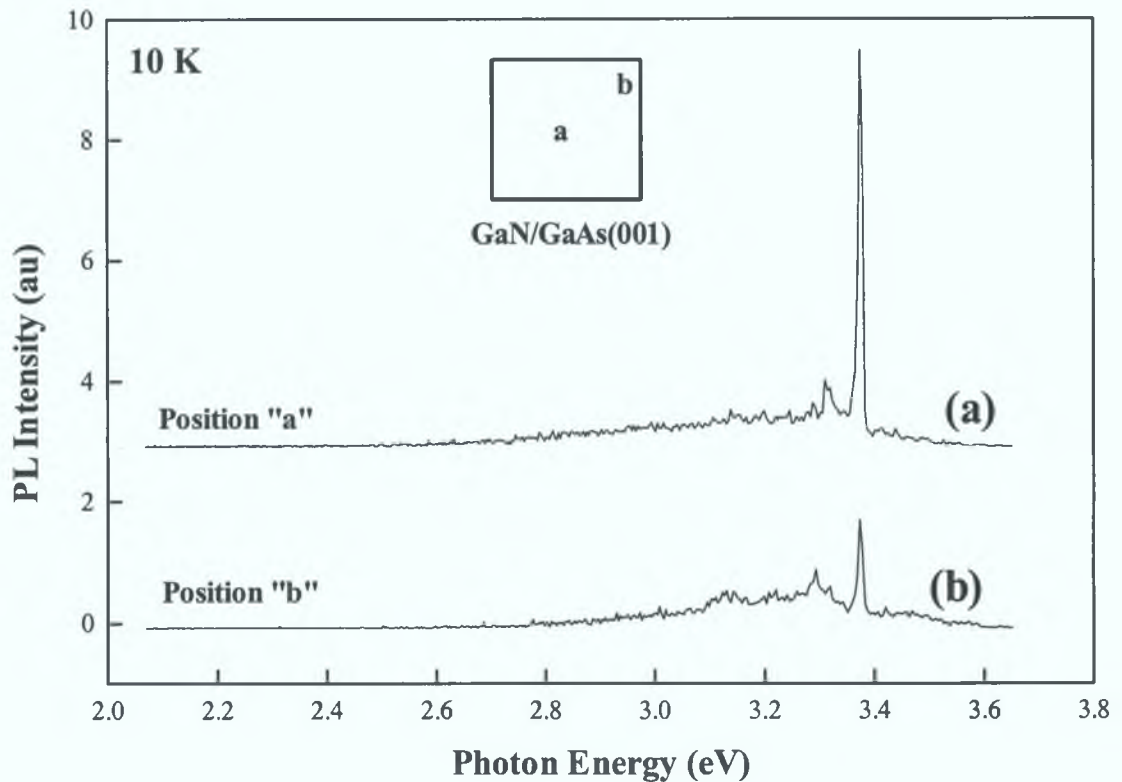


Figure 5.7 10K PL spectrum of GaN grown on GaAs (001) at different substrate positions.

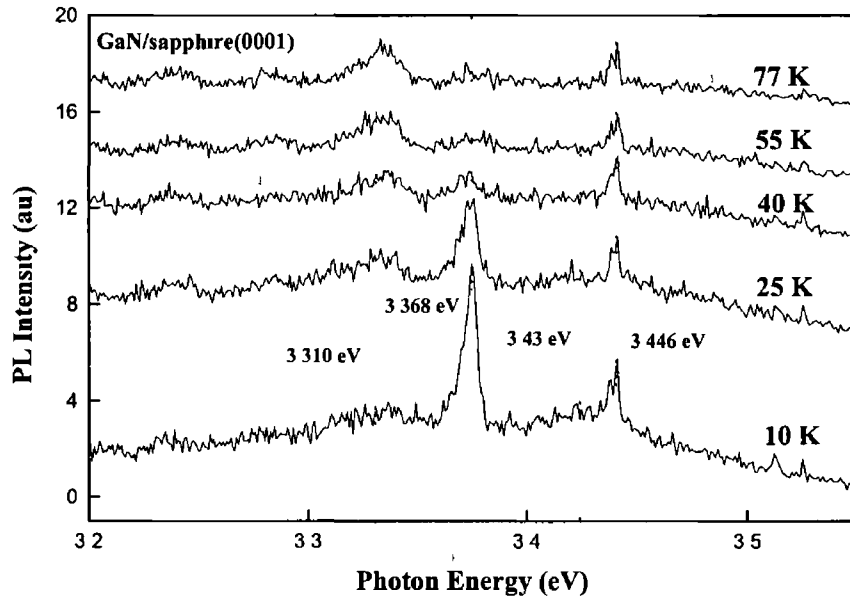
As mentioned in section 3.3, the thermal activation energy of PL transitions can be represented by the following expression:

$$I(T) = \frac{I_o}{1 + C_o \times \exp(-E_a/kT)} \quad (5.1)$$

Figure 5.8 shows on an expanded scale the temperature dependence of the PL spectra of our GaN samples grown on sapphire (0001) and GaAs (001) at $T_s = 800^\circ\text{C}$. The integrated intensities for 3.446 eV, 3.43 eV, 3.368 eV and 3.310 eV are fitted using equation (5.1) and the results are tabulated in table 6.1.

Chapter 5 Properties of GaN grown by the Liquid Target Pulsed Laser Deposition Technique in Nitrogen Atmosphere

(a)



(b)

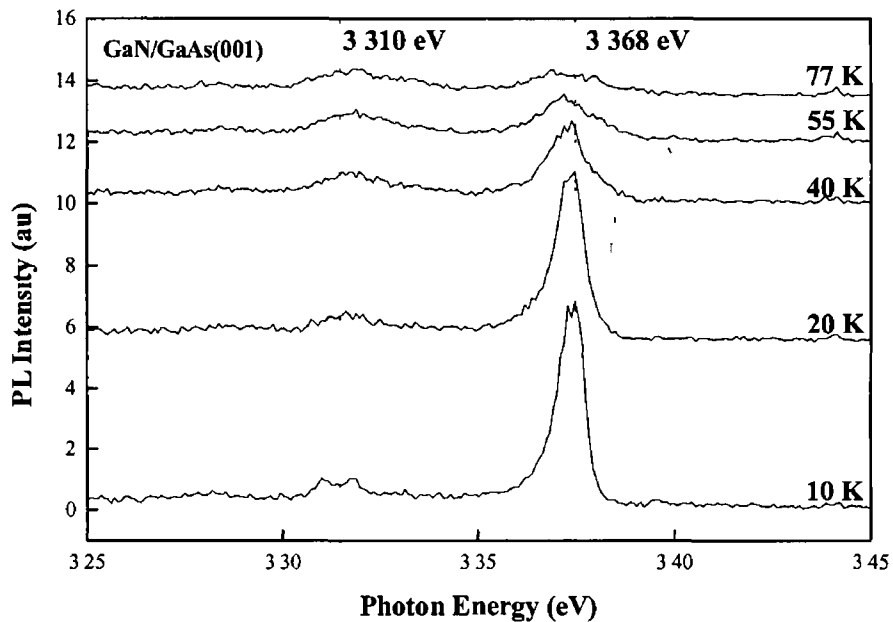


Figure 5 8 Expanded view of the temperature dependence PL spectra for GaN grown on (a) sapphire (0001) (b) GaAs substrate at $T_s = 800\text{ }^\circ\text{C}$

Chapter 5 Properties of GaN grown by the Liquid Target Pulsed Laser Deposition Technique in Nitrogen Atmosphere

PL Transition line	3 446 eV (sapphire)	3 43 eV (sapphire)	3 368 eV (sapphire)	3 310 eV (sapphire)	3 368 eV (GaAs)	3 310 eV (GaAs)
Activation Energy (E_a)	8 meV	15 meV	28±5 meV	5±1 meV	30±5 meV	3±1 meV

Table 5 1 The thermal activation energies (E_a) for various transitions in GaN grown on sapphire (0001) and GaAs (001) substrates

Table 5 1 shows that the 3 446 eV (donor exciton transitions) peak quenches with a donor activation energy of 8 meV, which is in reasonable agreement with the values of the binding energy of donor bound excitons in hexagonal GaN which range from 5 8 meV to 6 5 meV [14] The activation energy for the 3 43 eV line is found to be 15 meV, which is in agreement with the value of $E_a \sim 18$ meV obtained from our sample grown with the solid target PLD technique (see section 4 3 1)

As shown in Table 5 1, the 3 368 eV peak in GaN/GaAs(001) quenches with an activation energy of 30±5 meV, which agrees with the value ~ 27 meV reported by Wetzel *et al* [15] The activation energy of the 3 310 eV line in GaN/GaAs(001) is found to be 3±1 meV This suggests that the 3 310 eV line is almost insensitive to thermalisation effects, which indicates that the 3 310 eV transition involves a free electron The physical origins for the 3 368 eV and 3 310 eV transitions are still debated in the literature They were previously labelled I_3 and I_4 respectively by Wetzel *et al* [15] Similar lines were also reported in samples grown by other techniques such as MOCVD and ECR-MBE or using different types of substrates such as Si or fused silica [10, 15-18] Hong *et al* [10] attributed them to the near band-

Chapter 5 Properties of GaN grown by the Liquid Target Pulsed Laser Deposition Technique in Nitrogen Atmosphere

edge emission in cubic GaN. However, this explanation is inconsistent with recent measurements which place the band-edge emission in the cubic phase at 3.274 eV [11, 13]. Subsequently, other authors [15, 19] have interpreted I_3 and I_4 in terms of excitons localized at extended defects. However, this model could not explain the strong intensities of I_3 and I_4 in our spectra as defect-related luminescence normally involves non-radiative recombination. Moreover, the relatively small FWHM of I_3 (~6 meV) appears to be much smaller than the typical width of defect-related transitions [16]. This is because defect-related PL transitions always exhibit broad peaks (such as the yellow band in GaN) [20].

In view of our experimental results, we propose the following alternative interpretation. The cubic phase, likely to be formed by stacking faults at the layer-substrate interface [9, 21], is responsible for the transitions I_3 and I_4 . We suggest that I_3 and I_4 may arise from the quantum confinement of cubic material in the hexagonal matrix. The cubic phase inclusion (bandgap ~ 3.3 eV) in the hexagonal matrix (bandgap ~3.5 eV) act as sinks for the electrons, analogously to a type I "quasi" quantum well structure. The band diagram which pictures the I_3 and I_4 transitions in our model is shown in Fig. 5.9, where E_C and E_V refers to the conduction band and valence band, respectively. We labelled the quantum confinement energy for $n=1$ in E_C and E_V as $\Delta E_C^{n=1}$ and $\Delta E_V^{n=1}$, respectively. The shallow donor energy level, shallow acceptor energy level, quantum confinement exciton energy, quantum well width and height are labelled E_D , E_A , E_x , L and V_0 , respectively. The potential well V_0 spatially confines the electrons and holes, producing an effective 2-D recombination

Chapter 5 Properties of GaN grown by the Liquid Target Pulsed Laser Deposition Technique in Nitrogen Atmosphere

centre which will result in intense PL transitions. This model also explains the absence of cubic- and hexagonal- near band edge emissions in the sample grown on GaAs (001) (Fig. 5.6(c)) as most of the free electrons are confined. Hence, we propose I_3 as the transition involving an electron in ground level ($n=1$) to a hole in the cubic phase.

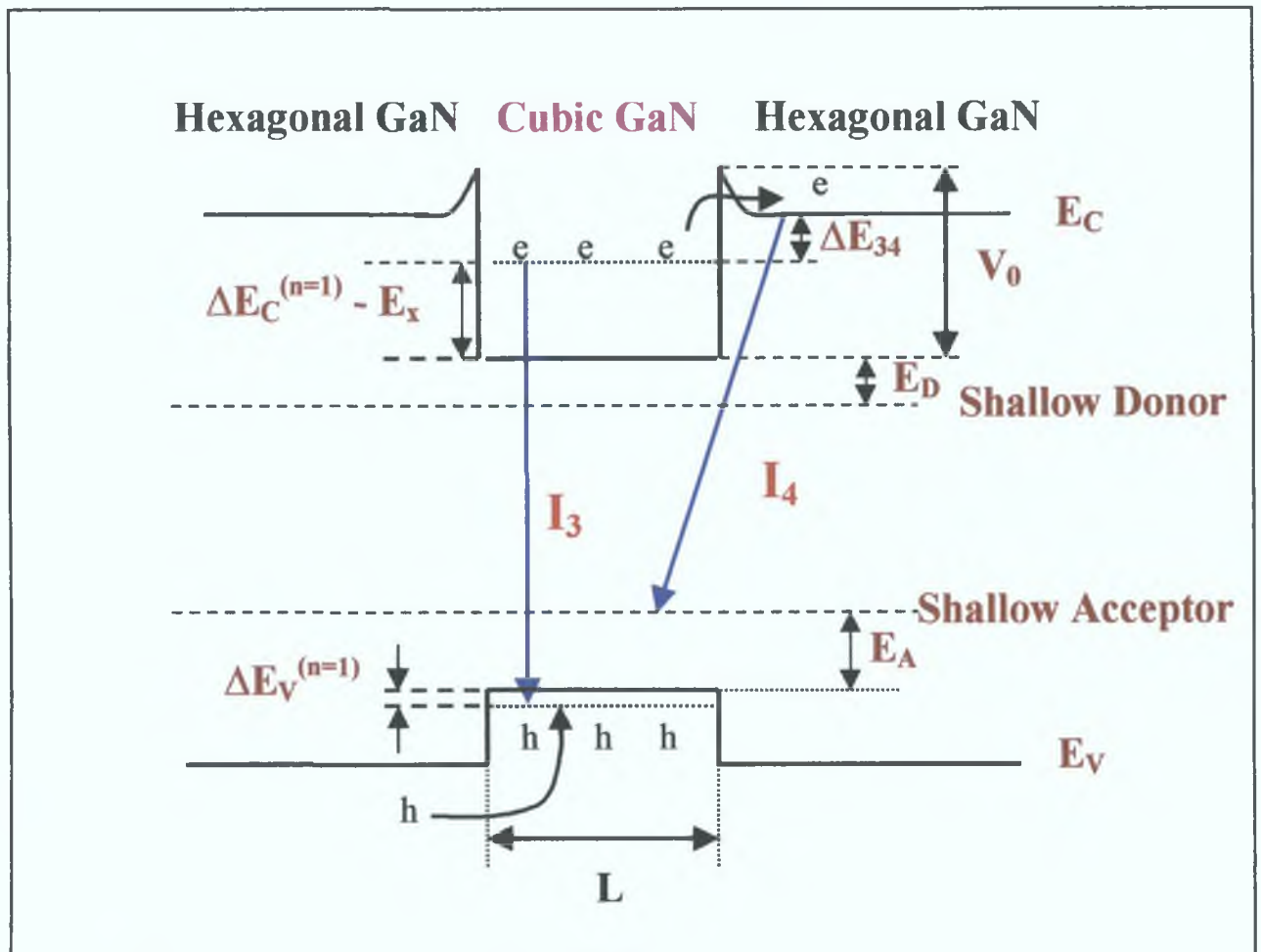


Figure 5.9 Band diagram summarising the PL transitions for both I_3 and I_4 .

Chapter 5 Properties of GaN grown by the Liquid Target Pulsed Laser Deposition Technique in Nitrogen Atmosphere

We use the following method to estimate the size of the cubic inclusions. The bandgap for cubic GaN (E_g^{cubic}) can be calculated as [13]

$$\begin{aligned}
 E_g^{\text{cubic}} &= \text{Donor bound exciton (D-X) transitions} + \text{Free exciton binding energy} \\
 &= 3.274 \text{ eV} + 26 \text{ meV} \\
 &= 3.30 \text{ eV}
 \end{aligned}
 \tag{5.2}$$

From Fig. 5.9, the confinement energies for $\Delta E_c^{n=1}$ and $\Delta E_v^{n=1}$ can be calculated by taking $E_x \sim 40 \text{ meV}$ [22]

$$\begin{aligned}
 \Delta E_c^{n=1} + \Delta E_v^{n=1} &= I_3 - E_g^{\text{cubic}} + E_x \\
 &= 3.368 \text{ eV} - 3.30 \text{ eV} + 40 \text{ meV} \\
 &= 108 \text{ meV}
 \end{aligned}
 \tag{5.3}$$

Taking the electron and hole effective mass in cubic GaN as $0.17 m_0$ and $0.82 m_0$ respectively [23], and using the quantum well model for the infinite potential well (Appendix A), the ratio of $\Delta E_c^{n=1}$ and $\Delta E_v^{n=1}$ becomes

$$\begin{aligned}
 \frac{\Delta E_c^{n=1}}{\Delta E_v^{n=1}} &= \frac{0.82}{0.17} \\
 \Rightarrow \Delta E_c^{n=1} &= 89 \text{ meV}, \quad \Delta E_v^{n=1} = 19 \text{ meV}
 \end{aligned}
 \tag{5.4}$$

Chapter 5 Properties of GaN grown by the Liquid Target Pulsed Laser Deposition Technique in Nitrogen Atmosphere

Hence, although the values of the conduction and valence band discontinuities are not known, it appears that the electron is the loosely bound particle. The depth of the quantum well (V_0) can be calculated in the following manner using the thermal dissociation value of 30 meV for the E_a of I_3

$$\begin{aligned}
 V_0 &= \Delta E_c^{n=1} + \text{Thermal Activation Energy for } I_3 \\
 &= 89 \text{ meV} + 30 \text{ meV} \\
 &= 119 \text{ meV}
 \end{aligned} \tag{5.5}$$

The value of the lowest confinement energy level ($n=1$) of the finite potential well is given by (See Appendix A)

$$\sqrt{V_0 - \Delta E_c^{n=1}} \approx \sqrt{\Delta E_c^{n=1}} \tan \left(\sqrt{\frac{\pi^2 \times m_e^* \times \Delta E_c^{n=1}}{2 \times \hbar^2}} \times L \right) \tag{5.6}$$

where $\hbar = 6.59 \times 10^{-16} \text{ eVs}^{-1}$, and m_e^* and L are the effective electron mass and the quantum well width, respectively

By substituting $\Delta E_c^{n=1}$ and V_0 values obtained from equation (5.4) and (5.5), the quantum well width (L) is calculated as $L \sim 3.1 \text{ nm}$. This value is in reasonable agreement with the value of $\sim 6 \text{ nm}$ for the height of the unintentional GaN cubic islands formed at the substrate-GaN interface and measured using TEM by Omitsuka *et al* [24]. We find a further justification for our model in the work of Wetzel *et al*

Chapter 5 Properties of GaN grown by the Liquid Target Pulsed Laser Deposition Technique in Nitrogen Atmosphere

[15] which describes an increase in the intensity of I_3 closer to the GaN-substrate interface region where the cubic phase was shown to dominate [12]

At this stage, it would be tempting to assign I_4 to the transition from the $E_{(n=1)}$ level to a shallow acceptor level in the cubic phase. However, such an assignment would lead to a value of E_A in the cubic GaN of

$$\begin{aligned} E_A &= I_3 - I_4 - \Delta E_V^{n=1} \\ &= 3.368 \text{ eV} - 3.310 \text{ eV} - 19 \text{ meV} \\ &= 39 \text{ meV} \end{aligned} \tag{5.7}$$

This value is inconsistent with the value of 90 meV reported by other authors [11, 13]. Another candidate for I_4 would be the transition involving an electron in the conduction band of the hexagonal phase with the shallow acceptor level of the cubic phase (see Fig. 5.9). This is because a small number of electrons may escape from the potential well due to the relatively small value of the potential barrier (i.e. $V_0 - (\Delta E_C^{n=1} - E_x) \sim 70 \text{ meV}$). The slight asymmetry of the I_4 peak, its small activation energy (table 5.1), and a blue shift with increasing of temperature (Fig. 5.8) are consistent with such a free to bound transition [16, 25]. In addition, the expected transition strength of recombination between different phases is consistent with the relative weakness of this feature. From Fig. 5.9, the acceptor binding energy (E_A) can be deduced from the I_4 transition energy using the following equation

Chapter 5 Properties of GaN grown by the Liquid Target Pulsed Laser Deposition Technique in Nitrogen Atmosphere

$$\begin{aligned} E_A &= V_0 + E_g^{\text{cubic}} - I_4 \\ &= 119 \text{ meV} + 3.30 \text{ eV} - 3.310 \text{ eV} \\ &= 109 \text{ meV} \end{aligned} \quad (5.8)$$

This value is in reasonable agreement with the shallow acceptor value E_A of 90 meV reported by other authors using PL excitation spectroscopy [11,13]

In quantum mechanics, the energy difference between I_3 and I_4 (i.e. ΔE_{34} as shown in Fig. 5.9) is related to the following expression

$$\frac{I_3}{I_4} = g \left(\frac{f_3}{f_4} \right) \exp\left(\frac{\Delta E_{34}}{kT} \right) \quad (5.9)$$

where g , f_3 and f_4 are the oscillation strength, the transition probability for I_3 and the transition probability for I_4 respectively

Hence, by plotting $\ln\left(\frac{I_3}{I_4}\right)$ vs $1/T$, it is possible to deduce ΔE_{34} from the slope of the curve. The corresponding plots are presented in Fig. 5.10

Chapter 5 Properties of GaN grown by the Liquid Target Pulsed Laser Deposition Technique in Nitrogen Atmosphere

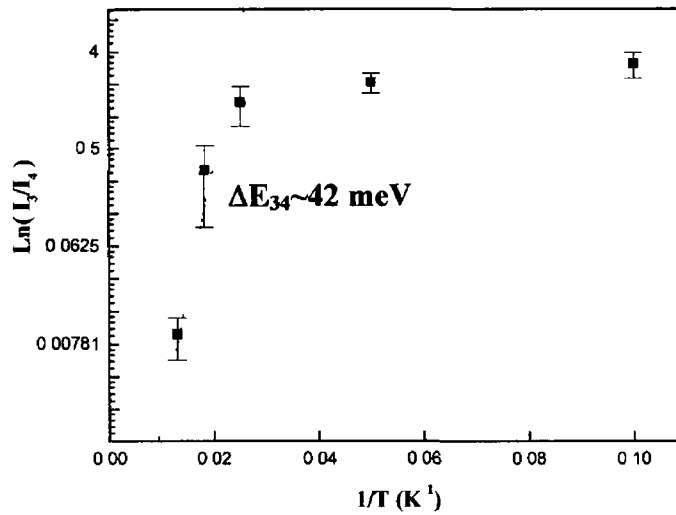


Fig 5 10 Integrated intensities of $\ln(I_3/I_4)$ as a function of $1/T$

Fig 5 10 shows that in the low temperature range ($T < 45$ K), the slope of $\ln(I_3/I_4) \sim 0$ which means that most of the electrons are confined within the quantum well and only a small portion of electrons in cubic hexagonal GaN make a transition to the acceptor level in cubic phase. As the temperature is increased, the electrons are thermalised out and add to the intensity of I_4 . The measured energy difference between I_3 and I_4 level ($\Delta E_{3,4}$) is ~ 42 meV, which is lower than the estimated value (~ 70 meV) from our QW model. One of the possible explanations is that the band bending at the interface of cubic and hexagonal structure (as shown in Fig 5 9) may 'effectively' lower the escape energy of electrons, where the electrons can escape to I_4 level via quantum tunnelling effects. A further study is required to validate this mechanism.

Chapter 5 Properties of GaN grown by the Liquid Target Pulsed Laser Deposition Technique in Nitrogen Atmosphere

5.4 Conclusion

In conclusion, this chapter examined some structural and optical properties of GaN thin films ($\sim 1 \mu\text{m}$) grown either on sapphire (0001) or GaAs (001) substrates using the liquid target pulsed laser deposition technique. GaN thin films grown on sapphire (0001) substrates at different temperatures ($T_s = 690^\circ\text{C}$ to 860°C) and laser repetition rate (3 Hz and 10 Hz) were characterized using XRD 2θ scans and low temperature PL. The optimum growth conditions were found to be $T_s \sim 800^\circ\text{C}$ at a laser repetition rate of 10 Hz, which resulted in a PL FWHM as narrow as 8 meV for the (D-X) transition. Following this, a GaN sample was grown on a GaAs (001) substrate for the same optimum growth conditions ($T_s = 800^\circ\text{C}$ and 5 Torr N_2). No hint of yellow band was detected in this sample. Two strong luminescence lines I_3 (3.368 eV) and I_4 (3.310 eV), were observed to dominate the low temperature (5K) PL spectra particularly for the sample grown on GaAs (001). We interpreted both peaks in terms of a model in which the carriers are confined in cubic inclusions within the hexagonal matrix analogously to a type I quantum well. We propose I_3 as the transition in which an electron makes a transition from the ground level ($n=1$) to a hole within the cubic phase, while I_4 corresponds to an electron in the hexagonal phase making a transition to a hole in the shallow acceptor level of the cubic phase.

Chapter 5 Properties of GaN grown by the Liquid Target Pulsed Laser Deposition Technique in Nitrogen Atmosphere

5.5 References

- 1 P R Willmott and J R Huber *Review of Modern Physics Pulsed Laser vaporization and deposition* **72**, 1, (2000)
- 2 R D Vispute, T Talyansky, R P Sharma, C Choopun, M Downes and T Venkatesan *Appl Phys Lett* **71**, 102 (1997)
- 3 R F Xiao, X W Sun, Z F Li, N Cue and H S Kwok, Q Z Liu and S S Lau *J Vac Sci Tech* **A15**, 2207 (1997)
- 4 M Gross, G Henn and H Schroder *Mat Sci Eng* **B50**, 16 (1997)
- 5 T Kurobe, Y Sekiguchi, J Suda, M Yoshimoto, H Matsunami *Appl Phys Lett* **73**, 2305 (1998)
- 6 N Grandjean, J Massies and M Leroux *Appl Phys Lett* **69**, 2071 (1996)
- 7 M Leroux, N Grandjean, B Beaumont, G Nataf, F Semond, J Massies and P Gibart *J Appl Phys* **86**, 3721 (1999)
- 8 P G Middleton, K P O'Donnell, C Trager-Cowan, D Cole, M Cazzanelh and J Lunney *Mat Sci Eng* **B59**, 133 (1999)
- 9 T F Huang, A Marshall, S Spruytte and J S Harris Jr *J Crys Growth* **200**, 362 (1999)
- 10 C H Hong, D Pavhdis, S W Brown and S C Rand *J Appl Phys* **77**, 1705 (1995)
- 11 J Wu, H Yaguchi, K Onabe, R Ito, Y Shirake, *Appl Phys Lett* **71**, 2067 (1997)

Chapter 5 Properties of GaN grown by the Liquid Target Pulsed Laser Deposition Technique in Nitrogen Atmosphere

- 12 S Ruvimov, Z Weber, J Washburn, T Drummond, M Hafich and S R Lee
Appl Phys Lett **71**, 2931 (1997)
- 13 D J As, F Schmilgus, C Wang, B Schottker, D Schikora and K Lischka Appl
Phys Lett **70**, 1311 (1997)
- 14 B Meyer Mat Res Soc Symp Proc **449**, 497 (1997)
- 15 C Wetzels, S Fischer, J Kruger, E E Haller, R J Molnar, T D Moustakas, E
N Mokhov, P G Baranov App Phys Lett **68**, 2556 (1996)
- 16 P Yu and M Cardona *Physics and Material Properties* Springer 1996
- 17 H Y Fan Phys Rev **82**, 900 (1951)
- 18 M Ilegems and R Dingle Appl Phys Lett **44**, 4234 (1973)
- 19 M Cazzanelli, D Cole, J F Donegan, J G Lunney, P G Middleton and K P
Donnel, C Viegoni and L Pavesi Appl Phys Lett **73**, 3390 (1998)
- 20 J Pankove *Optical Processes in Semiconductor* Dover, New York 1991
- 21 S Ruvimov, Z Weber, J Washburn, T Drummond, M Hafich and S R Lee
Appl Phys Lett **71**, 2931 (1997)
- 22 P Bigenwald, P Leffevre, T Bretagnon and B Gil Phys Stat Sol **216**, 371
(1999)
- 23 S Nakamura, S Pearton and G Fasol, *The Blue Laser Diode The Complete Story*,
2nd edition Springer, 2000 Page 44
- 24 T Onitsuka, T Maruyama, K Akimoto and Y Bando J Crys Growth **189/190**,
295 (1998)
- 25 D M Eagles, J Phys Chem Solids, **16**, 76 (1960)

CHAPTER 6

Study of the expansion dynamics of Ga and GaN ablation plumes using time-resolved extreme UV photoabsorption spectroscopy

As mentioned in section 2.3, the PLD growth technique presents a number of attractive features, for example PLD involves simple experimental procedures, it also preserves good film stoichiometry in most cases, allowing for the easy addition of various reactive gases during the deposition process. However, there are some drawbacks associated with the PLD technique. For example, the ablation plume is highly forward peaked, which leads to a non-uniform thickness of the film [1]. Another serious drawback is the possible contamination of the deposited films by micron sized droplets known as *particulates* which may be present in the ablation plume. The amount of the droplets is highly dependent on the experimental conditions [1-2]. The roughness of the GaN epilayers grown by PLD technique is closely linked to particulate formation [2-4]. Hence, knowledge of the plume composition during growth will be invaluable to optimise the thin film quality. To date, most of the PLD work on GaN has focussed on the evaluation of the thin film properties [2-8] rather than investigating the laser ablation plume. In this chapter, the expansion dynamics of Ga and GaN ablation plume in vacuum were studied using extreme ultraviolet time-resolved dual laser plasma (DLP) photoabsorption spectroscopy. Targets of either Ga metal or polycrystalline GaN, and a Nd-YAG laser (1.06 μm) at a fluence of 10 J cm^{-2}

Chapter 6 Study of the expansion dynamics of Ga and GaN ablation plumes using time-resolved extreme UV absorption spectroscopy

were used in this study. Spatio-temporal maps of the relative concentration of Ga^+ were constructed by measuring the transmission through the ablation plume of a pulsed beam of ultraviolet radiation tuned to $3p \rightarrow 3d$ *inner-shell* transitions in Ga^+ . Marked differences between the spectra of the Ga and GaN plumes were observed. The results of these experiments showed that the density of Ga^+ and Ga^{2+} active species becomes negligible over distances greater than 5 mm above the target surface. These observations shed new light on the general assumptions found in the literature that the active species in PLD are ionized throughout the plume, and that ionized species play a critical role in the deposition process [1,9]. We also found the emission of droplet (particulates) to last for $\sim 7 \mu\text{s}$ and the droplets to be present throughout the plume. Based on these observations, we conclude on the relationship between the quality of the GaN epilayers and the relevant ablation plume parameters.

6.1 Gallium Metal Target

We now discuss the results of a photoabsorption study of an ablation plume of gallium metal using the DLP technique (see section 3.4). The spectra were measured at different height above target (i.e. x -value) at various points across the plume diameter (y -value) (see Fig. 6.1), and for various time delays after the initiation of the plume.

Chapter 6 Study of the expansion dynamics of Ga and GaN ablation plumes using time-resolved extreme UV absorption spectroscopy

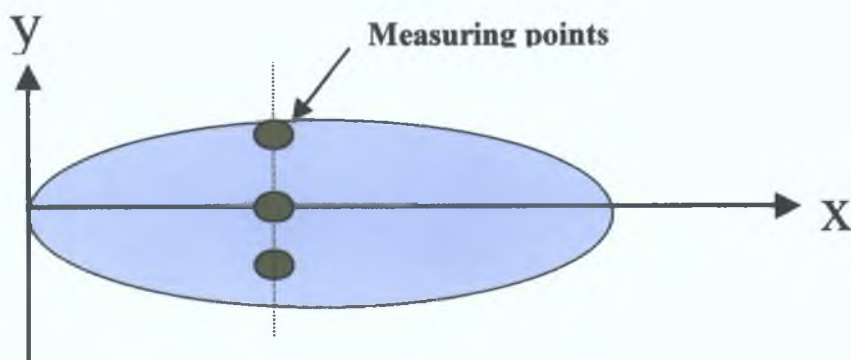


Figure 6.1 Schematic diagram of the ablation plume.

A typical spectrum taken at $x=0.15$ mm and $y=0$ mm is shown in Fig. 6.2 where $A = \ln\left(\frac{I_0}{I}\right)$ (I_0 = continuum background intensity and I = transmitted intensity) is plotted as a function of photon energy for various time delays. Ga^+ and Ga^{2+} absorption peaks are identified at 30.662 eV, 31.058 eV and 31.115 eV, respectively[10].

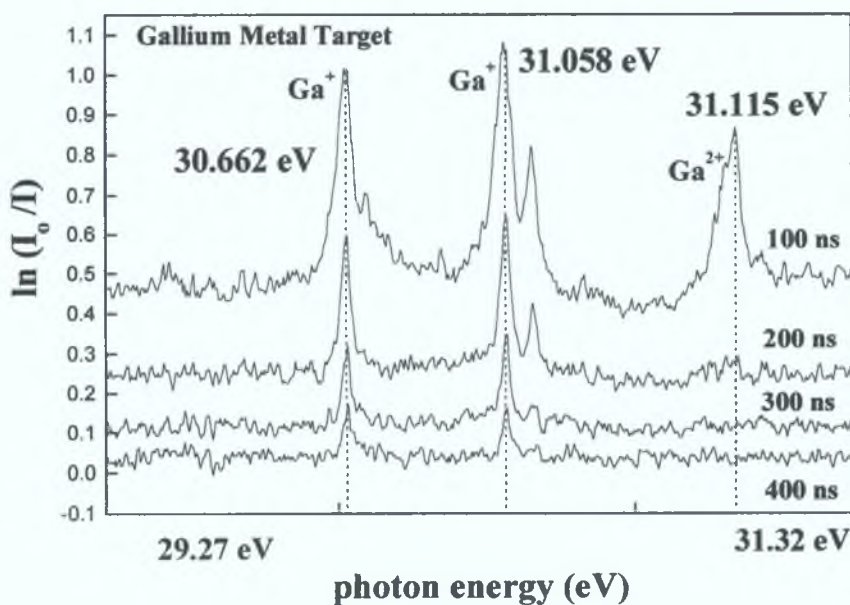


Figure 6.2 Typical absorption spectra of laser produced plasma at $x = 0.15$ mm

Chapter 6 Study of the expansion dynamics of Ga and GaN ablation plumes using time-resolved extreme UV absorption spectroscopy

During our experiment, the $x=0$ position was defined as the target position that allowed 90% of the background intensity (I_0) to reach the detector. These measurements were repeated for various values of y at fixed x and contour maps showing points of equal value of the absorption coefficient of the 33.66 eV transitions were drawn as a function of time delay. A typical contour map of this type is shown on Fig.6.3. The maximum absorption (A) value in Fig.6.3 is equal to 1.1 ($I/I_0 = 0.33$ at around 100 ns) and was the highest value recorded during the experiments with Ga metal. Similar measurements were repeated for different values of x and the corresponding time-of-flight curves for on-axis absorption ($y = 0$) are presented in Fig. 6.4.

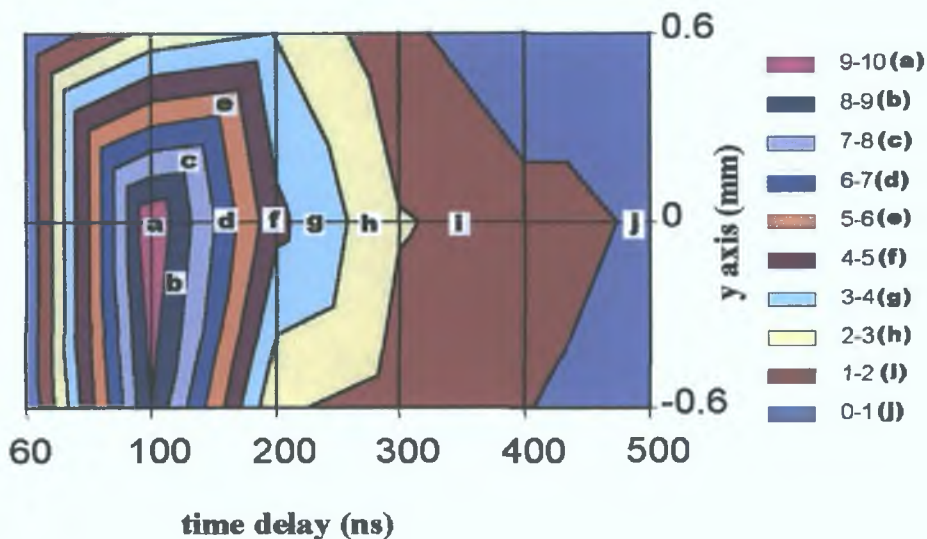


Figure 6.3 Contour maps of equal absorption at $x = 0.15$ mm and various y values as a function of time delay.

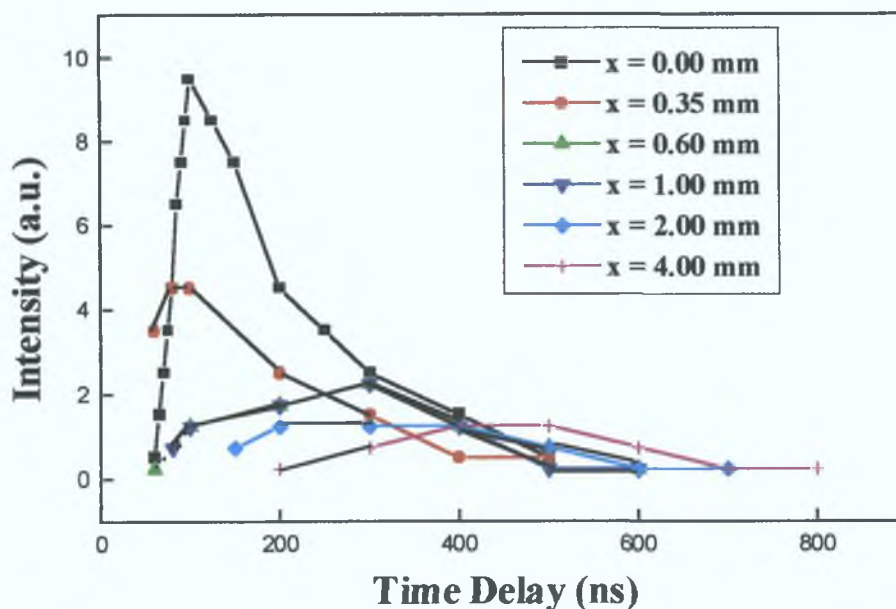


Figure 6.4 Time resolved extreme ultraviolet absorption of Ga^+ in a gallium ablation plume at various x- positions above the target surface

From Fig. 6.2, we observe that initially the plume absorption was dominated by Ga^{2+} but this ion disappeared rapidly after 100 ns due to recombination processes. The relative intensity of the absorption peaks to the intensity of the underlying photoionization continuum remains fairly constant (~ 2.8) between 100 ns and 400 ns (see Fig. 6.2). This suggests a high relative Ga^+ content in the ablation-plume. Close to the target surface and at early times the spatial distribution of the Ga^+ ions is dominated by steep gradients, see Fig. 6.3.

Fig. 6.4 shows the photoabsorption of Ga^+ at various x- positions as a function of time delays. We observed that the maximum population of Ga^+ in a gallium ablation plume

Chapter 6 Study of the expansion dynamics of Ga and GaN ablation plumes using time-resolved extreme UV absorption spectroscopy

produced by 1064 nm Nd YAG laser light at a fluence of 10 J cm^{-2} occurs close to the target surface around 100 ns after the plasma creation. It is clearly seen from Fig 6 4 that the further above the target, the later the maximum absorption occurs. This can be readily understood as the ionised species will require more time to travel to the larger values of x . In addition, Ga^+ content is dramatically reduced above $x = 4 \text{ mm}$. Indeed, we were unable to detect any absorption beyond this point. This phenomenon can be attributed to recombination of the ionised species [10-12]. From Fig 6 4, it is possible to deduce the x -position where the maximum absorption of the Ga^+ occurs as a function of time delays. The result is shown in Fig 6 5 below,

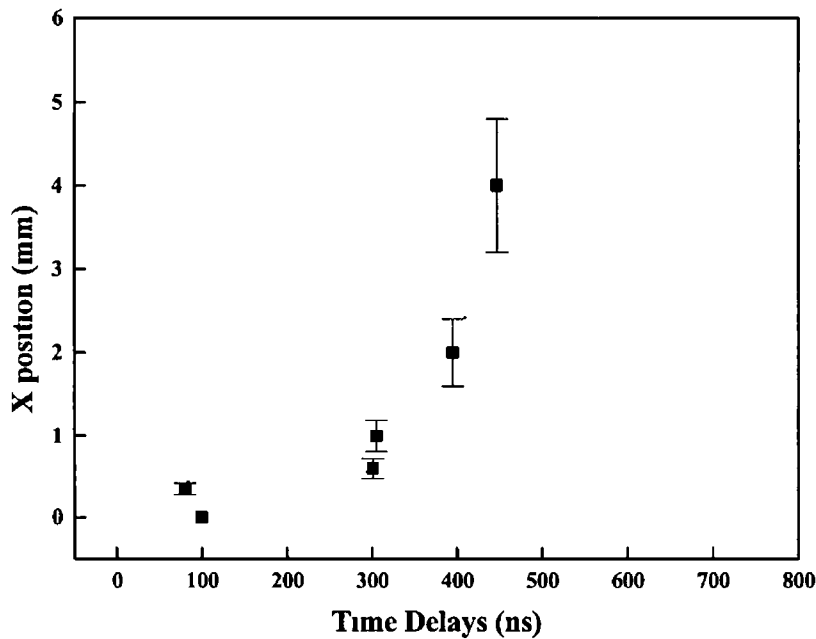


Figure 6 5 The x -position where the maximum absorption of Ga^+ occurs as a function of time delays

Chapter 6 Study of the expansion dynamics of Ga and GaN ablation plumes using time-resolved extreme UV absorption spectroscopy

A most probable velocity of $\sim 5 \times 10^5$ cms⁻¹ for Ga⁺ is measured from the slope in Fig 6.5. The corresponding temperature (T) of the plasma can be calculated from the following equation

$$V_{speed} = \left(\frac{2kT}{m} \right)^{1/2}, \quad (6.1)$$

where V_{speed} , k and m are the most probable Maxwell velocity distribution, Boltzmann constant and atomic mass for Ga respectively. This yields a temperature of the order of 4 eV ($\sim 46,400$ K) for the early phase of the plasma expansion.

6.2 Polycrystalline Gallium Nitride Target

This section presents the DLP study of the laser-ablation plume for the polycrystalline GaN target. These were prepared using the method outlined in Chapter 3 (section 3.1.1). Fig. 6.6 shows the absorption spectra of an ablation plume of GaN for (a) time delays less than 300 ns (b) $700 \text{ ns} < \text{time delays} < 7000 \text{ ns}$.

Chapter 6 Study of the expansion dynamics of Ga and GaN ablation plumes using time-resolved extreme UV absorption spectroscopy

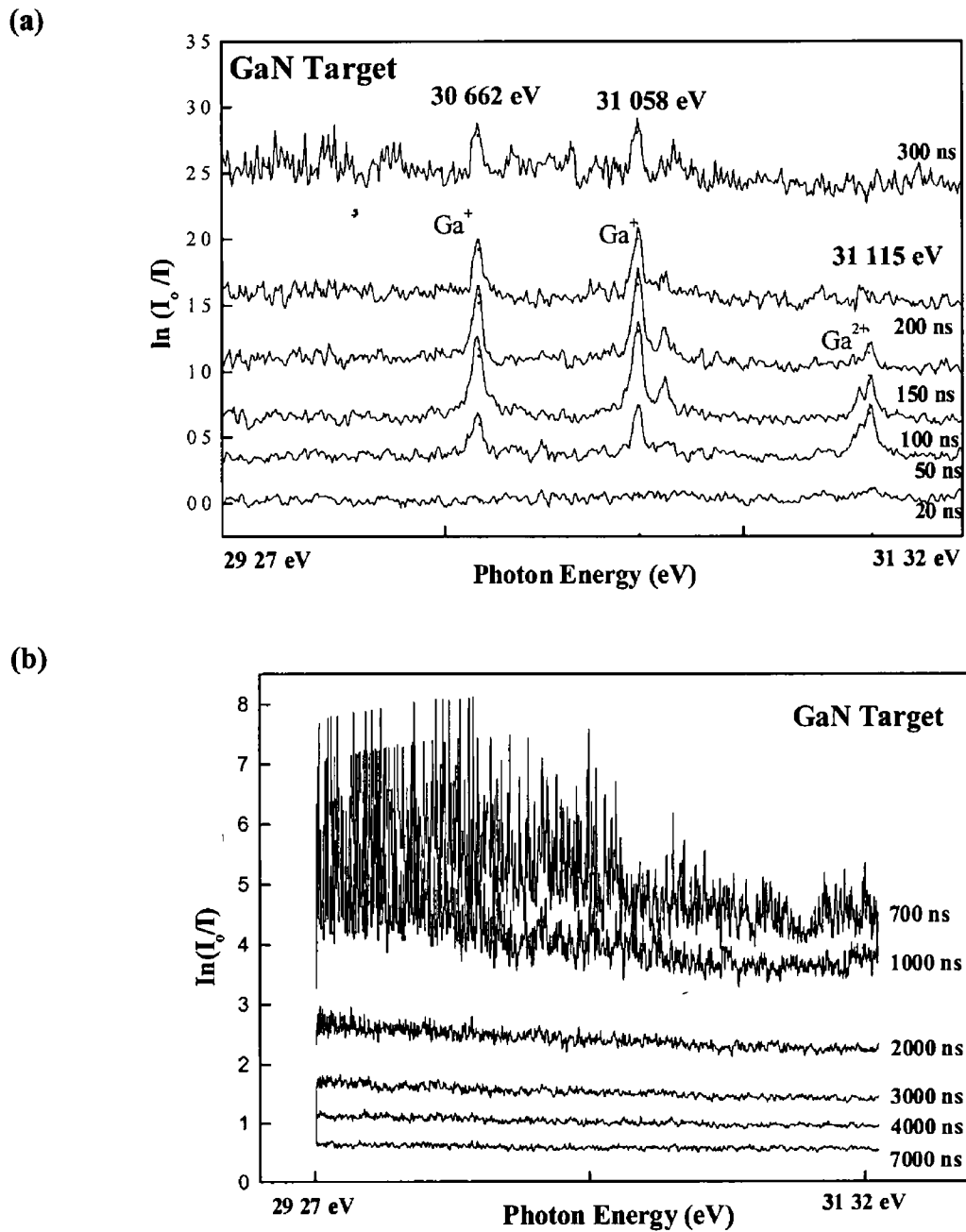


Figure 6 6 Absorption $\ln\left(\frac{I_0}{I}\right)$ spectra of laser produced plasmas of GaN measured at $x = 0.15$ mm above target surface for (a) time delays < 300 ns (b) 700 ns $<$ time delays < 7000 ns

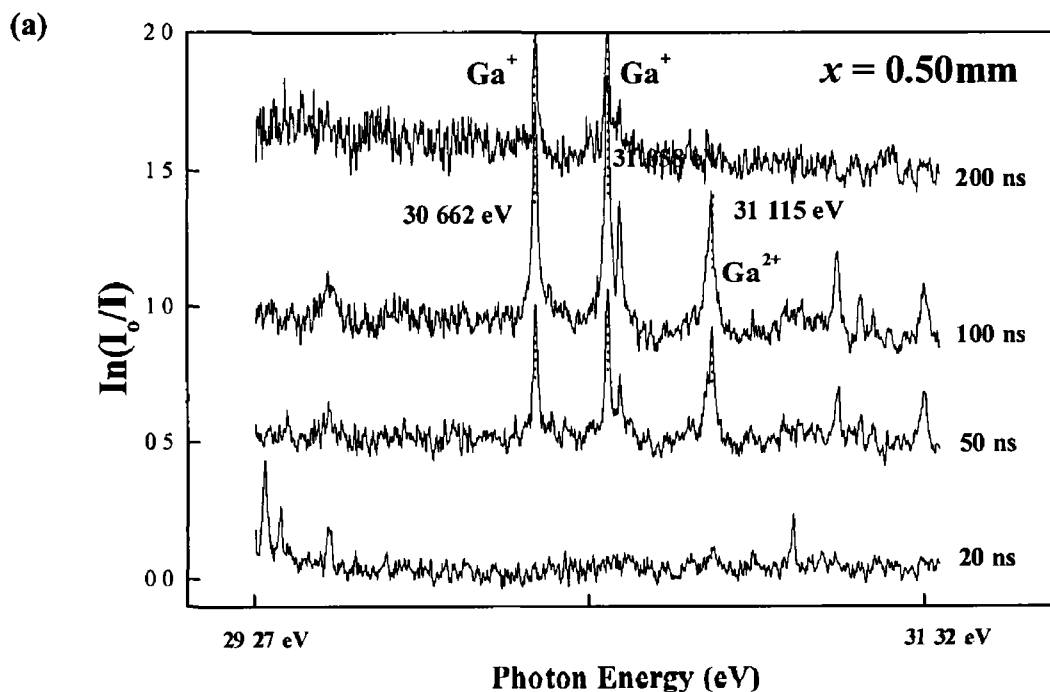
Chapter 6 Study of the expansion dynamics of Ga and GaN ablation plumes using time-resolved extreme UV absorption spectroscopy

The difference between the absorption behaviour of the Ga and GaN target is evident and the high absorption (A) values ($\ln(I_0/I) > 2$ for time delay greater than 200 ns in Fig 6 6(a)) indicate that saturation of the absorption has occurred for the GaN plasma after only a few 100's ns. This saturation effect precludes the plotting of meaningful contour maps of equal absorption. From Fig 6 6(a), we observe that the early behaviour of the GaN plasma close to the target surface is similar to the Ga plasma in Fig 6 2, i.e. dominated by Ga^+ and Ga^{2+} ions. One also observes a significantly higher level of continuous absorption which can be explained by the presence of atomic N in the plasma. The total photoionization cross-section of N at 30 eV is around 10 Mb [13]. However, at times greater than 200 ns, as the Ga^+ signal disappears, the continuum level is still increasing and the plasma becomes totally opaque after ~ 400 ns. We observed (as shown on Fig 6 6(b)) that it remained so for another few μs and only became completely transparent again to extreme UV radiation after $\sim 7\mu\text{s}$. Again, in this case, this behaviour is clearly incompatible with a plasma composed of free atomic or molecular species. This behaviour cannot be due to absorption by other Ga species because this was not observed when pure Ga metal was ablated (as shown in Fig 6 2). We therefore suggest that it can only be explained by the presence of a significant amount of non-atomized matter (i.e. "particulate"), at the liquid or solid density. In addition, the overall duration of the absorption (i.e. $7\mu\text{s}$) is consistent with the particulates emission time reported previously [14]. Hence, we suggest that the particulates that are generated from the GaN target and propagate throughout the GaN laser plasma plume are by and large absent in the ablation of Ga metal targets. This is in agreement with the observation by Xiao *et al* [5] that pure Ga

Chapter 6 Study of the expansion dynamics of Ga and GaN ablation plumes using time-resolved extreme UV absorption spectroscopy

provides a relatively particulate free laser ablation source compared to a solid GaN target

Figure 6 7 shows the absorption spectrum of laser produced plasma of GaN target at different positions (i.e. $x = 0.5$ mm, 2.00 mm and 5.00 mm). The absorption (A) values ($A = \ln(I_0/I)$) decrease with an increase in the x position, an effect due to the recombination within of ionised species as they travel further [12]. It is interesting to note that the Ga^+ species only exist in the spectrum for $x = 0.5$ mm and 2.00 mm (Fig. 6 7 (a) & fig. 6 7(b)), but are virtually absent in spectra taken at $x = 5$ mm (Fig. 6 7(c)). This suggests that Ga^+ species only exist within a few millimetres from the target position due to fast recombination processes during the plume expansion.



Chapter 6 Study of the expansion dynamics of Ga and GaN ablation plumes using time-resolved extreme UV absorption spectroscopy

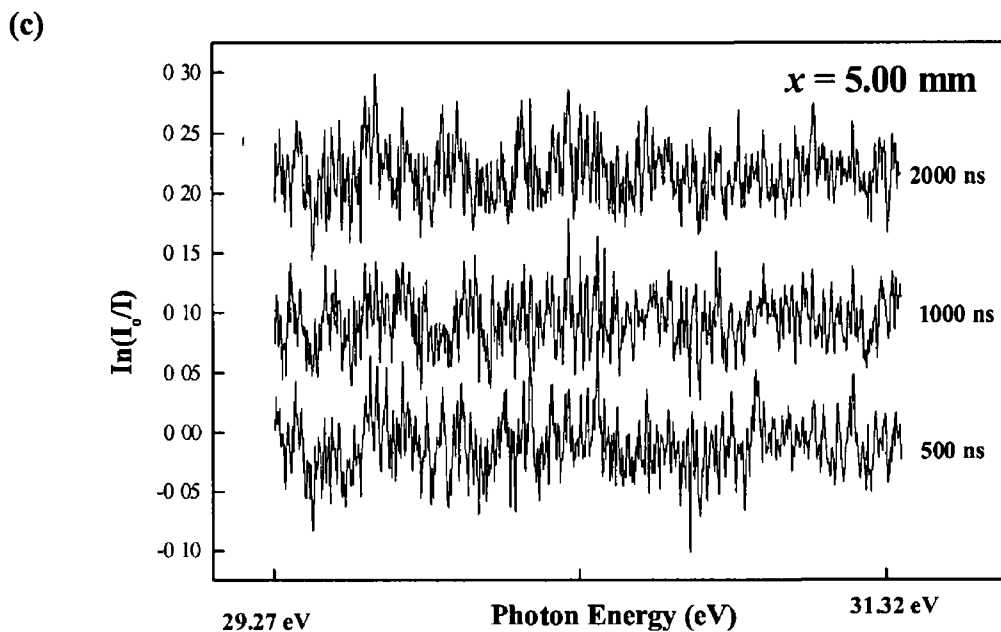
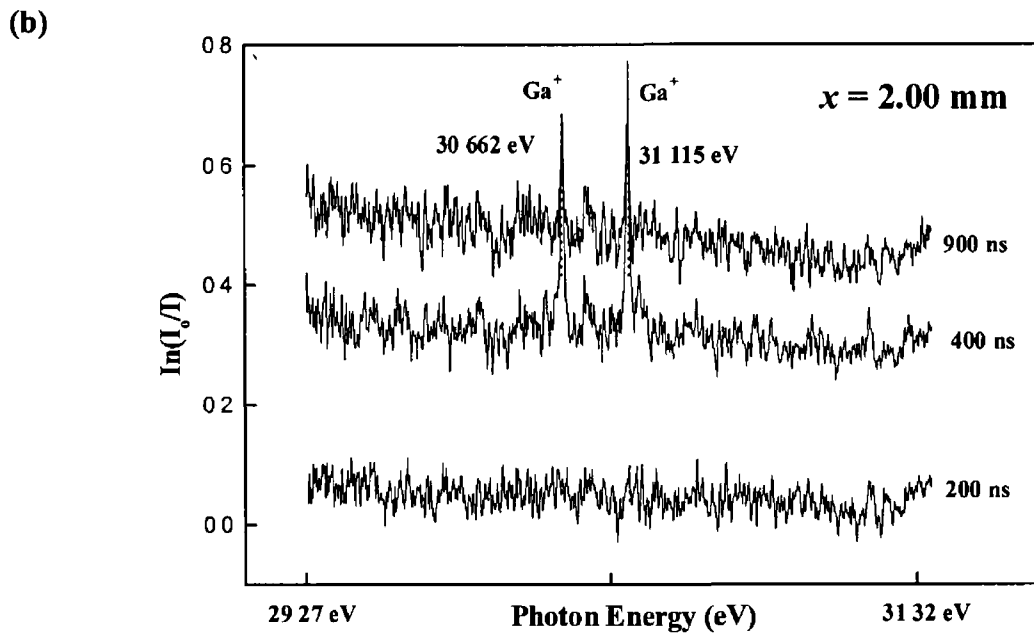


Figure 6 7 Extreme ultraviolet absorption spectrum of laser produced plasmas of GaN target measured at (a) $x = 0.5$ mm (b) $x = 2.00$ mm and (c) $x = 5.00$ mm above the target surface for various time delays

Chapter 6 Study of the expansion dynamics of Ga and GaN ablation plumes using time-resolved extreme UV absorption spectroscopy

In a typical solid target PLD system, the distance between the target and the substrate is typically a few cm's [2-5]. Our experiments indicate that the concentration of ionized species should be comparatively small at the substrate position. These observations are in contrast with the general beliefs [1,9] that the density of ablated ionized species such as Ga^+ plays a critical role in PLD growth. We suggest on the contrary that in the ablation of solid GaN in PLD system, only Ga neutral atoms, GaN molecules and particulates will reach the surface of the substrate with an appreciable concentration, a situation which is similar to the growth mechanism in solid source molecular beam epitaxy (MBE) systems [15]. This suggestion also explains why an increase in laser fluence in PLD system tend to increase particulate contamination instead of improving the surface quality [2]. An increase in laser fluence will emit a higher density of particulates which will eventually contaminate the substrate surface.

6.3 Conclusion

In conclusion, we have studied the Ga and GaN laser ablation plume using ultraviolet photoabsorption spectroscopy technique. The results suggest that metallic gallium is a more suitable target material for the PLD growth of GaN compared to a GaN target.

Chapter 6 Study of the expansion dynamics of Ga and GaN ablation plumes using time-resolved extreme UV absorption spectroscopy

6.4 References

- 1 D B Chrisely and G K Hubler, *Pulsed Laser Deposition of Thin Film* Wiley, New York (1994)
- 2 S Cho and H Okumura *Appl Phys Lett* **76**, 3861 (2000)
- 3 D Cole, J G Lunney, F P Logue, J F Donegan, J M D Coey, *Mat Sci Eng* **B48**, 239 (1997)
- 4 R D Vispute, V Talyansky, R P Sharma, S Choopun, M Downes and T Venkatesan, *Appl Phys Lett* **71**, 102 (1997)
- 5 R F Xiao, H B Liao, N Cue, X W Sun and H S Kwok *Appl Phys Lett* **80**, 4226 (1996)
- 6 T Ohyanagi, A Miyashita, K Murakami and O Yoda *Jpn J Appl Phys* **33**, 2586 (1994)
- 7 J Karpinski, J Jun and S Porowski, *J Crys Growth* **66**, 1 (1984)
- 8 J Karpinski and S Porowski, *J Crys Growth* **66**, 11 (1984)
- 9 M Gross, G Henn, J Ziegler, P Allenspacher, C Cychy and H Schroder *Mat Sci Eng* **B59**, 94 (1999)
- 10 P Dunne, G O Sullivan and V K Ivanov *Phys Rev* **A48**, 4358 (1993)
- 11 E T Kennedy, J T Costello, A Gray, C McGuinness, J-P Mosnier and P Van Kampen, *J Elec Spec Rel Phenom* **101**, 161 (1999)
- 12 W Whitty, J Costello, E T Kennedy, C Moloney and J-P Mosnier, *Appl Surf Sci* **127/129**, 686 (1998)
- 13 J A R Samson and C G Angel, *Phys Rev* **A42**, 1357 (1990)

**Chapter 6 Study of the expansion dynamics of Ga and GaN ablation plumes
using time-resolved extreme UV absorption spectroscopy**

14. N.Cherief, D.Givord, A.Lienard, K.Mackay, O.F.K.McGrath, J.P.Rebouillat,
F.Robaut and Y.Souche. *J. Mag. Mat.* **121**, 94 (1993).
15. S. F. Yoon, K. W. Mah and H. Q. Zheng. *J. Appl. Phys.* **85**, 7374 (1999).

CHAPTER 7

Conclusions and Recommendations for Future Works

7.1 Conclusions

The motivation for the present work originally lay in the inherent benefits that can be obtained from GaN-based related devices, in particular, from optoelectronic device applications. The basic theory of hexagonal and cubic GaN material systems were discussed in Chapter 2. We also briefly reviewed the basic principles of the various growth techniques in current use.

The principles of the two different types of Pulsed Laser Deposition (PLD) techniques, namely solid target PLD and liquid target PLD were introduced in Chapter 3. The principles of the characterisation techniques employed in this work, such as temperature dependent photoluminescence (PL) and x-ray diffraction (XRD) were also presented, as well as description of an extreme UV absorption spectrometer for laser plasma diagnostics.

A detailed description of the GaN/Sapphire material system grown by the PLD technique in N₂ atmosphere was presented in Chapter 4. The surface morphology of the GaN films was investigated using Atomic Force Microscopy (AFM) while the

Chapter 7 Conclusion and Recommendations for Future works

crystalline quality was studied using XRD scans. The optical properties of the material were studied using temperature dependent photoluminescence (PL) and room temperature Raman spectroscopy. X-ray diffraction and Raman spectroscopy showed predominantly the wurtzite structure, with some evidence for cubic inclusions. The 3.43 eV line in the PL spectra was interpreted as carriers transitions taking place at the interfacial region between the mixed hexagonal and cubic phases. The corresponding electrons are trapped in the defective region of the cubic phase and are spatially separated from the holes before radiative recombination occurs.

In Chapter 5, the optical and structural properties of GaN grown on sapphire(0001) substrates using the liquid target PLD technique were investigated. The material properties were studied as a function of substrate temperature (T_s) using low temperature PL and XRD. PL FWHM as narrow as 9 meV were recorded for the (D-X) transition in samples grown in the optimum conditions of $T_s \sim 800$ °C and a laser repetition rate of 10 Hz. This result is comparable to the best values (5-10 meV) previously reported for GaN films grown by MBE and MOCVD techniques. GaN thin films were also grown on GaAs (001) substrates and the properties of the sample were studied using temperature dependent PL down to 4K. No hint of the yellow band due to defects was detected in these samples. We observed the two transition lines at 3.368 eV (I_3) and 3.310 eV (I_4) to dominate the low temperature PL spectrum in samples grown on sapphire (0001) or GaAs (001) substrates at $T_s = 800$ °C. A model was proposed to explain the emission mechanism of both lines in terms of the confinement of the carriers in cubic inclusions within the hexagonal structure.

Chapter 7 Conclusion and Recommendations for Future works

analogously to a type I quantum well. I_3 was assigned to the transition involving an electron in the quantum well ground level ($n=1$) to a hole within the cubic phase, while I_4 was assigned to the transition involving a free electron in the hexagonal phase and a hole in the shallow acceptor in the cubic phase, respectively.

In Chapter 6, the expansion dynamics of Ga^+ in laser plasma of Ga metal and polycrystalline GaN were studied using photoabsorption spectroscopy. The analyses showed that Ga^+ species are detected only within distances less than 5 mm from the target surface, while particulates were observed throughout the ablation plume. The results suggest that metallic Ga is a more suitable target for PLD growth of GaN compared to GaN target. The relation between epitaxial material quality and growth parameters such as laser fluence and substrate temperature was also discussed.

7.2 Recommendations For Future Works

The following suggestions represent a collection of topics related to the present work which would constitute interesting lines of future research.

- 1) Further work is required to study the formation mechanism of cubic- phase GaN grown in N_2 atmosphere using PLD. This could be carried out by using scanning electron microscopy in conjunction with energy dispersive X-ray spectroscopy (SEM-EDX), micro-Raman and cross-section transmission electron microscopy (TEM).

Chapter 7 Conclusion and Recommendations for Future works

- 2) As mentioned in Chapter 4, N_2 is less reactive than ammonia due to the different bond strengths in these gases which results in lower growth rate. One possible solution is to "crack" the N_2 molecule by using the DC plasma source [1]
- 3) A comparative study of the properties of GaN films grown using different exciting laser wavelengths would be interesting
- 4) The properties of the PLD grown GaN/Sapphire interface should be studied in greater details, for example, the type of dislocation (i.e. screw dislocation or threading dislocation)[2], the control of the dislocation density under different growth conditions [3] and the uses of buffer layers to reduce these defects [4]
- 5) The growth of ternary nitride compounds such as Aluminium Gallium Nitride ($Al_xGa_{1-x}N$) [5] and Gallium Nitride Arsenide (GaN_xAs_{1-x}) [6] using multiple target PLD systems appears interesting. GaN/AlGaN and GaN/GaNAs multiple quantum well (QW) devices could be fabricated for the first time using these compounds
- 6) Most interesting would be the control of the doping (n or p) in GaN multilayers prepared by PLD. Doping is the most important issue that determines the quality of devices such as high electron mobility transistors (HEMT) or light emitting diodes (LED) [7-8]

7 3 References

- 1 P Merel, M Chaker, M Tabbal and H Pepin *Appl Surf Sci* **177**, 165 (2001)
- 2 X J Ning, F R Chien, P Pirouz, J W Yang and M A Khan, *J Mat Res* **11**, 580 (1996)
- 3 N Grandjean, J Massies, P Vennegues, M Lerous, F Demangeot, M Renucci and J Frandson *J Mater Res* **83**, 1379 (1998)
- 4 R F Xiao, X W Sun, Z F Li, N Cue and H S Kwok *J Vac Sci Technol* **15**, 2207 (1997)
- 5 T Huang and J S Harris *Appl Phys Lett* **72**, 1158 (1998)
- 6 S Cho and H Okumura *Appl Phys Lett* **76**, 3861 (2000)
- 7 M Micovic, N X Nguyen, P Janke, W S Wong, P Hashimoto, L M McCray, C Nguyen, *Electronics Letter*, **36**, 358 (2000)
- 8 T Wang, T Sugahara, S Sakai and J Orton *Appl Phys Lett* **74**, 1376 (1999)

AUTHOR'S PUBLICATIONS BASED ON THIS WORK

Journal Papers

- 1 K W Mah, J Castro, J T Costello, E T Kennedy, J G Lunney, E McGlynn, P van Kampen and J P Mosnier "Comparative study of the expansion dynamics of Ga⁺ ions in the laser ablation of Ga and GaN using time-resolved extreme UV absorption spectroscopy" *Applied Surface Science* Volume 168, Pages 150-153 (2000)

- 2 K W Mah, E McGlynn, J-P Mosmer, M O Henry, J Castro, D O' Mahony and J G Lunney "Photoluminescence Study of GaN Grown by Pulsed Laser Deposition in Nitrogen Atmosphere" *Materials Science and Engineering B*, Volume 82 Issues 1-3, Pages 128-130 (2001)

- 3 K W Mah, E McGlynn, J Castro, J G Lunney J-P Mosnier, D O' Mahony and M O Henry " Defect luminescence of GaN grown by pulsed laser deposition" *Journal of Crystal Growth*, Volume 222, Issues 3, Pages 497-502 (2001)

- 4 K W Mah, J-P Mosnier, E McGlynn, M O Henry, D O'Mahony and J G Lunney "Study of Photoluminescence at 3 310 eV and 3 368 eV in GaN/sapphire(0001) and GaN/GaAs(001) grown by Liquid Target Pulsed Laser Deposition" Accepted for publication, *Applied Physics Letter* (2002)

Conference Papers

- 1 K W Mah, S Beyrand, E McGlynn, P van Kampen and J-P Mosnier "Photoluminescence Study of GaN grown by Pulsed Laser Deposition in Nitrogen Atmosphere" *1st UK Nitride Consortium Conferences* Poster Presentation Sept 1999

- 2 K W Mah, J Castro, J T Costello, E T Kennedy, J G Lunney, E McGlynn, P van Kampen and J P Mosnier "Comparative study of the expansion dynamics of Ga⁺ ions in the laser ablation of Ga and GaN using time-resolved extreme UV absorption spectroscopy" Poster Presentation at Symposium D (Photon-induced Material Processing) *European Material Research Society (EMRS) 2000 Conference*

- 3 K W Mah, E McGlynn, J-P Mosnier, M O Henry, J Castro, D O'Mahony and J G Lunney "Photoluminescence Study of GaN Grown by Pulsed Laser Deposition in Nitrogen Atmosphere" Poster Presentation at Symposium C (Group III Nitride) *European Material Research Society (EMRS) 2000 Conference*

Lists Of Figures

Figure 2 1	(a) The basic interatomic bond (b) Three dimension structure of layers stacking along the [0001] direction in hexagonal GaN structure	17
Figure 2 2	The fundamental bandgap of hexagonal GaN	19
Figure 2 3	(a) The basic interatomic bond (b) Three dimension structure of layers stacking along the [111] direction in cubic GaN structure	21
Figure 2 4	A schematic diagram of a typical MOCVD GaN reactor	25
Figure 2 5	A schematic diagram of a typical PLD system	28
Figure 3 1	Schematic diagram (top view) of PLD system	37
Figure 3 2	Schematic diagram (cross section) of the radiative-type heater used in the system	38
Figure 3 3	Schematic diagram (side view) of the liquid target PLD system	40
Figure 3 4	Calibration curve for substrate heater	41
Figure 3 5	Schematic diagram of the Reflectivity System	42
Figure 3 6	Typical reflectivity curve of GaN thin film grown under nitrogen atmosphere	43
Figure 3 7	Schematic diagram of the XRD system operated in " θ - 2θ " mode	44
Figure 3 8	Schematic diagram of the PL experimental apparatus	50
Figure 3 9	Schematic diagram(Top view) of the DLP photoabsorption technique	52
Figure 3 10	Schematic diagram of the GaN plasma plume in the side view Typical cross section for the probing beam in this study $\sim(0.3 \times 0.5) \text{ mm}^2$	53

Figure 4 1	3-D AFM image of a GaN thin film taken near the edge of the sample	56
Figure 4 2	3-D AFM image of a GaN thin film taken around the centre of the sample	57
Figure 4 3	The “ θ -2 θ ” X-ray diffraction pattern for the GaN film	59
Figure 4 4	4 2 K photoluminescence (PL) spectrum of GaN measured at a laser excitation power of 0 3 W/cm ² . A very weak yellow band is observed around ~2 2 eV	60
Figure 4 5	Expanded view of the PL spectrum between 3 1 and 3 5 eV	61
Figure 4 6	Temperature dependence of PL spectra of GaN	62
Figure 4 7	Integrated Intensities of the (D-X), (D-A) and 3,41 eV transitions as a function of $\frac{1}{T}$. The dotted lines are best fitted curve	64
Figure 4 8	Schematic diagram of the band discontinuity at the interface between cubic and hexagonal GaN	67
Figure 4 9	Raman spectra for GaN films grown in N ₂ atmosphere	69
Figure 5 1	Average growth rate per pulse as a function of substrate temperature	74
Figure 5 2	Average growth rate per pulse as a function of pulse laser repetition rate (for T _s = 800 °C)	75
Figure 5 3	XRD scan of GaN samples grown on sapphire(0001) at various temperatures	76
Figure 5 4	XRD scans of GaN thin films in the conditions as indicated on the figure	78
Figure 5 5	10 K photoluminescence spectra of GaN/sapphire(0001) samples grown at various substrate temperatures	79

Figure 5 6	5 K PL spectrum for GaN thin films grown at $T_s \sim 800$ °C and 5 Torr in the conditions indicated in figure	81
Figure 5 7	10K PL spectrum of GaN grown on GaAs(001) at different substrate positions	83
Figure 5 8	Expanded View of the temperature dependence PL spectra for GaN grown in (a) sapphire(0001) (b) GaAs(001) substrate at $T_s = 800$ °C	84
Figure 5 9	Band diagram summarising the PL transitions for both I_3 and I_4	87
Figure 5 10	Integrated intensities of $\ln(I_3/I_4)$ as a function of $1/T$	92
Figure 6 1	Schematic diagram of the ablation plume	98
Figure 6 2	Typical absorption spectra of laser produced plasma at $x = 0.15$ mm	98
Figure 6 3	Contour maps of equal absorption at $x = 0.15$ mm and various y values as a function of time delay	99
Figure 6 4	Time resolved extreme ultraviolet absorption of Ga^+ in a gallium ablation plume at various x - positions above the target surface	100
Figure 6 5	The x -position where the maximum absorption of Ga^+ occurs as a function of time delays	101
Figure 6 6	Absorption $\ln\left(\frac{I_0}{I}\right)$ spectra of laser produced plasmas of GaN measured at $x = 0.15$ mm above target surface for (a) time delays < 300 ns (b) 700 ns $<$ time delays < 7000 ns	103
Figure 6 7	Extreme ultraviolet absorption spectrum of laser produced plasmas of GaN target measured at (a) $x = 0.5$ mm (b) $x = 2.00$ mm and (c) $x = 5.00$ mm above the target surface for various time delays	106

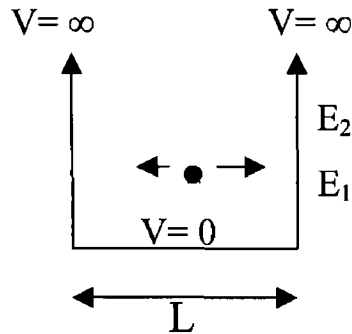
Lists Of Tables

Table 1 1	Summary of the bandgap and wavelength values for <i>Indium Nitride</i> (InN), <i>Gallium Nitride</i> (GaN) and <i>Aluminium Nitride</i> (AlN)	8
Table 2 1	Emissions energies for various transitions in hexagonal GaN at 4.2 K	20
Table 3 1	Theoretical XRD data for cubic and hexagonal GaN	45
Table 4 1	Activation energy of E_a and E_b derived from the best fitted curves	64
Table 5 1	The thermal activation energies (E_a) for various transitions in GaN grown on sapphire (0001) and GaAs (001) substrates	85

Appendix A: Quantum Well Theory

One dimensional infinite potential well

Let's consider a situation where a particle (e.g. electron) is in a one-dimensional infinite potential well as shown below



The potential is zero inside the well (i.e. $V = 0$) but infinite at the walls, so that the particle can't "penetrate" the wall and escape from the potential well. The Schrodinger equation can be simplified as

$$E\varphi = -\frac{\hbar^2}{2m^*} \times \frac{d^2}{dx^2} \varphi \quad (\text{A } 1)$$

Since the probability of finding the particle outside the well is zero (the particle must be in the well) the wave function must satisfy the following boundary conditions

$$\varphi(0) = \varphi(L) = 0 \quad (\text{A } 2)$$

$$\int_0^L \varphi^2 dx = 1 \quad (\text{A } 3)$$

Solving (A 1) & (A 2) & (A 3), give the following eigenvectors φ and eigenvalues E_n

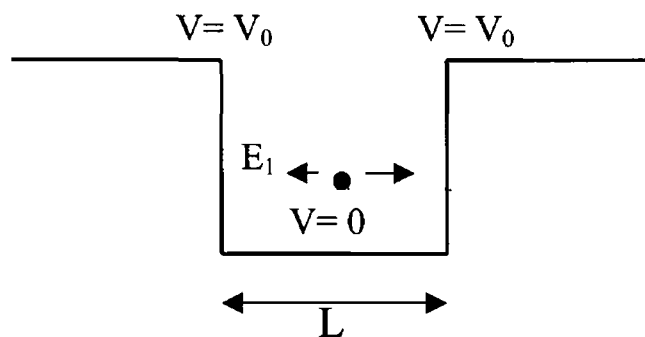
$$\varphi = \sqrt{\frac{2}{L}} \sin\left(\frac{n\pi x}{L}\right) \quad (\text{A 4})$$

$$E_n = n^2 \times \frac{\hbar^2 \pi^2}{2mL} \quad (\text{A 5})$$

For large values of L , E_n become continuous. This is commonly found in bulk semiconductors.

One dimensional finite potential well

In practise, the potential barrier in the "quasi" quantum well tends to be finite (i.e. $V_0 \neq \infty$). This means that there is a probability that the particle may "penetrate" (tunnelling) the potential well and exit the quantum well. In this situation, the potential well can be represented as $V(x) = 0$ for $0 < x < L$ and $V(x) = V_0$ for $x > L$ or $x < 0$. A schematic diagram for this is shown below.



In this case, the Schrodinger equations to be solved are

$$\frac{-\hbar^2}{2m} \frac{d^2\varphi}{dx^2} + V\varphi = E\varphi \quad 0 < x < L \quad (\text{A } 6)$$

$$\frac{-\hbar^2}{2m} \frac{d^2\varphi}{dx^2} = E\varphi \quad x < 0 \text{ and } x > L \quad (\text{A } 7)$$

The continuity of the wave function implies that the reflection (R) and transmission coefficients (T) must satisfy the condition

$$\mathbf{T + R = 1} \quad (\text{A } 8)$$

The wave function and its derivative must be continuous at the boundaries $x = 0$ and $x = L$ where

$$\varphi(0) = \varphi(L) \quad (\text{A } 9)$$

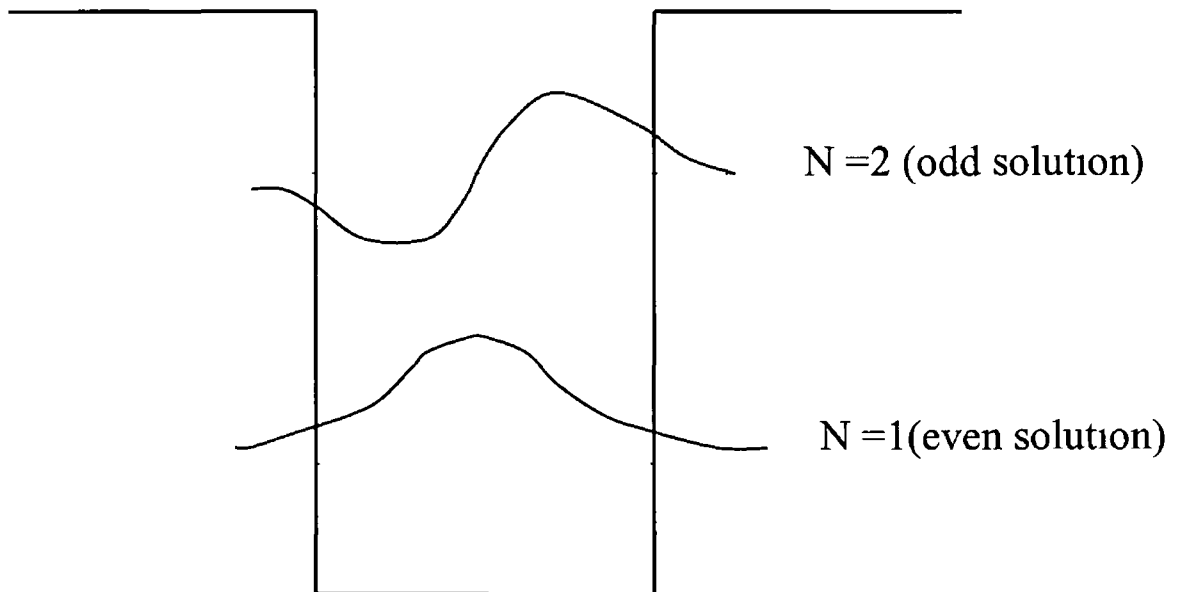
$$\left(\frac{d\varphi}{dx}\right)_{x=0} = \left(\frac{d\varphi}{dx}\right)_{x=L} \quad (\text{A } 10)$$

It can be shown that the first two energy levels ($n = 1, 2$) of the quantum well can be represented by the following solutions [1-2]

$$\sqrt{V_0 - \Delta E^{n=1}} \approx \sqrt{\Delta E^{n=1}} \tan \left(\sqrt{\frac{\pi^2 \times m_e^* \times \Delta E_c^{n=1}}{2 \times h^2}} \times L \right) \quad n=1 \quad (\text{A 11})$$

$$\sqrt{V_0 - \Delta E^{n=2}} \approx -\sqrt{\Delta E^{n=2}} \cot \left(\sqrt{\frac{\pi^2 \times m_e^* \times \Delta E_c^{n=2}}{2 \times h^2}} \times L \right) \quad n=2 \quad (\text{A 12})$$

Where $\Delta E^{n=1}$ and $\Delta E^{n=2}$ is the quantum confinement energy of the electron in $n=1$ and 2 respectively. The schematic diagram that represents (A 11) and (A 12) is shown below.



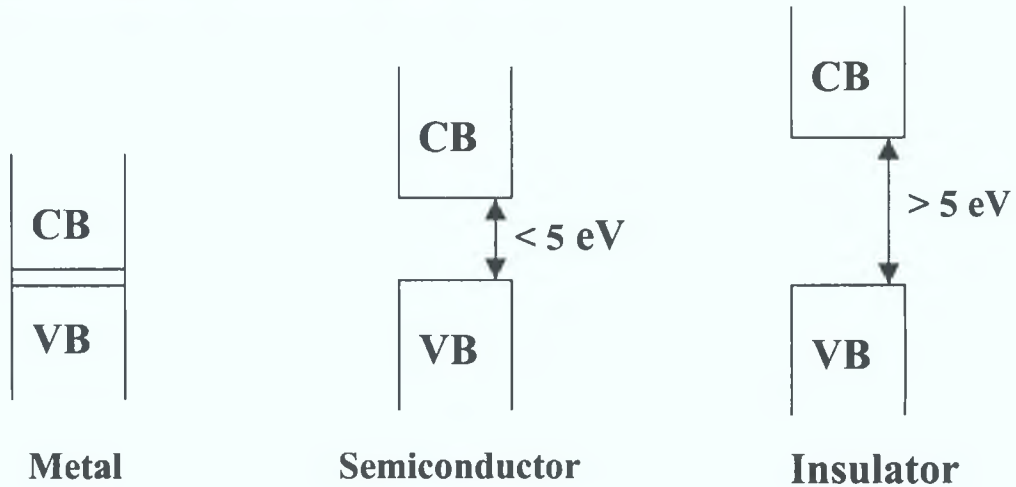
If we proceed to the higher energies level ($n > 2$), the wave solutions that represent the confinement energies will keep on repeating themselves. The quantum confinement only occurs in the case of ultra-thin material (i.e. a few nm) and at low enough temperature. It is worth to mention that quantum tunnelling is intimately bound to the Uncertainty Principle. This means that even when the barrier is sufficiently low (small V_0), we cannot say with certainty that the particle exists only on one side. However, the wave function amplitude for the particle in this situation is reduced by the barrier height, so that we can reduce the φ inside the quantum well which means that there is a higher probability to observe the particle outside the well. Tunnelling is important only over small dimensions (i.e. 1-10 nm range), but it can be of great importance in the mobility and optical properties of semiconductors.

References

- 1 P. Yu and M. Cardona *Physics and Material Properties* Springer 1996
- 2 J. Pankove *Optical Processes in Semiconductor* Dover, New York 1991

Appendix B: Band Theory

The magnitude of the forbidden band determines whether a solid is a metal, a semiconductor or an insulator. In principle, at 0 K a semiconductor has a completely full lower energy band (known as Valence Band or VB) separated from a completely unpopulated higher energy band (known as Conduction Band or CB). As a rule of thumb, any material that has a forbidden band > 0.01 eV and < 5 eV is considered to be a semiconductor. This is illustrated below:



The motion of a free electron through a crystalline solid of period T can be determined by solving the Schrodinger equation using a Bloch Function ($\varphi(r)$):

$$\left(\frac{-\hbar^2 k^2}{2m^2} \times \nabla^2 + V(r) \right) \varphi(r) = E \times \varphi(r) \quad (\text{B.1})$$

where $\varphi(r) = \nu(r) \exp(ik \cdot r)$ and $\nu(r)$ is a periodic function such that $\nu(r) = \nu(r + T)$.

The band structure of different solids is different due to their different crystal orientation and distance between the atoms. This means that the band structure varies with wave vector giving them a curved appearance in k-space. The consequence of this is that some crystals, depending of their lattice, will have their conduction band

(CB) minimum and valence band (VB) maximum at different points in k -space. In a **direct bandgap** material, the CB minimum and VB maximum occurs in the same k point ($k=0$). However, in the indirect bandgap material, the CB minimum and VB maximum occurs in the different k points in the material systems. A table of the direct (d) and indirect (i) bandgap energies in some important semiconductor materials is given in table below.

Crystal	Group	Bandgap (E_g)	Bandgap Type
Silicon	IV	1.20 eV	Indirect
Ge	IV	0.75 eV	Indirect
InAs	IV	0.42 eV	Direct
GaAs	III-V	1.40 eV	Direct
AlAs	III-V	2.22 eV	Indirect
InP	III-V	1.42 eV	Direct
GaP	III-V	2.34 eV	Indirect
AlP	III-V	2.50 eV	Indirect
InN	III-V	1.95 eV	Direct
GaN	III-V	3.40 eV	Direct
AlN	III-V	6.25 eV	Direct

An electron can be excited from the VB across the bandgap into the CB by electrical, optical (i.e. photoluminescence) or thermal effects. The properties of vacant orbitals in an otherwise filled band are very important in semiconductor physics. Vacant orbitals at the top of the VB are generally known as *holes*. Both electron and holes when in the presence of an applied field behave as if their masses were different from the no field situation. We say they have an effective mass m^* . The effective mass for

electron and holes in the cubic and hexagonal GaN material systems are tabulated in Appendix C

In the absorption process of a photon of energy $h\nu$ by an electron (such as in photoluminescence), two conservation rules must be satisfied before the absorption of electron can take place

a) *Conservation of Energy* The initial (E_i) and final (E_f) energies of the electron are related to

$$h\nu + E_i = E_f \quad (\text{B 2})$$

b) *Conservation of Momentum* The photon absorption process for the electron are related to

$$K_i \sim K_f \quad (\text{B 3})$$

Where K_i and K_f are the initial and final electron wave vector. The photon momentum magnitude is $h/\lambda \sim 0$ and can be ignored. Thus, the electromcs transitions due to photons are "vertical" in the $E(k)$ description. This explains why photo-absorption is not effective in indirect bandgap semiconductor

Donor-Acceptor Transition

Quiet often a semiconductor may contain both donor and acceptor atoms. By optical excitation, electron and holes can be created in the CB and VB respectively. In the decay some of the donor electrons will recombine radiatively with acceptor holes. This process is known as a donor-acceptor pair transitions or (D-A) transitions. The energy of a (D-A) transition is given by the following formula,

$$\hbar\omega = E_g - E_D - E_A + \frac{e^2}{\epsilon R} \quad (\text{B 4})$$

where E_D , E_A , e , ϵ and R are the donor and acceptor binding energy, electron charge, the dielectric constant and the distance between electron and hole, respectively. In GaN, the (D-A) pairs have been detected at ~ 3.25 eV (hexagonal GaN) and 3.17 eV

(cubic GaN) in the PL spectra Temperature dependent PL studies in hexagonal GaN reveal that E_D and E_A is ~ 25 meV and ~ 230 meV respectively These values are much higher than those of other III-V compound semiconductors such as GaAs (i.e. $E_A \sim 10$ meV)

Excitonic Transition

At sufficiently low temperatures, the Coulombic attraction between an electron and a hole will bind both these carriers together to produce a quasi particle known as exciton

When the material system contains a number of donor and acceptor in their neutral state, the exciton will be attracted to these impurities by van der Waals interactions These excitons are normally known as bound excitons There will be bound state of the exciton system having total energies lower than the bottom of the conduction band The exciton transition energy (E_n) in this situation is given by the following expression [1]

$$E_n = E_g - \frac{\mu e^4}{2\hbar^2 \epsilon^2 n^2} \quad (\text{B 5})$$

where E_g , n , ϵ and e are the bandgap energy, principle quantum number, dielectric constant and electron charge respectively μ is the reduced mass given by the following equation

$$\frac{1}{\mu} = \frac{1}{m_e} + \frac{1}{m_h} \quad (\text{B 6})$$

where m_e and m_h is the effective mass of the electron and hole respectively

The formation of excitons usually appears as narrow peaks in the absorption edge (bandgap) of direct semiconductors. Since the energy separation of the exciton state from the band edge is rather small, measurements to show the excitonic recombination of optical absorption must be carried out at low temperature. The exciton in the GaN material system is normally bound to the donor level near the conduction band, and is known as donor bound exciton or (D-X) transition which emits an energy at 3.473 eV in the low temperature PL spectra. The FWHM of the (D-X) transition in our PLD-grown GaN is about ~ 10 meV.

References

1 C. Kittel, *Introduction to Solid State Physics* John Wiley & Son NY1997

Appendix C: Hexagonal GaN vs Cubic GaN

The small covalent radius of N (1 e 0.7 Å compared to 1.1 Å for phosphorus and 1.2 Å for arsenic) results in significantly reduce lattice parameters for GaN compared with other III-V compounds, and the larger bond energy (3.4 eV compared to 1.4 eV for InP, 1.5 eV for GaAs) imply a higher melting temperature. The relatively small size of N compared with other group III atoms appears to play an important role in determining the crystal structure, the thermodynamically stable structure for GaN is the hexagonal (wurtzite) one. It should be pointed out that the cubic (zinc blende) structure does exists, but so far most research has focused on the hexagonal form. The two structures are very closely related as the bonding to the nearest neighbours is tetrahedral.

The physical properties of both structures are shown in the table 1 below,

	Wurtzite	Zincblende
Direct Bandgap (4 K)	3.5 eV	3.3 eV
Second Valley Bandgap	5.3 eV	4.7 eV
Effective Electron Mass	0.2 m_0	0.20 m_0
Effective Hole Mass	0.26 m_0	2.20 m_0
Electron Mobility	1000 cm^2/Vs	1450 cm^2/Vs
Thermal Conductivity	1.3 w/cm K	0.95 w/cm K
Dielectric Constant	8.9 ϵ_0	9.1 ϵ_0
Index of refraction	$n(1 \text{ eV}) \sim 2.33$ $n(3.38 \text{ eV}) \sim 2.67$	$n(3.38 \text{ eV}) \sim 2.55$
Piezoelectric Constant	$C_{11} = 367$ $C_{12} = 135$ $C_{13} = 103$ $C_{14} = 405$ $C_{33} = 95$ $C_{44} = 202$	$C_{11} = 293$ $C_{12} = 159$ $C_{44} = 155$

Table 1 Physical properties of cubic and hexagonal GaN

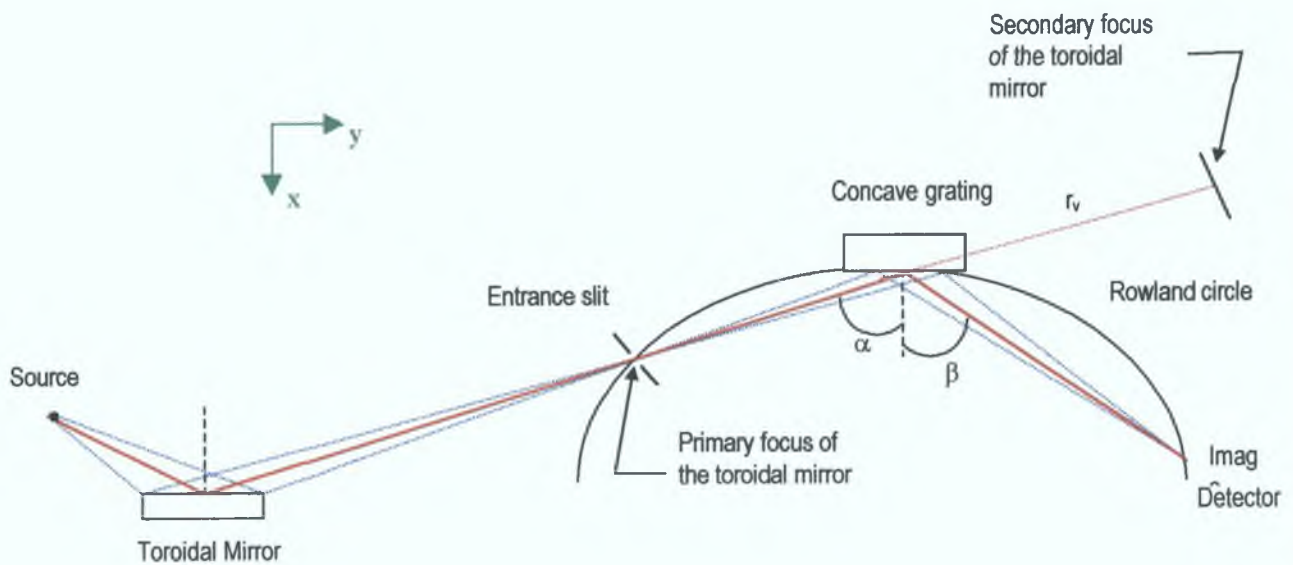
The zone centre phonon energies in GaN material system have been measured by several groups using both Raman scattering and infrared transmission methods and there is a high degree of consistency between all the results. In hexagonal GaN, the optical phonon modes can be classified under the irreducible representations of the point group C_{6v} , there are A_1 and E_1 modes on both the TO and LO branches, together with the so called 'low' and 'high' E_2 modes. The A_1 modes are polarized parallel, and the E_1 modes perpendicular to the crystal c -axis. Cubic GaN has zincblende structure and belong to the point group $T_d = 43m$. Zincblende-type material have close to $k=0$ a doubly degenerate TO and a single LO phonon with higher frequency. Two A_1 , one E_2 and two E_1 modes out of eight sets of modes predicted by Group Theory are Raman active. The wurtzite material can be considered as having a slightly distorted zincblende structure with a small change in the nearest neighbour distance, hence the energy difference between the Raman modes of hexagonal and cubic GaN is not very large. The phonon frequencies of hexagonal and cubic GaN are shown in table 2 below.

Hexagonal Modes	$A_1(\text{TO})$	$E_1(\text{TO})$	E_2	$A_1(\text{LO})$	$E_1(\text{LO})$
Frequency(cm^{-1})	540	560	575	735	762
Cubic Modes		$E_1(\text{TO})$		$A_1(\text{LO})$	
Frequency(cm^{-1})		555		740	

Table 2 Phonon frequencies in hexagonal and cubic GaN in room temperature

Appendix D: Optical Setup of the DLP System

The continuum radiation and the absorbing plasma are created by two Nd:YAG lasers focussed onto a tungsten rod (using a plano-convex lens) and a sample target, respectively The synchronisation of the lasers is controlled by a digital Delay Generator. The optical configuration of our DLP system is shown below,



Optical path of the DLP system

During the experiment, the continuum light that passes through the absorbing plasma is collected and focused by a toroidal mirror onto the entrance slit which is positioned on the Rowland circle. The toroidal mirror improves the grating efficiency of the spectrometer by eliminating astigmatism. The radii of curvature of the toroidal mirror were adjusted to produce uniform spectral lines on the Rowland circle. The concave grating sits on the Rowland Circle and focuses the dispersed light onto the detector (combination of a Micro-Channel Plate (MCP) and Photo-Diode Array (PDA) detector). By moving the detector along the Rowland circle, it is possible to record spectra in a different photon energy range. The output of the PDA signal is then processed by an Optical Multi-Channel Analyser (OMA) which is computer controlled.

The Nd YAG Laser

The YAG laser in our laboratory is a pulsed SL800 oscillator/amplifier system supplied by Spectron Laser Systems. It can be operated in both free running or Q-switched modes. Operated in Q-switched mode the output is ~1.2 J with pulse length of 15 ns at a fundamental lasing wavelength of 1.064 μm . As mentioned, the synchronisation of the lasers is done on a multi-channel delay function generator. The delay function generator employs the use of a 4145-2 programmable time delay card which is commercially available. This signal is applied simultaneously to both input channels of the delay generator. The first output of the function generator is connected to the flash lamp trigger of the first Nd YAG laser (the one that creates the laser plasma), while the second output is connected to the flash lamp trigger of the second Nd YAG laser (the one that “probes” the laser created plasma). The jittering caused by the system is less than 3 ns.